

2017

Mast Cells and Lipid Cross-Talk in Skin Inflammation

Piper Alexandra Wedman
University of South Carolina

Follow this and additional works at: <https://scholarcommons.sc.edu/etd>



Part of the [Medical Sciences Commons](#)

Recommended Citation

Wedman, P. A. (2017). *Mast Cells and Lipid Cross-Talk in Skin Inflammation*. (Doctoral dissertation). Retrieved from <https://scholarcommons.sc.edu/etd/4158>

This Open Access Dissertation is brought to you by Scholar Commons. It has been accepted for inclusion in Theses and Dissertations by an authorized administrator of Scholar Commons. For more information, please contact digres@mailbox.sc.edu.

Mast Cells and Lipid Cross-Talk in Skin Inflammation

By

PIPER ALEXANDRA WEDMAN

Bachelor of Science
Metropolitan State College of Denver, 2011

Submitted in Partial Fulfillment of the Requirements

For the Degree of Doctor of Philosophy in

Biomedical Science

School of Medicine

University of South Carolina

2017

Accepted by:

Carole Oskeritzian, Major Professor

Mitzi Nagarkatti, Chair, Examining Committee

Gregorio Gomez, Committee Member

Joseph Janicki, Committee Member

Angela Murphy, Committee Member

Maria Marjorette Peña, Committee Member

Cheryl L. Addy, Vice Provost and Dean of the Graduate School

© Copyright by Piper Alexandra Wedman, 2017
All Rights Reserved.

DEDICATION

I was 21 when I met my husband, Scott, and decided to return to high school to complete the 15 English credits needed to earn my high school diploma. I graduated that spring and started college Fall 2006. The reason was simple, I wanted to return to school to ensure my kids would have a good future. From the beginning, Scott has been supportive of my decisions and helped me raise our kids while I attended school. I dedicate this work to them, my family, Scott, Korbin and Kyra, you inspire me to do my best!

ACKNOWLEDGEMENTS

There are so many people who have been there for me throughout this journey...

Dr. Carole, thank you for giving me the honor of working with you. You have both challenged me and supported me and because of that I have grown in ways I didn't think possible! Alena, your friendship and coffee breaks made all the difficult days easier. Ahmed, thank you for your happiness and positivity. Dr. John, thank you for your expertise and your stories. My committee members, Dr. Nagarkatti, Dr. Murphy, Dr. Gomez, Dr. Peña and Dr. Janicki, thank you for your time and commitment to me throughout the years! To all the people in the PMI department, your willingness to help was always appreciated!

Scott, thank you for believing in me when I didn't believe in myself. Without you, this path would have been even more challenging! Korbin and Kyra, thank you for loving me unconditionally! Mom, thanks for making time to visit the kids and I each year. Your love and guidance encouraged me to reach for the stars! Alia and Brady, thank you for always listening to me and for helping me weigh the pros and cons when I can't make decisions. The rest of my family and friends, thank you for your time and laughter. I love you all!

This work was supported by NIH/NIAID R01 AI095494 and NIH/NIAMS R21 AR067996 to CAO.

ABSTRACT

Atopic dermatitis (AD) is an inflammatory skin disease whose pathogenic mechanisms remain unclear. Using a validated human AD-like mouse model, we observed that skin remodeling started at a pre-symptomatic stage of AD that included cellular infiltration of the hypodermis, accompanied with activated/degranulated mast cells (MC). Local MC activation was quantified using a novel method of computer-assisted image analysis we developed and reported. Using a variation of this method, we defined morphometric parameters allowing for quantitation rather than scoring of cellular infiltration. Cell recruitment correlated with MC activation, chemokine production and increased levels of sphingolipid sphingosine-1-phosphate (S1P), produced by sphingosine kinase-1 (SphK1). MC or SphK1 deficiency significantly hindered early AD inflammation.

Chronic AD features skin barrier dysfunction leading to skin lesions due to decreased lipid ceramide (CER) content. Interestingly, local CER species C16 and C24 were significantly increased in pre-symptomatic AD. Accordingly, skin CER synthase (CerS, CER synthesis) CerS4, 5 and 6 mRNA mRNA levels were statistically augmented. Because of the overall proapoptotic functions of CER, we next measured local cleaved/activated caspase 3 levels, the executioner caspase in apoptosis. Skin cleaved caspase 3/apoptosis was significantly augmented in early AD and correlated with increased endoplasmic reticulum (ER) stress-related molecular players. To substantiate the importance of MC in

ER stress-induced apoptosis, CER profiling was similarly conducted in treated skin samples collected from MC-deficient mice. MC deficiency prevented CER increase and local apoptosis that were restored following MC reconstitution.

Epigenetic regulation of the molecular pathways that drive AD is unknown. We identified and validated a microRNA triad 34a-485-486 whose downregulation promoted the AD-related pathogenic pathways we have unraveled.

We conclude that MC may initiate AD by driving early skin remodeling and cell recruitment through local chemokine and S1P production and CER-elicited apoptosis. Moreover, the down-regulation of a miRNA triad de-represses these key players of AD pathogenesis. Targeting these pre-symptomatic effector mechanisms may offer new prophylactic strategies for AD whose treatment remains a clinical challenge.

TABLE OF CONTENTS

DEDICATION.....	iii
ACKNOWLEDGEMENTS	iv
ABSTRACT	v
LIST OF TABLES.....	ix
LIST OF FIGURES.....	x
LIST OF ABBREVIATIONS.....	xii
FOREWORD	1
CHAPTER 1: INTRODUCTION	5
1.1 MAST CELLS AND SPHINGOSINE-1-PHOSPHATE IN EARLY ALLERGIC LUNG INFLAMMATION.....	5
1.2 ATOPIC DERMATITIS	6
1.3 STATEMENT OF HYPOTHESIS AND AIMS.....	8
CHAPTER 2: A NEW IMAGE ANALYSIS METHOD BASED ON MORPHOMETRIC AND FRACTAL PARAMETERS FOR RAPID EVALUATION OF IN SITU MAMMALIAN MAST CELL STATUS	10
2.1 INTRODUCTION.....	10
2.2 MATERIALS AND METHODS	12
2.3 RESULTS.....	18
2.4 DISCUSSION	21

CHAPTER 3: MAST CELLS AND SPHINGOSINE-1-PHOSPHATE UNDERLIE EARLY PATHOGENIC REMODELING IN PRE-LESIONAL ECZEMA	34
3.1 INTRODUCTION.....	34
3.2 MATERIALS AND METHODS	36
3.3 RESULTS AND DISCUSSION	43
CHAPTER 4: A MAST CELL-MEDIATED ELEVATION OF CERAMIDES TRIGGERS APOPTOSIS IN PRE-LESIONAL ATOPIC DERMATITIS	62
4.1 INTRODUCTION.....	62
4.2 MATERIALS AND METHODS	64
4.3 RESULTS.....	67
4.4 DISCUSSION	70
CHAPTER 5: A MIRNA TRIAD EPIGENETICALLY REGULATES AD PATHOGENESIS.....	80
5.1 INTRODUCTION.....	80
5.2 MATERIALS AND METHODS	82
5.3 RESULTS.....	83
5.4 DISCUSSION AND FUTURE DIRECTIONS	85
CHAPTER 6: SUMMARY AND CONCLUSIONS	91
6.1 MOLECULAR MECHANISMS UNDERLYING EARLY SKIN REMODELING AT THE ONSET OF ATOPIC DERMATITIS.....	91
6.2 SPHINGOSINE-1-PHOSPHATE AND MAST CELLS CONTRIBUTE TO SKIN INFLAMMATION IN EARLY-PHASE ATOPIC DERMATITIS.....	91
6.3 OVA TRIGGERS MC-RELATED PRODUCTION OF PRO-APOPTOTIC CERAMIDES AT ATOPIC DERMATITIS ONSET	93
6.4 DOWN-REGULATION OF MIRNA 34A, 485 AND 486 REGULATES AD PATHOGENESIS	94
REFERENCES.....	97
APPENDIX A: PERMISSION TO REPRINT.....	122

LIST OF TABLES

Table 3.1 Mouse primer sequences used for qPCR in AD experiments	61
Table 4.1 Mouse primer sequences used for qPCR in CER experiments.....	79
Table 5.1 Mouse primer sequences used for qPCR in miRNA experiments	90

LIST OF FIGURES

Figure 2.1 Methylene-blue stained mouse skin for MC detection and analysis...	30
Figure 2.2 Mass descriptors distinguish intact from degranulated MC.....	31
Figure 2.3 Fractal dimension (D) independently validates definitions of intact vs. degranulated MC	32
Figure 2.4 D of degranulated MC is higher than D of intact MC.....	33
Figure 3.1 Skin remodeling starts after a single epicutaneous (EC) exposure to OVA	52
Figure 3.2 Chemokines are up-regulated after a single exposure to OVA.....	54
Figure 3.3 Mast cells degranulation and S1P levels increase in OVA-treated skin tissues.....	55
Figure 3.4 Skin remodeling and chemokine expression are mitigated in mice deficient for SphK1 or mast cells: S1P-mediated skin mast cell degranulation and mast cell-dependent local S1P production.....	57
Figure 3.5 Cellular infiltration, mast cell degranulation and S1P increase are abated in mouse back skins exposed to LPS-free OVA.....	59
Figure 4.1 Skin exposure to OVA leads to increased ceramides in WT mice	74
Figure 4.2 Increased cleaved Caspase 3 is observed following OVA exposure .	75
Figure 4.3 OVA treatment leads to endoplasmic reticulum stress-induced apoptosis	76
Figure 4.4 Ceramides, mRNA coding for genes involved in ceramide production remain unaltered and apoptosis undetectable upon OVA treatment of Kit ^{W-sh/W-sh} MC-deficient mice	77
Figure 4.5 In vitro S1P stimulation triggers ceramide generation in BMMC	78
Figure 5.1 Down-regulation of skin miRNA up-regulates AD-associated gene expression	88

Figure 5.2 A newly identified AD-associated microRNA signature is also relevant to AD pathogenesis with validated target gene de-repression 89

Figure 6.1 Inflammatory changes occur early after topical application of LPS-containing OVA in an established mouse human AD-like model 96

LIST OF ABBREVIATIONS

A	Area
AD.....	Atopic Dermatitis
Ag	Antigen
ATF4.....	Activating Transcription Factor 4
BiP	Binding Immunoglobulin Protein
BMMC.....	Bone Marrow-Derived Mast Cells
Bv.....	Blood Vessel
C	Carbon
Casp3	Caspase 3
CER	Ceramides
CerS.....	Ceramide Synthase
CHOP	CCAAT-Enhancer-Binding Protein Homologous Protein
CS.....	Chondroitin Sulfate
CTLA-4	Cytotoxic T Lymphocyte-Associated Antigen 4
CTMC	Connective Tissue Mast Cells
D	Fractal Dimension
DNP	Dinitrophenol
EC.....	Epicutaneous
ER.....	Endoplasmic Reticulum
FcεR1α.....	High-Affinity IgE Receptor
FTY720	Fingolimod

GAPDH	Glyceraldehyde 3-Phosphate Dehydrogenase
GV	Pixel Gray Value
H&E	Hematoxylin and Eosin
H(GV).....	Gray Level Histogram
HSA	Human Serum Albumin
HSI.....	Hue, Saturation, Intensity
HPF.....	High Power Field
IgE	Immunoglobulin E
IOD	Integrative Optical Density
LPS.....	Lipopolysaccharide
MB	Methylene Blue
MC	Mast Cells
MCP-1, CCL2.....	Monocyte Chemoattractant Protein 1
MIP-1 α , CCL3.....	Macrophage Inflammatory Protein 1 α
MMC	Mucosal Mast Cells
OVA	Ovalbumin
PSA.....	Passive Systemic Anaphylaxis
PVDF	Polyvinylidene Difluoride
RANTES, CCL5...	Regulated on Activation, Normal T-Cell Expressed and Secreted
ROI	Regions of Interest
S1P.....	Sphingosine-1-Phosphate
S1PR	Sphingosine-1-Phosphate Receptor
SC.....	Stratum Corneum
SCF.....	Stem Cell Factor
Snord96a	Small Nucleolar RNA, C/D Box 96A

SphK..... Sphingosine Kinase
UPR Unfolded Protein Response
WT Wild-Type
XBP-1 X-box Binding Protein 1

FOREWORD

Mast cells are immune cells of hematopoietic lineage. Differentiation and maturation of MC occurs as they reach the vascularized tissues where they will reside (Kitamura, 1989). MC exist as two distinct subsets, distinguishable by the protease composition of secretory granules. In humans, MC_{TC} contain tryptase, chymase, and other proteases, while MC_T contain only tryptase (Oskeritzian *et al.*, 2005). MC_{TC} (equivalent to connective tissue MC, CTMC) are located in the skin, heart, muscle, and submucosa of the small intestines while MC_T (equivalent to mucosal MC, MMC) are localized to airway epithelia and small intestine mucosa (Schwartz, 2005).

MC, uniquely identified by dual expression of c-kit, stem cell factor (SCF) receptor, and high affinity immunoglobulin (Ig) E receptor (FcεRI), are key effector cells of IgE-mediated immune responses, including allergic diseases. IgE-dependent MC activation occurs following antigen (Ag) cross-linking of surface-bound IgE, triggering the release of many mediators. Some mediators, such as vasoactive amines (e.g. histamine), neutral proteases (e.g. tryptases and chymases), proteoglycans (e.g. heparin) some cytokines and growth factors and sphingolipid S1P are pre-stored within MC and released immediately upon activation, while prostaglandins, leukotrienes and other pro-inflammatory lipid mediators are produced *de novo*. In addition, MC can secrete a wide variety of

growth factors, cytokines, and chemokines in response to various stimuli in a tissue and/or species-dependent manner (Galli *et al.*, 2015).

Human MC and mouse bone marrow-derived MC (BMMC) are important tools for analyzing MC responses *in vitro*. Primary MC can be isolated from tissues and expanded *ex vivo* in the presence of MC-specific growth factors, which include SCF (and interleukin (IL)-3 for mouse MC). In addition, MC lines are available. The most common MC lines are rat basophilic leukemia (RBL)-2H3 cells, human HMC-1 and LAD2 cells, derived from patients with MC leukemia (Butterfield *et al.*, 1988; Kirshenbaum *et al.*, 2003), and commercially available LUVA cells, that spontaneously developed from human blood CD34⁺ cells (Laidlaw *et al.*, 2011). While convenient, cell lines present transformed phenotypes with constitutively activated signaling pathways, making primary cells preferable for studying MC functions *in vitro*.

MC-deficient mice have proven useful for studying the relevance of MC in health and disease. Kit, receptor for stem cell factor (SCF, previously called MC growth factor), is expressed on all hematopoietic stem cells. While most cells gradually lose Kit expression as they mature, MC remain Kit⁺. *Kit*^{W/W^{-v}} and *Kit*^{W^{-sh}/W^{-sh}} MC-deficient mice feature *c-kit* mutations. *Kit*^{W^{-sh}/W^{-sh}} mice present fewer abnormalities than *Kit*^{W/W^{-v}} mice, which are anemic and difficult to breed. In addition, *Kit*^{W/W^{-v}} mice display other phenotypic abnormalities including decreased numbers of TCRγδ and spontaneous dermatitis, thus *Kit*^{W^{-sh}/W^{-sh}} mice are preferred (Grimbaldeston *et al.*, 2005). Nonetheless, mutations in Kit may alter other cells than MC. To avoid the collateral issues related to *c-kit* mutations,

alternative MC-deficient mice were generated, in which Cre recombinase (Cre) is expressed under the control of “MC-restricted” promoters. The mast cell protease (*Mcpt*) 5-*Cre*; *R-DTA* mice feature diphtheria toxin alpha (DTA)-induced deletion of CTMC only and have an otherwise normal immune system (Dudeck *et al.*, 2011). *Cpa3^{Cre/+}*, or “Cre-Master”, mice display a carboxypeptidase A3 (*Cpa3*)-directed activation of Cre, which results in eradication of all MC, but also affects some T cell populations and basophils (Feyerabend *et al.*, 2011). *Cpa3-Cre;Mcl-1^{fl/fl}*, affectionately called “Hello Kitty” mice by Dr. Steve Galli who generated them, are similar to the *Cpa3^{Cre/+}* strain as constitutive reduction in all MC is observed with concomitant depletion of basophils (Lilla *et al.*, 2011). Perhaps more clinically relevant than MC-deficient models, another approach has been to induce MC ablation when desired. To this end, *Mcpt5-Cre;iDTR* mice (Dudeck *et al.*, 2011), “Mas-TRECK mice (Otsuka *et al.*, 2011; Sawaguchi *et al.*, 2012), and *Cpa3-Cre;iDTR* mice (Reber *et al.*, 2014) are all inducible models of MC depletion (Galli *et al.*, 2015). To confirm the importance of MC to a specific disease state, MC-deficient mice can be conveniently reconstituted through adoptive transfer of BMDC from WT or knockout mice of similar C57Bl/6 genetic background.

Sphingosine-1-phosphate (S1P) is a potent sphingolipid metabolite important for cell trafficking, proliferation and survival responses. The pleiotropic properties of S1P can be attributed to the fact that S1P can bind to 5 specific G protein-coupled receptors, termed S1P receptors (S1PR1-5), expressed in

various combinations by a variety of different cell types, including T and B cell lymphocytes, dendritic cells and mast cells (Spiegel and Milstien, 2011).

MC can produce S1P both constitutively and upon IgE/Ag activation, which concomitantly activates SphK (Oskeritzian *et al.*, 2008) that phosphorylate sphingosine to produce S1P. The two isoforms of SphK have distinct functions in MC. SphK2 is most important for production of S1P in the nucleus and other subcellular compartments, while SphK1-derived S1P may be transported outside of the cell to ligate cell surface S1PR in an autocrine and/or paracrine manner (Mitra *et al.*, 2006; Oskeritzian *et al.*, 2008). MC express S1PR1, which plays a role in immune cell trafficking and migration, and S1PR2, which stops movement mediated by S1PR1 and triggers release of MC granules (Jolly *et al.*, 2004; Spiegel and Milstien, 2011).

CHAPTER 1: INTRODUCTION

1.1 MAST CELLS AND SPHINGOSINE-1-PHOSPHATE IN EARLY ALLERGIC LUNG INFLAMMATION

We recently demonstrated the importance of MC/S1P signaling, through S1PR2, for early T cell recruitment to inflamed lungs in a model of passive systemic anaphylaxis (PSA) (Oskeritzian *et al.*, 2015). Mice were passively sensitized with IgE anti-2,4-dinitrophenyl (DNP) and later challenged with antigen (Ag) DNP-human serum albumin (DNP-HSA). We found that the neutralization of extracellular S1P with a specific anti-S1P mAb (Sphingomab™), prior to Ag challenge, resulted in significantly decreased levels of circulating histamine, monocyte chemoattractant protein 1 (MCP-1)/CCL2, macrophage inflammatory protein 1 α (MIP-1 α)/CCL3 and RANTES/CCL5 compared to an isotype-matched negative control Ab. We established that these chemokines were important for CD3+ T cell recruitment. Moreover, we identified MC as a local source of CCL2 and CCL5. Significantly reduced levels of circulating chemokines were detected in MC-deficient Kit^{W-sh/W-sh} mice following Ag challenge, compared to WT controls. Furthermore, when MC-deficient mice were reconstituted with MC by adoptive transfer of BMDC, production of circulating chemokines observed in WT mice was restored. Following Ag challenge, Sphingomab recipients and MC-deficient mice were protected from the drastic drop in core body temperature

indicative of anaphylaxis and early pulmonary edema observed in isotype or WT controls. These results highlighted MC/S1P axis as a major contributor of tissue remodeling during the early phase of allergic responses in the lungs and were publicized as the Editor's Choice of The Journal of Allergy and Clinical Immunology and again as a part of the "Advances and highlights in mechanisms of allergic disease in 2015" (Wawrzyniak *et al.*, 2016).

1.2 ATOPIC DERMATITIS

Atopic dermatitis (AD) is a recurring inflammatory skin disease which affects 10-25% of individuals residing in developed countries. Primarily starting in early childhood, 85% of patients experience onset of symptoms prior to age 5. Individuals affected with AD often develop other allergic disorders, such as asthma, food allergies or rhinitis later in life, making it the first manifestation of allergies in what has become known as the atopic march. AD occurrence has increased in recent years, but is less prevalent in rural areas supporting the "hygiene hypothesis" which states that early exposure to infectious agents aids immune system development and decreases susceptibility to allergic (and autoimmune) disease (Bieber, 2010).

AD pathogenesis has been attributed to Ag penetration through a compromised barrier, which triggers activation of skin resident cells and release of many pro-inflammatory mediators, leading to severe itchiness, dry-flaky skin and lesions. AD skin displays thickening of the epidermis and dermis layers accompanied by accumulation of immune cells (Bieber, 2010; Yoon *et al.*, 2016), including effector T cell subsets (Th1, Th2, Th17 and Th22) and MC (Auriemma

et al., 2013; Werfel *et al.*, 2016). Molecularly, inflammatory pathways of AD are biphasic. The acute phase is thought to be driven by Th2 cells whereas Th1 immune responses dominate chronic lesions (Bieber, 2010). Observations of chronic inflammation associated with AD has prompted many studies, resulting in suggested potential targets for therapeutic intervention, including cytokines and chemokines present once the disease has developed. Available treatment options, for moderate to severe AD, consist in symptom management with undesirable side effects such as diabetes, hypertension, gastric ulcers, osteoporosis, glaucoma, growth retardation, renal toxicity, liver dysfunction and leukopenia (Simon and Bieber, 2014).

For mild AD, moisturizers can contribute to restoration of the skin barrier. Many of these topical skin care products feature addition of the sphingolipid ceramide (CER), critical for maintaining barrier functions in healthy individuals. AD patients present a loss of very long chain ceramides that compose the stratum corneum (SC) layer of epidermis. It has been thought that adding ceramides to moisturizer would positively affect SC structure and lipid organization. However, a recent study, comparing efficacy of ceramide-rich moisturizer on AD patients, found no significant difference in disease severity when compared with other moisturizing products (Miller *et al.*, 2011).

Inflammation results from the coordinated actions of diverse molecular pathways driving a variety of altered gene and protein expression. The discovery of miRNA, small noncoding molecules that control translation of target mRNA and therefore post-transcriptionally fine-tune many biological processes, has

prompted new lines of research to better understand AD etiology (Plank *et al.*, 2013). Sonkoly *et al.* were the first to conduct a genome-wide analysis of miRNA expression in human biopsies of healthy, psoriatic and AD skin samples but were ultimately unable to define an AD-specific signature (Sonkoly *et al.*, 2007). In a later study, they linked overexpression of miR-155, which targets cytotoxic T lymphocyte-associated antigen 4 (CTLA-4), to increased proliferation of T_H cells in AD (Sonkoly *et al.*, 2010). More recently, Rebane *et al.* reported that miRNA 146a is upregulated in keratinocytes from chronic lesions of AD patients, contributing to suppression of innate immune responses (Rebane *et al.*, 2014). However, there is no study defining the miRNA signature of AD pathogenesis.

1.3 STATEMENT OF HYPOTHESIS AND AIMS

Allergenic stimulation releases the multifaceted sphingolipid S1P from tissue-resident MC (Mitra *et al.*, 2006; Oskeritzian *et al.*, 2008; Oskeritzian *et al.*, 2010). Our most recent studies revealed that S1P serves to further propagate inflammatory responses through autocrine/paracrine stimulation of MC, creating an inflammatory amplification loop, which we have shown is essential to the onset of acute pulmonary inflammation. As MC are present in normal skin at homeostasis and they become more numerous and activated in inflamed skin (Bieber, 2010; Liu *et al.*, 2011), we suggest a similar critical role for MC and S1P in the onset and progression of skin inflammation. We are proposing to establish the contribution of MC in diseased mouse skin samples, compared to healthy skins, at the initiation of AD. We anticipate an early-defined MC-driven molecular signature at AD onset that may allow for the design of new prophylactic

strategies to prevent further disease development. Next, we propose local S1P plays a key role in inflammatory cell recruitment through its stimulatory effects on MC degranulation, likely propagating inflammation. Moreover, since AD is associated with loss of skin barrier functions and because lesional skin of AD patients displays decreased ceramide content, we will investigate changes in CER levels at early-phase skin inflammation, a time-point which may be more receptive to repair strategies. As little is known pertaining to the epigenetic regulation of AD by miRNAs, we also propose to investigate miRNA expression during AD pathogenesis.

For this study, we designed the following aims:

- Aim 1: Establish the molecular mechanisms underlying early skin remodeling at the onset of AD
- Aim 2: Examine how S1P and MC contribute to skin inflammation in early-phase AD
- Aim 3: Investigate ceramide species at the initiation of AD
- Aim 4: Define the regulatory function of miRNA in AD development and progression

To study the direct implication of MC during AD inception, we first developed a computer-automated system to measure MC activation status *in situ*.

CHAPTER 2: A NEW IMAGE ANALYSIS METHOD BASED ON MORPHOMETRIC
AND FRACTAL PARAMETERS FOR RAPID EVALUATION OF IN SITU
MAMMALIAN MAST CELL STATUS¹

2.1 INTRODUCTION

Mast cells (MC) are long-lived tissue-dwelling cells, found in all vascularized tissues at homeostasis, especially at the host/environment interfaces, including skin, airways and the gastrointestinal and genitourinary tracts (Galli *et al.*, 2011). There is mounting evidence that MC manifest substantial immunomodulatory functions in many physiological processes through the vast repertoire of mediators they release upon activation (Galli *et al.*, 2011; Oskeritzian, 2015). Degranulation represents the canonical process through which activated MC secrete mediators (Wernersson and Pejler, 2014). It refers to rapid exocytosis of granules that occupy about 80% of MC cytoplasm and harbor a wide array of preformed bio-active substances (Galli and Tsai, 2012; Moon *et al.*, 2014). A spectrum of receptor-dependent and independent stimuli can activate MC, including physical and mechanical triggers, and the

¹ Wedman, P., A. Aladhami, M. Beste, M.K. Edwards, A. Chumanevich, J.W. Fuseler, and C.A. Oskeritzian. 2015. A New Image Analysis Method Based on Morphometric and Fractal Parameters for Rapid Evaluation of In Situ Mammalian Mast Cell Status. *Microsc Microanal* 21:1573-1581.

Reprinted here with permission of publisher.

subsequent secretion of histamine, proteases, lipid mediators, cytokines, and chemokines (da Silva *et al.*, 2014). To date, investigators are taking advantage of MC cytoplasm replete with granules as intragranular proteoglycans interact with metachromatic dyes such as methylene blue (MB) to allow for visualization, anatomical distribution and enumeration of MC in tissue sections (Wolters *et al.*, 2005). The interaction of these highly sulphated structures with dye molecules yields a distinct blue/purple color uniquely staining MC cytoplasmic granules (Lagunoff, 1974; Wolters *et al.*, 2005). Other commonly used histological methods include chloroacetate esterase, but this technique may also stain granulocytes (Rafail *et al.*, 2015). Although local MC identification may be straightforward, microscopic discrimination between intact and degranulated MC could be daunting even for trained observers as tissue MC are polymorphic and staining intensity may vary even when routinely used. Thus, the universally accepted method to substantiate MC activation remains circulating level determination of MC-restricted mediators, including tryptase (Schwartz *et al.*, 1987). However, while unequivocally quantitative, systemic measurements do not reflect *in situ* alterations of MC. Because of their strategic location, MC can regulate vascular permeability and cell recruitment to initiate local inflammation, therefore exerting important pathogenic functions (Marshall, 2004). We reasoned that image analysis could aid to develop a reproducible, objective and thus reliable method to quantify rather than score MC activation. To this end, we investigated normal mouse skin samples for MC using the well-established MB staining of tissue sections. Images of a large number of MC were captured from

four different mice. Next, we considered MC granule-filled cytoplasm as an object and MC as regions of interest (ROI), endowed with size, volume and staining intensity parameters. We reasoned that an intact MC should feature higher values for these parameters, compared to degranulated MC. Our results demonstrate these morphometric parameters precisely classify MC into two objective groups, intact and degranulated MC. We further complemented these measurements by quantification of fractal dimension values for each cellular state. Taken together, we have established a rigorous analytical method based on acquisition of morphometric data collected from digitized images of tissue sections that allows for reliable and objective quantitation of MC activation status. Thus, MC disorders may involve aberrant proliferation of MC exemplified by mastocytosis, a myeloproliferative neoplasm, but many primary MC diseases feature normal MC numbers of abnormal hyperactivity (Hamilton *et al.*, 2011; Valent *et al.*, 2011). Chronic MC activation could be challenging to diagnose, often accompanied with mild, episodic or atypical symptoms of idiopathic origin (Valent *et al.*, 2011). Based on our study, pathological specimens could be surveyed for MC status at a greater scale for diagnostic/prognostic purposes in MC related disorders or in diseases where MC dysfunction is suspected in the absence of pathognomonic signs.

2.2 MATERIALS AND METHODS

Reagents

All chemicals were purchased from Fisher Scientific (Pittsburgh, PA, USA).

Animals

Gender- and aged- matched C57BL/6 mice were purchased from Charles River NCI (Frederick, MD, USA). All mice were used at 8–12 weeks of age and maintained in a pathogen-free facility. Studies were performed in accordance with institutional animal care and use committee guidelines.

Histology

For skin tissue collection, mice were euthanized by CO₂ asphyxiation. The skin from the dorsal back was shaved. Skin samples were collected and fixed in 10 %-buffered formalin. Fixed tissues were embedded in paraffin, sectioned (5 μm thickness) and mounted on microscope slides. Some slides were stained with hematoxylin and eosin. Other slides were de-paraffinized in xylene, hydrated through graded alcohols, and equilibrated in phosphate-buffered saline. To visualize MC, slides were placed in 0.1 % methylene blue (MB) for 5 s, rinsed with water, dehydrated in 100 % ethanol and mounted under coverslips with cyto seal 60 (Wolters *et al.*, 2005). Sections were imaged with a Nikon E-600 microscope (Nikon Inc., Melville, NY, USA) equipped with a Micropublisher digital camera and images collected with 10x and 40x objectives. Fourteen adjacent images were recorded from each section as TIFF files. Morphometric parameters of MC were measured using the MetaMorph® 6.1 Microscopy Automation and Image Analysis software (MolecularDevices, Sunnyvale, CA, USA).

Descriptors of MC Morphology in the Skin

The morphometric descriptors of area (A), integrated optical density (IOD) to generate relative density (IOD/A), and fractal dimension (D) were measured

for thresholded and isolated MC residing in the hypodermis and dermis of isolated regions of the skin (n = 4 mice).

Isolation and Area of MC

In the hypodermis and dermis of digitized images, MC were isolated as individual ROI using the hue, saturation, intensity (HSI) color model of the set color threshold subroutine of MetaMorph 6.1 software. The area of the cell measured excluded holes (non-stained regions) within the ROI.

IOD of MB-stained MC

The HSI values were adjusted to isolate the blue/purple metachromatic color characteristic of MC as a thresholded region. The cytoplasmic blue/purple metachromatic color distinguishes MC from other blue staining in the tissue. From the thresholded region, the area (A) of the cell and its IOD were measured using the integrated morphometry subroutine of MetaMorph 6.1. The image of the individual isolated MC was converted to a gray scale image for further analysis of its fractal dimension using the free HarFa imaging software (www.fch.vutbr.cz/lectures/imagesci/).

When using threshold boundaries in an image, the IOD is defined as the weighted sum of the image histogram in which each term in the histogram is multiplied by the gray value it represents (Walter and Berns, 1981) and is expressed by the following equation:

$$IOD(T1, T2) = \sum_{GV=T1}^{T2} H(GV) \times GV$$

where T1 and T2 represent the upper and lower thresholds defining the ROI in the histogram, GV the gray value of each pixel, and H(GV) the gray level

histogram. Values of IOD were calculated directly from the integrated morphometry subroutine of MetaMorph 6.1 software. Using the software's optical calipers, the measurements were refined by setting specific boundary conditions for area and IOD for acceptance of the signal from the individual MC and to minimize or eliminate the contributions of any non-specific and background staining. This concept of IOD representing the mass or total amount of stained material in an ROI of an image is well-established and has been previously applied to diverse topics including the translocation of nuclear factor κ B in the nucleus (Fuseler *et al.*, 2006; Rogers and Fuseler, 2007), changes in actin cytoskeleton in cardiac fibroblasts (Fuseler *et al.*, 2007) and adult stromal stem cells (Fuseler and Valarmathi, 2012), and comparison of the architecture of normal and tumor microvasculature (Fuseler *et al.*, 2010).

The IOD measured for the MB-stained MC is a representation of the mass and a measurement of the total amount of material in the delineated region. The values of the IOD were normalized by being divided by the area (A) of the thresholded ROI for the MC. The resulting term of IOD/A allows for comparisons to be made between intact MC and MC that have experienced degranulation as result of activation. Additionally, IOD/A provides the concept of mass density or relative density (Smith *et al.*, 1996) of the intact and degranulated MC. As a mass measurement, the values of IOD/A provide further information on the structure and distribution of pixels constituting the mass MC granules present within the ROI.

Fractal Dimension

MC granular cytoplasm is an irregular and complex object composed of proteoglycan-containing granules at different levels of resolution, which are functionally and physiologically similar (self-similar). Because of the complexity of form, MC cytoplasm cannot be characterized or defined by regular Euclidean geometry or dimensions. Regular Euclidean dimension assigns an integer to each point or set of points in Euclidean space and includes the familiar geometrical descriptors or numbers: 0 to a point, 1 to a straight line, 2 to a plane surface, and 3 to a volume or three dimensional figures. These integer descriptors are exponents of power functions that describe these objects (Brown *et al.*, 2002). Complex macro- or micro-anatomical structures cannot be analyzed by regular Euclidean geometry, but can be described quantitatively by fractal geometry (Mandelbrot, 1983; Smith *et al.*, 1996). The fractal dimension of complex or irregular structures can be described by non-integer numbers, with values falling between two-integer topological dimensions. These non-integer numbers are described as non-Euclidean and define the fractal dimension (D) of an object. The concept of fractals currently provides a useful method to quantify the inherent irregularity or complexity of phenomena (Zhang *et al.*, 2006). In general, a fractal is any rough and irregular object consisting of parts that are in some way similar to the whole. Because of the self-similar conditions, MC cytoplasm can be considered a fractal object and its fractal dimension (D), expressed by a non-integer number lying between two Euclidean integer topological dimensions (Grizzi *et al.*, 2005). In the case of the two-dimensional

images analyzed in this study, the values of D characterizing MC cytoplasm are therefore fractional and lie between the Euclidean integers of 1 and 2.

The box-counting method has been the most widely used and general model for applying fractal analysis to biological and non-biological systems and is expressed by the formula:

$$D = \lim_{e \rightarrow 0} \frac{\text{Log}N(e)}{\text{Log}\left(\frac{1}{e}\right)}$$

The box-counting method consists of a grid of boxes of side length size (e) superimposed over the image of the structure and N(e) the smallest number of boxes of side (e) required to cover the surface or outline of the object completely (Dioguardi *et al.*, 2006; Fuseler *et al.*, 2007; Grizzi and Dioguardi, 1999). Since a zero limit cannot be applied to a biological object, here the MC, the fractal dimension is determined as the slope of a regression line when Log [N(e)] is plotted against Log(1/e) i.e., $D = \text{Log} [N(e)]/\text{Log}(1/e)$. From the images of previously isolated and thresholded MC, the D values of the ROI were determined using HarFA (full version 5.5.31) software (Nezadal *et al.*, 2001). The thresholded images of MC are assigned mesh sizes of boxes with (e) values ranging from 2 to 215 pixels and 30 steps within this range were calculated to generate the Log [N(e)] versus Log(1/e) plots, the slopes of which determine the D values. In these 40x images, one pixel is equal to 0.229 μm . Fourteen images were analyzed from each skin section of each animal (n = 4 mice).

Statistics

Data are expressed as means \pm SEM. Significance was determined by analysis of variance and an appropriate *post hoc* test for multiple comparisons

using Sigma-Plot software (Systat Software Inc., San Jose, CA, USA) and is shown in figures.

2.3 RESULTS

Methylene Blue Staining of Normal Mouse Skin Sections for MC Detection and Analysis

We used a classic staining technique to visualize MC in skin tissue sections. Methylene blue (0.1 % MB) stains all nuclei of cells in blue. Because of the metachromatic nature of the proteoglycans that compose the frame of MC granules, the interaction of the dye molecules with proteoglycans results in an absorption spectrum shift from blue to purple. Thus, metachromasia features blue/purple cytoplasmic granules, unique to MC (Wolters *et al.*, 2005). Even though the metachromatic cytoplasmic staining is MC-specific, Figure 2.1a shows that *in situ* MC detection can be challenging, at low magnification using a 10× objective of MB-stained skin section. Higher magnification using a 40× objective (or High Power Field, HPF) of similar MC-stained skin tissue sections allows for MC identification, but illustrates the difficulty to decide, even with blinded analysis and microscope aided human eyes, whether a particular MC presents features of an intact or a degranulated cell (Fig. 2.1b). We developed a method for rapid and unequivocal identification of MC status, as follows: an intact MC was defined as a MC within and/or at the periphery of which no distinct granule could be singled out in high power field (HPF) (Fig. 2.1b, Intact MC). Next, we defined as degranulated, MC for which distinct individual granules could be observed within and at the periphery of the cell in HPF (Fig. 2.1b,

Degranulated MC). Figure 2.1c describes the analytic flow chart employed to quantitatively identify and distinguish between an intact and a degranulated MC. To this end, two MC were randomly selected (Fig. 2.1b, Intact MC and Degranulated MC), and then isolated as specific ROI to remove the background (Fig. 2.1c, upper panels). Next, isolated MC images were color-thresholded (Fig. 2.1c, middle panels, orange coloring). The thresholding process was followed by the actual determination of pixel intensity (Fig. 2.1c, lower panels, green coloring) to measure the IOD parameter which sums the values of all the pixels in the selection (cell). We noticed that the area occupied by and the morphology of each MC could vary greatly. To take this variable into account, the area (A) occupied by each cell was measured next and expressed in square μm . Because intact MC granules are fully equipped with a variety of mediators whereas degranulated MC have partly released the mediators harbored in their granules, we reasoned that intact and degranulated MC must be characterized by differential mass or IOD/A measurements, allowing for objective definition of each of these cellular states.

Relative Mass Calculations Based on IOD/A Ratios Distinctly and Quantitatively Characterize Intact and Degranulated MC

We further analyzed skin tissue sections collected from four different animals, and randomly selected 90 intact and 90 degranulated MC, as described above. Next, IOD and A parameters were calculated as described in Figure 2.1. Quantitation of IOD/A ratios were carried out. As shown in Figure 2.2, intact MC exhibit an average IOD/A ratio of 15.459 ± 2.18 , which was significantly

decreased to 11.782 ± 2.109 in degranulated MC. Importantly, these results quantitatively substantiate the notion that intact MC feature a higher mass compared to degranulated MC. This procedure actually measures relative MC mass and demonstrates this parameter to be significantly attenuated upon degranulation, in agreement with the biological relevance of the process.

Fractal Dimension Analysis Constitutes a Suitable Analytical Approach to Further Define Morphometric Evaluations of Intact and Degranulated MC

We next considered that the size and volume parameters previously calculated for each MC status could be complemented by quantification of comparative fractal dimension values. To this end, we sought to determine whether fractal dimension, a measure of chaos and space filling capacity, could be a useful discriminating factor between intact and degranulated MC, as there is an increasing use of applied fractal geometry in the medical field for pattern recognition, texture analysis and segmentation. This type of analysis has been performed to study cell nuclei and nuclear chromatin and has been demonstrated as a useful prognostic tool in cancer (Ferro *et al.*, 2011; Streba *et al.*, 2015). Therefore, we reasoned that the more ordered cytoplasm of an intact MC should display contrasted fractal characteristics compared to a more heterogeneous, less uniform cytoplasm of a degranulated MC. Figure 2.3a shows the procedure to first isolate cells to be analyzed from the tissue and second, proceed with binarization of the image (i.e., generate a black and white image from a gray-scale one). Binarized images are next used to calculate fractal dimension (D), therefore quantifying the structural density of MC cytoplasm. D values of the two-

dimensional images analyzed were between the Euclidean values of 1 (a straight line) and 2 (an irregular, complex structure). Of note, fractal dimensions constitute numerical descriptors which are exponents of power functions, i.e., nonlinear functions.

Fractal Analysis is a Reliable Method for Objective Quantification of in situ MC Degranulation

Analysis of normal skin samples collected from four different mice was conducted using 14 images per animal and randomly chosen intact MC (n = 29 - 60 cells per animal) and degranulated MC (n = 14 - 29 cells per animal). The fractal dimension of each cell was determined. The discriminatory performance of D parameters is shown in Figure 2.4, indicating mean D values of 1.378 ± 0.621 and 1.484 ± 0.0489 for intact and degranulated MC, respectively. Surprisingly, the D values characterizing each MC status were very consistent from animal to animal, suggesting the potential relevance of fractal signatures to objectively evaluate MC activation status. Moreover, mean D values of degranulated MC were significantly augmented compared to mean D values of intact MC. We established that computer-assisted morphometric MC analysis performed on microscopy images of tissue samples may overcome the time-consuming and subjective examination that necessitates expertise and extensive observer training.

2.4 DISCUSSION

Key components of innate immunity, MC are present in tissues apposed to the vasculature in homeostatic conditions (Reber *et al.*, 2012). They harbor

numerous intracytoplasmic granules, large dense core vesicles composed of a proteoglycan matrix where many mediators are pre-stored, including vasodilating histamine, cytokines and chemokines (Wernersson and Pejler, 2014). Beside their canonical activation through the cross-linking by antigen (Ag) of immunoglobulin E (IgE) bound to their high-affinity receptors, MC express a plethora of receptors, including Toll-like receptors, and receptors for complement, cytokines, chemokines, neurotransmitters and sphingosine-1-phosphate (S1P), the ligation of which could also trigger further MC activation (Oskeritzian, 2015; Oskeritzian *et al.*, 2008; Oskeritzian *et al.*, 2015; Oskeritzian *et al.*, 2010; Theoharides *et al.*, 2012). Moreover, microenvironmental physical/mechanical, pH, osmolarity and temperature alterations and UV radiation can also activate MC. Degranulation or the exocytosis of granules is the most prominent process indicative of MC activation. MC stimulation is traditionally monitored through the detection of granule-associated mediators measured in the circulation upon release. However, a systemic appreciation of MC activation, though relevant and sometimes life-threatening such as upon anaphylactic shock, does not inform on the status of local MC in tissues. As outlined above, the distinctive ability of MC to produce and pre-store large concentrations of many mediators positions these cells as first-line responders thus shaping the initial local response to trauma. We have previously reported that IgE/Ag- and S1P-mediated activation of MC delivers locally several cell-recruiting chemokines, thus endowing MC with early guidance of inflammatory events (Oskeritzian *et al.*, 2008; Oskeritzian *et al.*, 2015; Oskeritzian *et al.*, 2010). This is particularly important in skin disorder

pathogenesis as the positioning of large numbers of MC is substantiated in the dermis and the hypodermis, subcutaneous fatty tissue layer of rodent and human skin (Hart *et al.*, 1999; Hart *et al.*, 1998). Strong evidence suggests an association between MC-derived functions and the mediator repertoire they differentially release owing to the nature of stimulation (Galli *et al.*, 2008; Kalesnikoff and Galli, 2008).

Intragranular proteoglycan interaction with dye molecules of MB results in a metachromatic staining of granules specific to MC, the only tissue-resident cells that display these distinct blue/purple-colored granules in their cytoplasm. Of note, although circulating basophils share some phenotypic and functional features, they differ from MC in many aspects of natural history, granule contents and functions (Voehringer, 2013). Relevant to our study, basophils are not found in normal tissues (Arock *et al.*, 2002), but could be recruited into inflamed sites (Voehringer, 2013). Importantly, the main histochemical difference that allows distinguishing MC from basophils resides in differential metachromatic staining. Namely, MC granules comprise both heparin and chondroitin sulfate (CS) proteoglycans, whereas basophil granules present CS but do not contain heparin and are fewer in number compared to MC granules, thus resulting into weak staining with basic dyes (Voehringer, 2013). Other distinct features of MC are their round nuclear morphology and a cell size ranging from 5 to 10 μm , conversely to basophils that display lobulated, indented or segmented nuclei and an overall smaller size of 5 – 7 μm compared to MC (Voehringer, 2013).

While easy to identify in MB-stained tissue sections, defining MC activation status remains challenging even for a trained observer and is a source of considerable inter-observer variability. Since MC are tissue-resident and could initiate or suppress immune responses, they constitute an emerging target candidate for fine-tuning the local microenvironmental responsiveness, therefore pathogenesis and carcinogenesis (Oskeritzian, 2015). There is increasing need for a better understanding pertaining to the relationship of MC in inflammation and cancer as it seems diversified and therefore ill-understood (Giannou *et al.*, 2015; Oldford and Marshall, 2015; Oskeritzian, 2015; Ribatti, 2013). Indeed, many studies acknowledge the presence of increased MC numbers in numerous pathological conditions, yet reporting the more relevant and tractable local percentage or number of degranulated MC is not recognized as strong univariate data that often needs to be validated by quantitating MC-derived mediators in biological fluids.

In this study, we developed a computerized method for morphometric analysis of MC based on objective parameter measurements in routinely MB-stained normal skin tissue sections. Of relevance to MC granularity and morphology, these criteria include mass and relative density measurements based on IOD and area (A) ratios and fractality, which implies scale-independent self-similarity. We discovered that, independent of the subject, intact skin MC are consistently characterized by a mass (IOD over A ratio) significantly higher than degranulated MC. Of note, the IOD/A ratios of intact or degranulated MC were surprisingly consistent from cell to cell in each group and from animal to animal,

further highlighting the reproducibility and validity of our newly developed analytical method. Interestingly, the use of IOD and A parameters have previously been applied to dermal MC as a tool to quantify histamine content, but not to provide a measurement of MC activation as demonstrated herein (Hart *et al.*, 1999; Hart *et al.*, 1998).

The examination of fractal characteristics has been convincingly relevant to analyze chromatin structure and nuclear texture, providing important diagnostic and prognostic information for patients with acute leukemia and multiple myeloma (Ferro *et al.*, 2011). Fractal analysis has been widely applied in the past to quantify cytoskeleton morphology (Fuseler *et al.*, 2007; Fuseler and Valarmathi, 2012; Qian *et al.*, 2012), cellular shape (Jelinek *et al.*, 2011; Sedivy *et al.*, 2002; Wick *et al.*, 2003), vasculature structure (Anderson *et al.*, 2005; Di Ieva *et al.*, 2007; Fuseler *et al.*, 2010; Grizzi *et al.*, 2005), vascular sprouting (Doubal *et al.*, 2010; Moledina *et al.*, 2011) and tumor microvasculature (Di Ieva, 2012; Fuseler *et al.*, 2010). More recently, it was successfully applied to quantify collagen fibrotic lesions of the liver (Dioguardi *et al.*, 2008; Dioguardi *et al.*, 2006) and the heart (Zouein *et al.*, 2014). Microscopy evaluation of the MC degranulation process requires high magnification analysis and could be difficult given staining variations occurring in routine slide preparations. We took advantage of the fact that fractals are scale independent and their determination based on thresholded images less dependent on staining intensity. Methylene blue is one of the most common metachromatic staining methods and well-established histological approach to detect MC through the unique staining of

their granules (Wolters *et al.*, 2005). As such, it could be used to distinguish intact from degranulated MC. However, observer-based analysis often yields inconsistent data, varying with the individual grading of MC status and provides semi-quantitative estimates of MC degranulation rather than reliable quantitation partly because of the irregular shapes tissue MC display in situ. Thus, MC cytoplasm, 80% of which is occupied by granules, is highly polymorphic and irregular in shape. To overcome these conditions, we considered the granule/cytoplasm mass as a fractal object, a concept developed by Mandelbrot (1982) that provides a theoretical framework for many biological processes and objects. Thus, the fractal property relates to a measurement variable and a fractal object or process can reveal fractal characteristics of many different variables or features. We measured the fractal dimension (D) of intact and degranulated MC, as a measure of the comparative space filling capacity and complexity or structural density of MC in these two different biological stages, using digitized two-dimensional images. We discovered that D associated with intact MC is consistently and significantly lower than D of degranulated MC in a reproducible manner. These important results suggest that the measure of D can quantitatively distinguish intact from degranulated MC, regardless of cellular morphology which could greatly vary. Together with the relative density measurements provided by the IOD/A ratios, which determines the structure and/or distribution of the granular material within a MC (our region of interest), we demonstrate that the measure of D generates a quantitative description of mammalian MC status. We are currently exploring the feasibility of acquiring

these data in a semi-automated manner for potential diagnosis/prognosis applications to compare the analysis of healthy and diseased tissue sections in MC related disorders. We attributed the detection of some degranulated MC in normal skin to the procedure for sample preparation that requires shaving of the mouse back skin. This mandatory step constitutes a mild but perhaps significant mechanical stimulus leading to a low but detectable incidence of dermal MC activation.

Despite the differences between mouse and human skin, mouse models of human disease remain prevalent, and in many cases genes of interest are deregulated and/or mutated in both species (Gerber *et al.*, 2014). The vast abundance of disease models, knockout and transgenic strains ensure that mouse models will remain a highly relevant mainstay to the study of skin biology (Gerber *et al.*, 2014). Therefore, our morphometric method of MC analysis was first developed using mouse skin samples. Applying this morphometric method to human samples would assist clinicians and hospitals with providing a rapid determination of MC activation status, including in suspected cases of MC activation syndrome, mastocytosis, and anaphylactoid versus genuine anaphylactic reactions (Akin *et al.*, 2010; Hamilton *et al.*, 2011; Valent *et al.*, 2011). A previous report applied fractal dimension and lacunarity or measurement of roughness to characterize MC degranulation in rainbow trout (Manera *et al.*, 2014). Although informative, this study did not use mammalian MC. Moreover, MC degranulation was triggered in a receptor-independent manner using compound 48/80, a synthetic polyamine basic secretagogue

composed of mixed polymers of phenylethylamine cross-linked by formaldehyde of undetermined ratio thus precluding calculation of molar concentrations (Manera *et al.*, 2014). Our study establishes that mouse skin MC status can be quantified at homeostasis using fractal geometry, image analysis and readily available standard bright field microscopy on tissue sections routinely stained with MB, providing in situ quantification of MC activation. We are currently applying similar approaches to complementary MC immunohistochemistry staining techniques designed to phenotype MC subsets. Introduction of the fractal theory in biology and medicine has already led to a better understanding of many physiological processes, including allosteric enzyme kinetics, intracellular bioenergetic dynamics, metabolic rate, drug clearance modeling, angiogenesis, cardiovascular physiology and tumor growth (Aon *et al.*, 2008; Ferro *et al.*, 2011; McNally and Mazza, 2010; Thamrin *et al.*, 2010). Here we demonstrate in situ quantification of MC status in mammalian tissue samples, combining relative density and fractal dimension measurements of MC cytoplasmic density and order. Furthermore, we propose that this morphometric analysis is applicable to patient samples and provide quantitative data pertaining to local MC activation in tissue sections in clinical settings.

We demonstrate the ability to quantify in situ MC activation using computer-assisted image analysis and biological specimens, based on fractality and mass measurements. Reproducible, consistent and quantitative data were collected from multiple skin samples, establishing that significantly different morphometric parameters are featured in intact and degranulated MC. This

method may be further developed as a rapid diagnostic tool for the formulation of MC involvement in research and clinical settings.

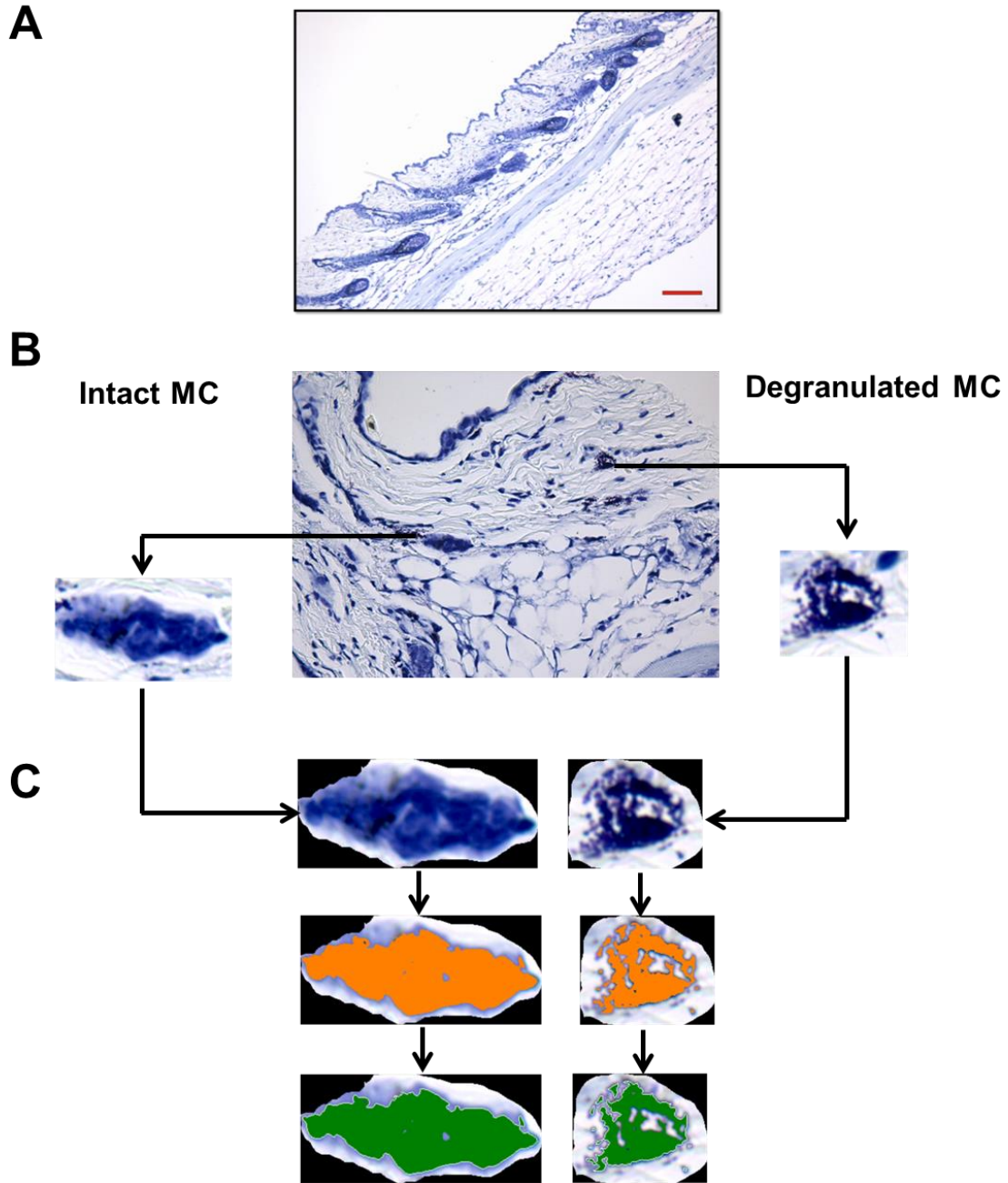


Figure 2.1 Methylene-blue stained mouse skin for MC detection and analysis. a: Methylene blue (MB)-stained mouse skin tissue section. Scale bar is 200 μm . b: MB-stained mouse skin tissue section with a selection of two randomly selected and isolated mast cells (MC) (Scale bar = 50 μm); an intact MC and a degranulated MC. c: Isolated MC images are color-thresholded (orange), followed by measurement overlay (green) to allow for relative density and mass measurement IOD/A determinations.

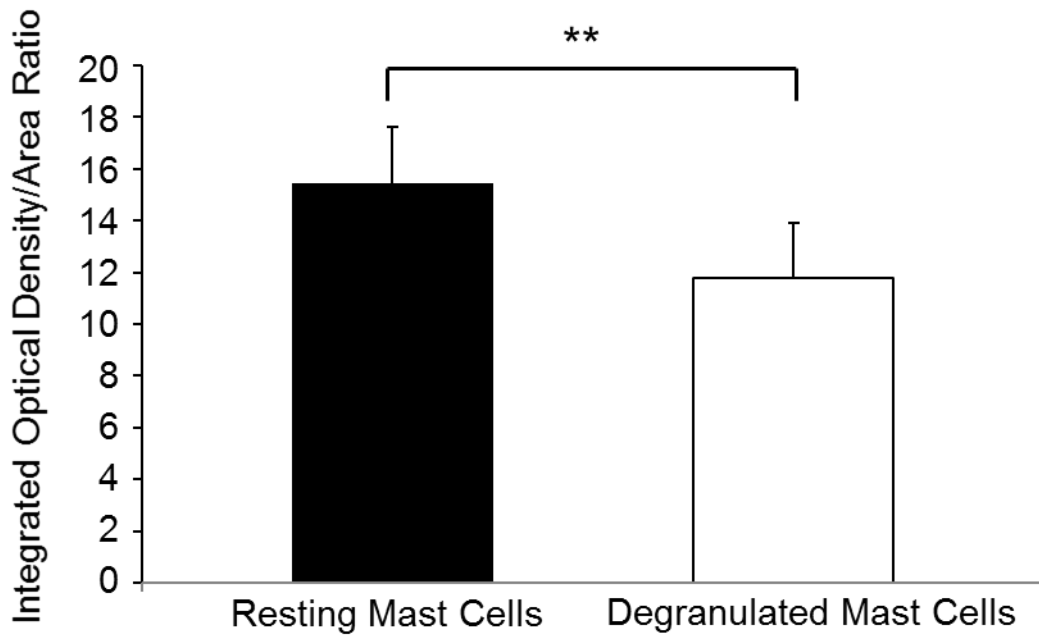


Figure 2.2 Comparison of mass between intact and degranulated MC. Comparative relative density and mass measurements as integrated optical density (IOD) over Area (A) ratios for intact and degranulated MC in skin samples of four different normal mice (** $p < 0.001$).

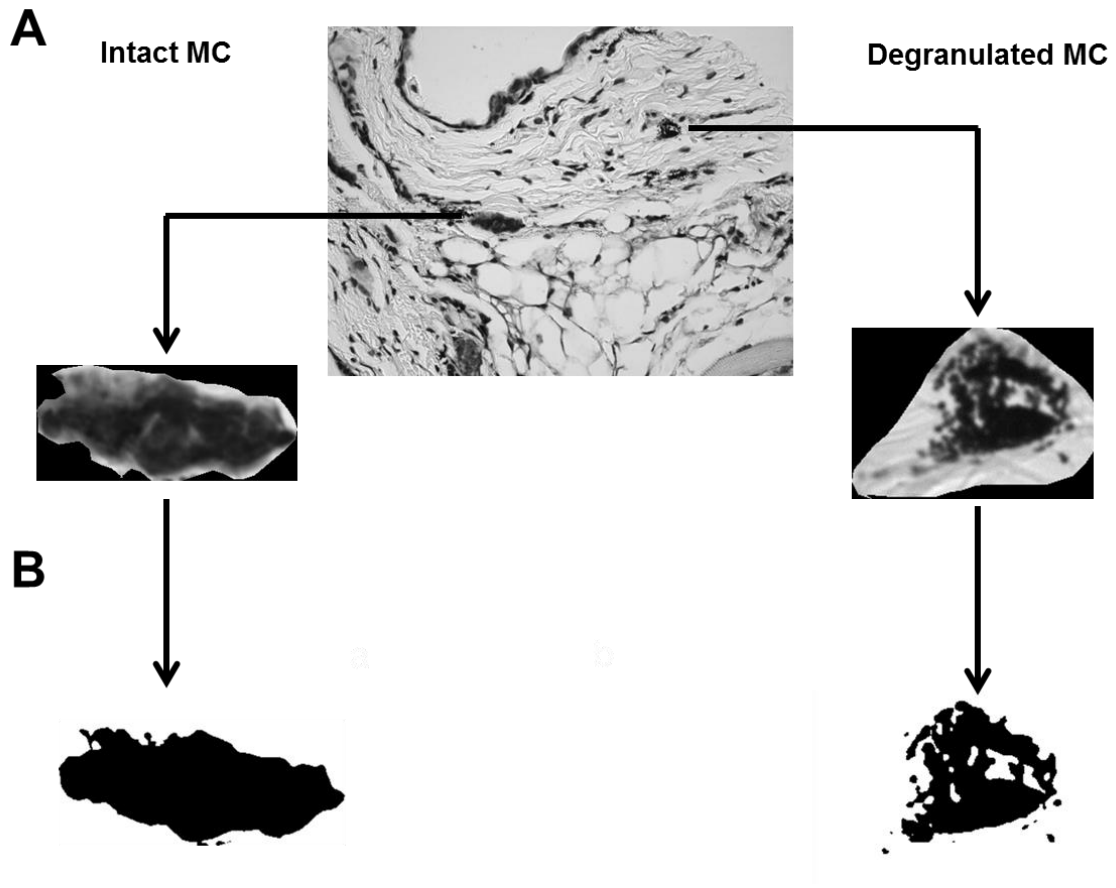


Figure 2.3 Fractal dimension to identify intact and degranulated MC. Fractal dimension (D) is a morphological descriptor of chaos and space filling capacity of MC cytoplasm. a: For measurement of D , the digitized image in Figure 2.1b was thresholded to generate a black and white 8-bit gray scale image from the color image. b: Threshold images were generated using the free HarFa software, which includes several filtration algorithms to eliminate thermal noise associated with the digital camera and illumination variations (gray scale) across the image. Scale bar is 50 μm .

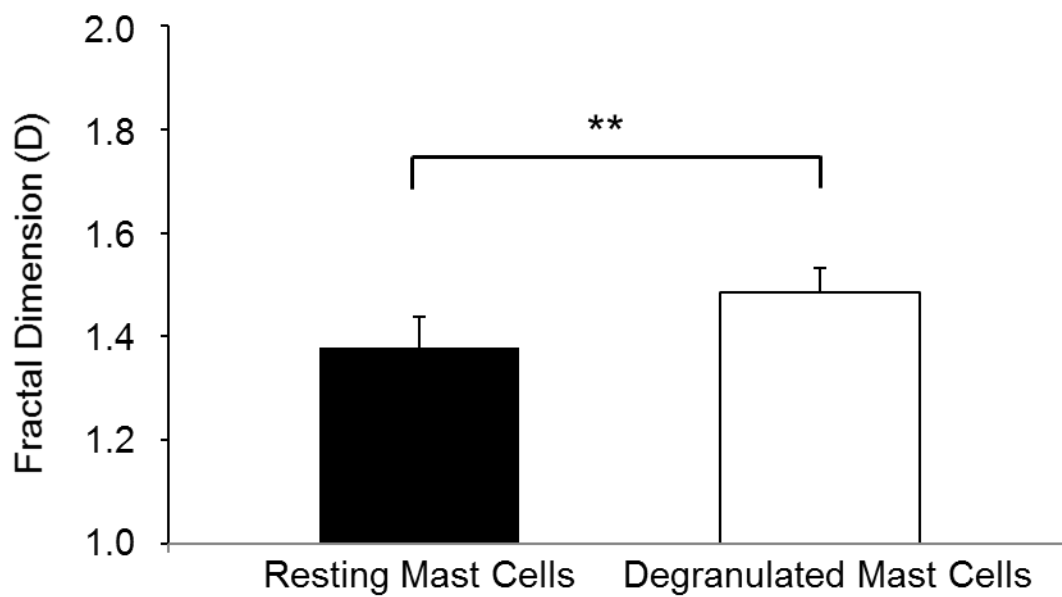


Figure 2.4 Fractal dimension of degranulated MC is higher than intact MC.

Comparative fractal dimension (D) analysis for intact and degranulated MC in skin samples of four different normal mice (14 images per animal were analyzed). Degranulation of MC increased the D values significantly and consistently, compared to D values of intact MC (** $p < 0.001$).

CHAPTER 3: MAST CELLS AND SPHINGOSINE-1-PHOSPHATE UNDERLIE EARLY PATHOGENIC REMODELING IN PRE-LESIONAL ECZEMA²

3.1 INTRODUCTION

Atopic dermatitis (AD) is a chronic relapsing inflammatory skin disease that affects 15-30% children and 2-10% adults world-wide (Auriemma *et al.*, 2013; Darlenski *et al.*, 2014; Eyerich and Novak, 2013; Graham and Nadeau, 2014; Liu *et al.*, 2011; Nakamura *et al.*, 2013; Patrizi *et al.*, 2011; Szegedi *et al.*, 2015). This complex multifactorial disorder often features hypersensitivity to environmental agents and immune dysfunction (Auriemma *et al.*, 2013; Elias, 2014; Eyerich and Novak, 2013; Kim *et al.*, 2014; Liu *et al.*, 2011; Mu *et al.*, 2014; Patrizi *et al.*, 2011). Yet, the sequential events leading to eczematous lesions and AD etiology are not completely understood.

Interestingly, 70-80% of AD patients have increased levels of total serum IgE antibodies (Ando *et al.*, 2013; Auriemma *et al.*, 2013; Darlenski *et al.*, 2014; Kendall and Nicolaou, 2013; Liu *et al.*, 2011; Patrizi *et al.*, 2011). Perivascular accumulation of lymphocytes and mast cells (MC) are observed in chronic lesions (Ando *et al.*, 2013). However, few studies have investigated the initial phase leading to lesions, including events prior to IgE production (Gittler *et al.*,

² Wedman, P., A. Aladhami, A. Chumanevich, J.W. Fuseler, and C.A. Oskeritzian. 2017. Mast Cells and Sphingosine-1-Phosphate Underlie Early Pathogenic Remodeling in Prelesional Eczema. Under Revision. *Allergy*, 03/29/2017.

2012; He *et al.*, 2007; Kim *et al.*, 2014; Spergel *et al.*, 1998; Wang *et al.*, 2007; Zhu *et al.*, 2015). Equipped with surface receptors for IgE (FcεRI) and other ligands and tissue-resident at homeostasis, MC play an important role as initiators of inflammation and first-line responders to inflammatory signals (Griffith *et al.*, 2014; Oskeritzian, 2015; Oskeritzian *et al.*, 2015; Oskeritzian *et al.*, 2010). Moreover, MC present the unique ability to produce and store many vasoactive and cytoactive mediators in their cytoplasmic granules prior to trauma and also neo-synthesize bioactive products upon activation (Galli and Tsai, 2012; Kalesnikoff and Galli, 2008; Mu *et al.*, 2014; Nakamura *et al.*, 2013; Oskeritzian, 2015; Oskeritzian *et al.*, 2015; Oskeritzian *et al.*, 2010; Zhu *et al.*, 2015). We recently established that MC and a potent sphingolipid metabolite, sphingosine-1-phosphate (S1P) are at the nexus of inflammatory infiltration in early lung allergic responses (Oskeritzian *et al.*, 2015). We previously reported that MC-derived S1P, produced by sphingosine kinase (SphK), can be exported out upon activation, amplify MC cytokine/chemokine production by autocrine binding to S1P receptors and regulate cell trafficking (Mitra *et al.*, 2006; Oskeritzian, 2015; Oskeritzian *et al.*, 2008; Oskeritzian *et al.*, 2015). S1P can also activate MC independently of the canonical IgE/FcεRI pathway (Chumanevich *et al.*, 2016; Kendall and Nicolaou, 2013; Oskeritzian *et al.*, 2015; Oskeritzian *et al.*, 2010).

In the current study, we investigated AD pathogenesis using a variation of a well-established human AD-like mouse model and collected skin samples for analysis after a *single* epicutaneous (EC) exposure to OVA Ag (Spergel *et al.*, 1998). We discovered a new pathogenic pathway leading to AD that links cell

infiltration of the hypodermis to local MC activation and S1P elevation. Next, we examined skin remodeling in mice deficient for SphK1 or MC and after LPS-free OVA exposure and established an essential role for MC, S1P and LPS at the onset of AD.

3.2 MATERIALS AND METHODS

Atopic dermatitis model

AD was induced in 8 to 12 weeks of age-matched female C57Bl/6J (WT), SphK1 KO (SphK1^{tm1Rlp}), and MC-deficient *Kit^{W-sh/W-sh}* (B6.Cg-*Kit^{W-sh}*/*sh*/HNhrJaeBsmGlljJ) mice as previously described (Spergel *et al.*, 1998), purchased from Charles River NCI (Frederick, MD) and The Jackson Laboratory (Bar Harbor, ME). After simple randomization using shuffled pieces of paper that indicated saline, OVA or LPS-free OVA, mice were assigned to either experimental group. Then, 100 µl of OVA solution (100 µg OVA (Sigma-Aldrich, St Louis, MO) or LPS-free OVA (100 µg EndoGrade® OVA (Hyglos GmbH, Munich, Germany) in 0.9% saline) or 0.9% saline only (saline control) were pipetted on a 1 cm x 1 cm square gauze pad (patch) placed on the shaved and tape-stripped upper-back skin area. Next, this area was occluded with a Tegaderm Transparent Dressing (3M HealthCare, St Paul, MN) using bandages. Patch was removed after seven days and skin samples collected from euthanized mice. For patch 3-IgE determinations, the full AD protocol was conducted exactly as previously described (Spergel *et al.*, 1998). Briefly, each patch was secured for one week followed by two weeks of rest before next exposure week. Patch 1 and patch 3 sera were prepared from blood collected by cardiac puncture

immediately after euthanasia and stored at -80°C until use. Animal experiments and all experimental protocols were approved by the University of South Carolina Institutional Animal Care and Use Committee. Animal experiments and all methods were performed in accordance with the relevant guidelines and regulations.

Histology and Microscopy

Skin tissues collected from euthanized mice were fixed in 4% fresh paraformaldehyde. Fixed tissues were embedded in paraffin, sectioned (4 µm thickness) and mounted on microscope slides. One group of slides was stained with Hematoxylin and Eosin (H&E) for skin morphometric analysis. To visualize MC, a second group of slides was placed in 0.1% methylene blue (MB) for five seconds, rinsed with water, dehydrated in 100% ethanol and mounted under coverslips with cyto seal 60 (Wolters *et al.*, 2005). Sections were imaged with a Nikon E-600 microscope (Nikon Inc., Melville, NY) equipped with a Micropublisher digital camera model 5.0 and images collected as TIFF files with the Micropublisher software at low (10x, numerical aperture 0.30) and high (40x, numerical aperture 0.75) magnification for analysis. Images were analyzed as 24-bit color images or 8-bit monochrome images, as required, using the QImaging software version 2.0.13 (QImaging Corp., Surrey, BC, Canada). Morphometric and fractal parameters of nuclei (infiltration, 25-30 ROIs/image, a minimum of twelve 40x-images/skin section; 4 skin sections/2 mice/treatment group) and MC (percent degranulation, fifty 40x- total images/310-485 total MC; 4 skin sections/2 mice/treatment group) were measured using the MetaMorph®

6.1 Microscopy Automation and Image Analysis software (Molecular Devices, Sunnyvale, CA) and the free HarFa imaging software (www.fch.vutbr.cz/lectures/imagesci/), as previously described (Wedman *et al.*, 2015). For these and all quantifications described below, the investigators who were making measurements were blind to slide group allocations (single blind studies).

Morphometric measurement of skin remodeling

The thickness of each skin layer (epidermis, dermis and hypodermis) was measured in saline- and OVA-treated specimens using an ocular micrometer (Klarmann Rulings, Inc., Litchfield, NH). From each slide, uniform regions of the epidermis, dermis and hypodermis were selected and the average thickness was measured (n= 3-5 measurements/3-5 animals/treatment group/skin layer (i.e, epidermis, dermis, hypodermis)).

Computer-assisted quantification of hypodermal cellular infiltration

A recent computer-assisted imaging method developed by our laboratory (Wedman *et al.*, 2015) was adapted to quantify cellular infiltration. A minimum of twelve high-magnification H&E images per animal was used to determine cellular infiltration in the hypodermis. To this end, nuclei were isolated by means of color thresholding using the set color threshold subroutine of the MetaMorph software (orange color overlay) and quantified by applying a fixed circular region of interest (ROI, diameter=75 μ m) of constant area that was moved sequentially to adjacent regions to survey the entire hypodermis of each section (n=25-30 ROIs/section, 2 sections/slide, 2 slides/animal, 2 animals/treatment). The

morphometric parameters of the nuclei (area, perimeter and integrated optical density determined using the Integrated Morphometry Analysis subroutine of MetaMorph) were used to refine nuclei measurements and eliminate any background noise.

Validation of cellular infiltration quantification by independent fractal dimension analysis

As described above, fixed circular ROIs were isolated and collected as TIFF file images throughout the hypodermis of H&E images in each section. The hue, saturation and intensity values were adjusted to isolate the nuclei in orange as a thresholded region. The images of the individual isolated and selected nuclei (green) were converted to a 8-bit gray scale image for further fractal dimension measurements using the free HarFa imaging software (www.fch.vutbr.cz/lectures/imagesci/), which converts the gray-scaled image into a binary one, as we previously described (Wedman *et al.*, 2015). Briefly, an area featuring cellular infiltration is an irregular and complex object composed of nuclei, which are fundamentally similar (self-similar). Because of its complexity, infiltration cannot be described by regular Euclidean geometry that uses integer descriptors (Brown *et al.*, 2002; Wedman *et al.*, 2015). Instead, it can be described quantitatively by fractal geometry using non-integer numbers, with values falling between two-integer topological dimensions (Mandelbrot, 1983; Smith *et al.*, 1996). These non-integer numbers define the fractal dimension (D) of an “object”, here, the distribution of nuclei within a hypodermal ROI. As discussed previously (Wedman *et al.*, 2015), the concept of fractals provides a

useful method to quantify the inherent irregularity or complexity of phenomena. In the case of the two-dimensional images analyzed in the current study, the values of D characterizing cellular infiltration are therefore fractional and lie between the Euclidean integers of 1 and 2.

***In situ* determination of mast cell degranulation**

The MC granular cytoplasm is an irregular and complex object composed of proteoglycan-containing granules at different levels of resolution that are functionally and physiologically similar (self-similar). Thus, it can be considered as a fractal object and analyzed accordingly. Using this approach, we previously demonstrated (Wedman *et al.*, 2015) that MC cytoplasm cannot be characterized by regular Euclidean geometry because of its complexity of form but can be described quantitatively as degranulated or intact by fractal geometry and dimension (Mandelbrot, 1983; Smith *et al.*, 1996), with values ranging between 1 and 2. We previously established that the fractal dimension (D) value uniquely characterizing intact MCs is 1.378 ± 0.062 and the D value describing degranulated MCs is 1.484 ± 0.048 (Wedman *et al.*, 2015). These values were used as a baseline for non-subjective quantification of intact and degranulated MC numbers in the skin samples of saline- and OVA-treated animals (n=2 animals/treatment).

Quantitative Real-Time qPCR

Skin samples were collected, snap-frozen and stored at -80°C until RNA extraction. Total RNA from saline-treated skin samples (n=4-8 animals) and OVA-treated skin samples (n=6-10 animals) was isolated and purified with the

miRNeasy kit (Qiagen, Valencia, CA), following the manufacturer's procedure. The iScript cDNA synthesis kit (Bio-Rad, Hercules, CA) was used according to the manufacturer's specifications to reverse transcribe cDNA. QPCR was performed on a CFX Connect (Bio-Rad) with SensiFAST™ SYBR No-ROX Kit (Bioline, Taunton, MA). Primer sets used in real-time qPCR amplification are displayed in Table 3.1. The real-time qPCR conditions were as follows: initial step at 95°C for 5 min and cycles ($n=40$) consisted of 10 s at 95°C, followed by 1 min annealing at 55°C and extension at 72°C. All reactions were performed in duplicate. Data were analyzed with CFX Manager™ Software and are normalized expression to saline-treated samples and directly proportional to the amount mRNA of the target gene relative to the amount of mRNA of the reference gene, GAPDH mRNA levels. Primers were purchased from Thermo Fisher Scientific, Inc. (Waltham, MA).

Multiplex Assays

The following chemokines were measured in mouse serum or in mouse skin protein extracts ($n=10-12$ mice/treatment/sample type) with a Bio-Plex Array Reader (LUMINEX 100; Bio-Rad Laboratories, Hercules, CA) with murine Milliplex panels (EMD Millipore, Billerica, MA): CCL2/monocyte chemoattractant protein 1, CCL3/macrophage inflammatory protein 1 α and CCL5/RANTES. Mouse skin protein extracts were obtained from skin specimens harvested after one week of exposure to OVA or saline, weighed, and frozen in liquid nitrogen. Each sample was homogenized with a mortar and pestle and digested for 2 h at 4°C in Reporter lysis buffer (Promega, Madison, WI) supplemented with

complete mini-protease inhibitor tablets (Roche Diagnostics, Indianapolis, IN). Supernatants were stored at -80°C and quantified for chemokine content, as indicated above.

Total Serum IgE ELISA

Mouse total serum IgE was measured by ELISA, according to manufacturer's instruction (R&D Systems, Minneapolis, MN). N=6 animals/experimental groups for one exposure and n=9 animals/experimental groups for three exposures.

Lipidomics

Lipids were extracted from snap-frozen skin tissues and S1P was measured by using liquid chromatography-electrospray ionization-tandem mass spectrometry (4000 QTRAP; AB Sciex, Foster City, CA), as previously described (Hait *et al.*, 2009). Quantification of S1P was normalized to weight of skin sample. N=3-4 samples per experimental group.

Statistics

Data are expressed as means \pm SEM (unless otherwise stated) and were analyzed by using the unpaired 2-tailed Student *t* test, with Welch's correction for samples of unequal variance (Prism 6; GraphPad Software, La Jolla, CA). Significance for all statistical tests is shown in figures. Experiments were repeated at least 3 times in triplicates with consistent results. *In vivo* experiments were repeated 3 times, and each experimental group consisted of 5 to 6 mice.

3.3 RESULTS AND DISCUSSION

OVA triggers rapid skin remodeling and cellular infiltration

We previously reported that systemic Ag stimulation leads to early lung remodeling in sensitized mice (Oskeritzian *et al.*, 2015). These studies prompted us to revisit the development of another inflammatory disease of atopic nature, AD, for which the initiating mechanisms remain ill-understood (Leung and Guttman-Yassky, 2014; Malajian and Guttman-Yassky, 2015). We found that epidermal and dermal thickening that is observed in the 49-day AD mouse model (Spergel *et al.*, 1998; Wang *et al.*, 2007), was already significant albeit modest after one OVA application, compared to one saline treatment (Figures 3.1a-c).

We observed a marked cellular infiltration in the hypodermis, compared to saline controls (Figures 3.1a-c). We adapted our recently established image quantification method (Wedman *et al.*, 2015), to measure cellular infiltration (Figure 3.1d) in a defined region of interest (ROI) (circle in Figure 3.1e) sequentially moved across the entire hypodermis. Figure 3.1g shows whole hypodermis survey of infiltration in a representative saline-treated skin sample compared to an OVA-treated one, in which blood vessel (Bv)-containing ROI are depicted in red. Saline treatment triggered some infiltration, increased around Bv. The OVA application drastically increased hypodermal cell numbers, also around Bv (Figure 3.1g). The statistical validation of these results was demonstrated by analyzing multiple samples (Figures 3.1f, h).

Having previously established the relevance of fractal dimension to define morphometric descriptors (Wedman *et al.*, 2015), we reasoned fractals or

measures of space filling capacity could also represent an accurate method to quantify cellular infiltration. Figures 3.1i-j describe the procedure established to isolate nuclei/cells. Next, binary images (Figure 3.1k) were generated to calculate fractal dimensions (D) of ROI by quantifying the structural density of the “objects” (nuclei) or cellular infiltration. Figure 3.1l independently confirmed the increased cellular infiltration substantiated in Figures 3.1f-h after OVA treatment as measured by D values of multiple skin samples. The discriminatory performance of D was further validated in Figure 3.1m, also showing increased infiltration around the BV.

Importantly, the present study analyzed prelesional skin specimens, therefore identifying novel histo-pathological mechanisms of pre-symptomatic AD. We described a new morphometric method to quantify rather than score cellular infiltration that uncovered a prevalent although previously unnoticed hypodermal infiltration after a single OVA treatment, suggesting an important function for the hypodermis at the onset of AD. We propose this initial infiltration, also reported in acutely inflamed airways (Oskeritzian *et al.*, 2015), could constitute a novel target to prevent disease manifestation.

OVA stimulates local and systemic chemokines

We next investigated chemokine expression in treated skin samples collected from both treatment groups. Skin mRNA expression for CCL2, CCL3 and CCL5, three members of the chemokine network we previously identified as major contributors to airway inflammation (Oskeritzian *et al.*, 2015) were all significantly increased after OVA exposure (Figure 3.2a). Interestingly, skin CCL2

(Figure 3.2b) and CCL3 (Figure 3.2c) (but not CCL5 (data not shown)) protein levels were also increased upon OVA application, compared to saline controls. As expected, circulating chemokine levels did not exactly corroborate local levels. Serum CCL2 levels remained unchanged after EC OVA (Figure 3.2d), whereas serum CCL3 and CCL5 were enhanced (Figures 3.2e-f). Recently, a meta-analysis also described increased chemokine mRNA expression in patients with AD (Ewald *et al.*, 2015). CCL2 and CCL3 genes were also identified in patients with moderate-to-severe AD by next-generation RNA-sequencing (Suárez-Fariñas *et al.*, 2015). Combined with our finding, these studies also suggest an important role of infiltration in the establishment of AD.

OVA exposure elicits significant IgE-independent skin MC degranulation and S1P elevation

Further interrogating skin gene expression, we found that mRNA coding for the α chain of Fc ϵ RI (Fc ϵ RI α) was significantly up-regulated in OVA-treated mouse skin samples (Figure 3.3a). Importantly, the α chain is responsible for IgE binding to its receptor and initiates MC activation during allergic responses (Metzger *et al.*, 1986). Although expressed by Langerhans (Haas *et al.*, 1993) and other cells (Ying *et al.*, 1998), we reasoned that skin-resident MC could also contribute to the enhanced Fc ϵ RI α mRNA detection in these samples.

Microscopy examination of methylene blue (MB)-stained skin sections revealed that metachromatic MC were distributed throughout the skin layers, irrelevant of treatment (Figures 3.3b-c). Using our previously reported MC morphometrics, skin sections were analyzed for MC activation (Wedman *et al.*, 2015). Figures

3.3b-c show representative examples of resting (green-framed insert, circle and arrow) MC and degranulated (red-framed insert, circle and arrow) MC. MC activation was morphometrically measured in whole hypodermis of samples to calculate the percentage of MC degranulation. Figure 3.3d demonstrated that skin MC were significantly more degranulated after OVA than after saline application. While it has been shown that AD features increased perivascular MC (Damsgaard *et al.*, 1997; Kawakami *et al.*, 2009), MC numbers were unaltered in either treatment in the current study (data not shown). Of note, a recent report delineated a protective role for MC during the development of spontaneous AD-like disease in a transgenic mouse model but did not measure local skin MC activation (Sehra *et al.*, 2016). Our finding of increased *in situ* MC degranulation at this early subclinical stage of AD was novel and intriguing. As expected, seven days of OVA exposure did not suffice to enhance circulating IgE levels (Figure 3.3e), compared to its abundant detection after 3 OVA treatments (Figure 3.3e) as originally described (Spergel *et al.*, 1998).

MC can be activated by S1P, an influential sphingolipid metabolite resulting from the phosphorylation of its precursor sphingosine by SphK (Chumanevich *et al.*, 2016; Oskeritzian *et al.*, 2008; Oskeritzian *et al.*, 2015; Oskeritzian *et al.*, 2010; Rivera *et al.*, 2008). Quantitative lipid analysis of skin samples, using lipidomics mass spectrometry (Hait *et al.*, 2009), revealed that S1P was significantly increased in mouse skin after one exposure to OVA, compared to saline controls (Figure 3.3f). In agreement, SphK1 skin mRNA expression was also augmented after a single OVA application (Figure 3.3g). We

have shown that S1P-mediated MC activation led to the release of cell recruiting chemokines (Oskeritzian *et al.*, 2008; Oskeritzian *et al.*, 2015; Oskeritzian *et al.*, 2010; Price *et al.*, 2013) and MC may serve as a local source of S1P (Mitra *et al.*, 2006; Oskeritzian *et al.*, 2008), including when activated by mechanical stress such as tape-stripping, and induce leukocyte rolling in inflamed mouse venules and human endothelial cells (Nussbaum *et al.*, 2015). MC are established chemokine producers in the chronic phase of AD (Griffith *et al.*, 2014; Zhu *et al.*, 2015) and mediate leukocyte recruitment (Gonzalo *et al.*, 2007; McAlpine *et al.*, 2012; Ohsawa and Hirasawa, 2012; Oskeritzian, 2015; Wu *et al.*, 2013), although dispensable in a genetic mouse model (Sulcova *et al.*, 2015). In the present study, it is noteworthy that local chemokine detection and MC activation occurred prior to IgE production. While augmented in most AD patients (Ando *et al.*, 2013; Liu *et al.*, 2011; Patrizi *et al.*, 2011), our data suggest that IgE may contribute to AD progression rather than initiation. Importantly, our results strongly support MC and S1P as early contributors to the development of pre-AD-related skin alterations.

SphK1 or MC deficiency protects against OVA-driven skin remodeling and infiltration

To determine the relevance of S1P in the observed pre-symptomatic skin changes, we repeated the adapted AD protocol in SphK1 KO mice (Allende *et al.*, 2004), of genetic background similar to the WT mice we used so far (Figures 3.1-3.3). SphK1 deficiency mitigated OVA-initiated skin remodeling (Figures 3.4a vs. 3.1c). The SphK1-null hypodermis surveying revealed a slight but significant

increase in nuclei (i.e., cell) numbers after OVA, compared to saline-treated skins (Figure 3.4b), that was less pronounced than in SphK1-sufficient mice (Figures 3.4b vs. 3.1f) and absent around the Bv (Figures 3.4c vs. 3.1h). Consistent with these results, the pattern of OVA-restricted chemokine gene induction in corresponding WT skin samples (Figure 3.2a) was not observed in SphK1 KO mouse skins (Figure 3.4d). Importantly, genetic ablation of SphK1 prevented OVA-initiated local up-regulation of FcεRIα mRNA expression (Figures 3.4d vs. 3.3a) and skin MC degranulation (Figures 3.4e vs. 3.3d). These results strongly suggest that S1P is a driving mediator of IgE-independent skin remodeling and infiltration through local skin MC degranulation in AD pathogenesis.

To investigate MC's contribution to skin remodeling, we conducted OVA or saline EC exposure of MC-deficient *Kit^{W-sh/W-sh}* (Grimbaldeston *et al.*, 2005) mice. Although some epidermal thickening was observed, *Kit^{W-sh/W-sh}* dermal layers were unaltered (Figure 3.4f), compared to MC-sufficient mice of similar genetic background (Figure 3.1c). Furthermore, MC deficiency prevented cellular infiltration of the hypodermis (Figures 3.4g-h), suggesting a critical role of MC in skin inflammatory responses. This was further confirmed by the absence of OVA-induced up-regulation of chemokine, FcεRIα and SphK1 mRNA levels (Figure 3.4i). It is noteworthy that skin-associated S1P levels were significantly lower and not increased upon OVA application in *Kit^{W-sh/W-sh}* mice (Figure 3.4j), compared to the corresponding WT mice (Figure 3.3f), supporting skin MC as a relevant local source of S1P.

Thus, it is tempting to speculate that MC may act as causative agents of inflammatory response of the skin, similar to our recent report pertaining to lung allergic responses (Oskeritzian *et al.*, 2015). Moreover, local elevations of S1P in inflamed skins may contribute to early MC activation at the inception of AD, perhaps prompting MC themselves to further produce S1P. Keratinocytes (Oizumi *et al.*, 2014) and Langerhans cells (Japtok *et al.*, 2012) could also contribute to local S1P release. Nonetheless, our results suggest an important function for MC activation at the onset of AD, linking S1P and chemokines to early skin remodeling, thus setting the stage for the progression to AD. Decreased S1P in human AD has been evoked but not measured (Japtok *et al.*, 2014). In agreement with previous studies (Dillahunt *et al.*, 2013; Oskeritzian *et al.*, 2008), our data evoke a strong interdependency not only between 1) the presence of SphK1 and skin MC activation but also 2) skin S1P level alterations and the presence of MC. Thus, our study evokes local S1P and MC as potential triggering components of skin remodeling in early AD.

Cellular infiltration, MC activation and local S1P elevation are abrogated in mice treated with lipopolysaccharide (LPS)-free OVA

Yoon *et al.* recently established that endogenous TLR4 ligands are essential to epidermal thickening observed in EC-sensitized skin after tape-stripping (Yoon *et al.*, 2016). Furthermore, commercial-grade OVA, used in this and most studies, contains high LPS levels, a TLR4 ligand (Watanabe *et al.*, 2003). To investigate the LPS contribution to the early skin inflammation upon EC OVA exposure, experiments were repeated using LPS-free OVA. EC LPS-

free OVA-triggered hypodermal infiltration was similar to the one observed in saline-treated animals (Figures 3.5a-b). Moreover, local MC were not activated (Figure 3.5c) and S1P and SphK1 mRNA levels remained unaltered following LPS-Free OVA exposure (Figures 3.5d-e). These results suggest that the LPS co-administered with OVA Ag participated in the early skin inflammatory responses. This makes sense as most environmental Ag penetrate the body likely combined with LPS, thus mimicking natural Ag exposure. Several studies have investigated the effect of LPS “contamination” of OVA in allergic responses. While some studies reported that LPS/TLR4 signaling prime pro-inflammatory responses to OVA (Dong *et al.*, 2009; Eisenbarth *et al.*, 2002), others described protective effects of LPS in airway allergic responses (Watanabe *et al.*, 2003). Our study is the first to compare the effects of OVA to LPS-free OVA in a mouse model of skin inflammation. Furthermore, our results suggest that LPS exposure may prime initial inflammatory responses, as recently suggested (Yoon *et al.*, 2016), and promote local MC activation and endogenous S1P production. Of note, topical exogenous S1P administration attenuated contact dermatitis in a hapten-induced murine AD-like model (Reines *et al.*, 2009) and topical application of Fingolimod (FTY720), a structural analog of sphingosine also phosphorylated by SphK that acts as an S1P receptor agonist, could attenuate skin inflammation (Sun *et al.*, 2016). Thus, we propose that endogenously produced S1P can exert varied pro-inflammatory functions, compared to exogenously applied, anti-inflammatory S1P.

The small but statistically significant structural and molecular alterations between saline and OVA treatment were expected, as these pathogenic events occurred prior to any overt sign of disease. Therefore, these primary and newly uncovered responses could not be compared to the large differences often reported when comparing acute to chronic AD skin lesions and further emphasize the relevance of our findings to pre-symptomatic AD pathogenesis. These initial signs of skin remodeling set the stage to forthcoming clinical features of AD, including eczematous lesions observed later in this preclinical model (after 3 OVA exposures) and in human AD. These findings highlight perhaps new prophylactic approaches for this disease whose treatment management still remains a clinical challenge.

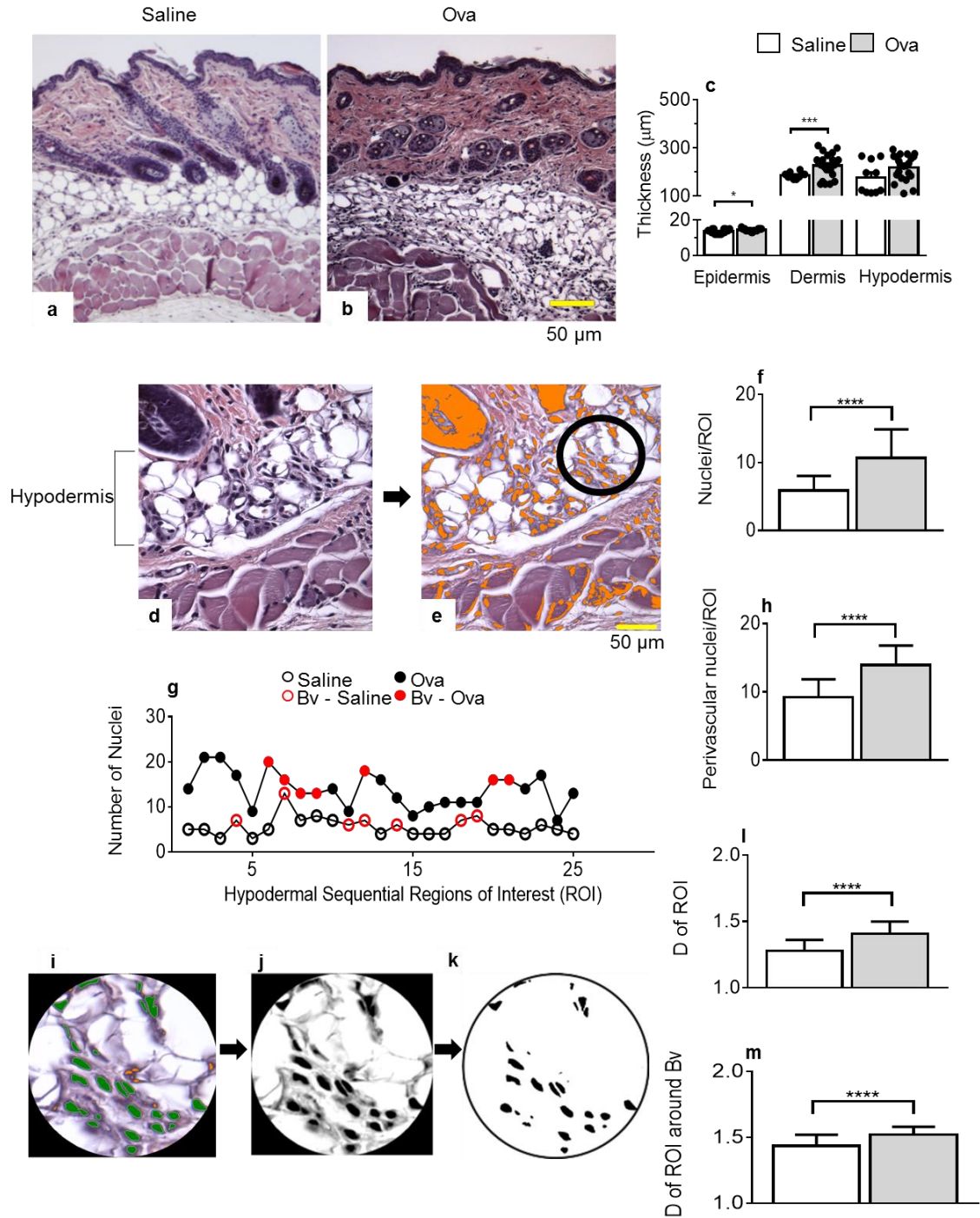


Figure 3.1 Skin remodeling starts after a single epicutaneous exposure to OVA. (a-b) H&E staining of skin tissues exposed to saline (a) or OVA (b). Panels a-b are representative images. Original magnification, $\times 100$. (c) Thickness of the epidermis, dermis and hypodermis layers, as measured in H&E-stained tissues.

For epidermis thickness, $n = 18$ (saline, empty bars), 19 (OVA, grey bars), for dermis, $n = 10$ and 25 and for hypodermis, $n = 10$ and 25 individual measurements collected from 3-5 animals/treatment group/skin layer. (d) Example of H&E stained skin section focusing on the hypodermis (red arrow, original magnification, $\times 400$) in which (e) nuclei are color-thresholded (orange) and a fixed circular region of interest (ROI, black circle) defined. (f) Nuclei numbers per ROI of multiple saline treated mice, compared to OVA treated mice. (g) Representative nuclei enumeration performed in each ROI ($n = 25$ ROI) throughout the hypodermis of one saline-treated mouse (empty circles) and of another exposed to OVA (filled circles). Red symbols refer to blood vessel (Bv)-containing ROI. (h) Infiltration analysis focusing around Bv. (i) Nuclei within ROI were color-thresholded as in (e) and enumerated (green). (j) Colored nuclei images were gray-scaled and (k) a binary image was software-created to calculate the fractal dimension (D) of each ROI. Panels i-k are representative images of an isolated ROI. (l) D of ROI in skin specimens treated with saline or OVA. (m) Similar determinations of D were performed focusing around Bv. For all ROI determinations, 25-30 ROIs/image, a minimum of twelve 40x-images/skisection; 4 skin sections/2 mice/treatment group were analyzed (f, h, l, m). Statistical differences were determined with unpaired 2-tailed Student's t test with Welch's correction. Bar = 50 μm . * $p = 0.0142$, *** $p = 0.0004$, **** $P \leq 0.0001$.

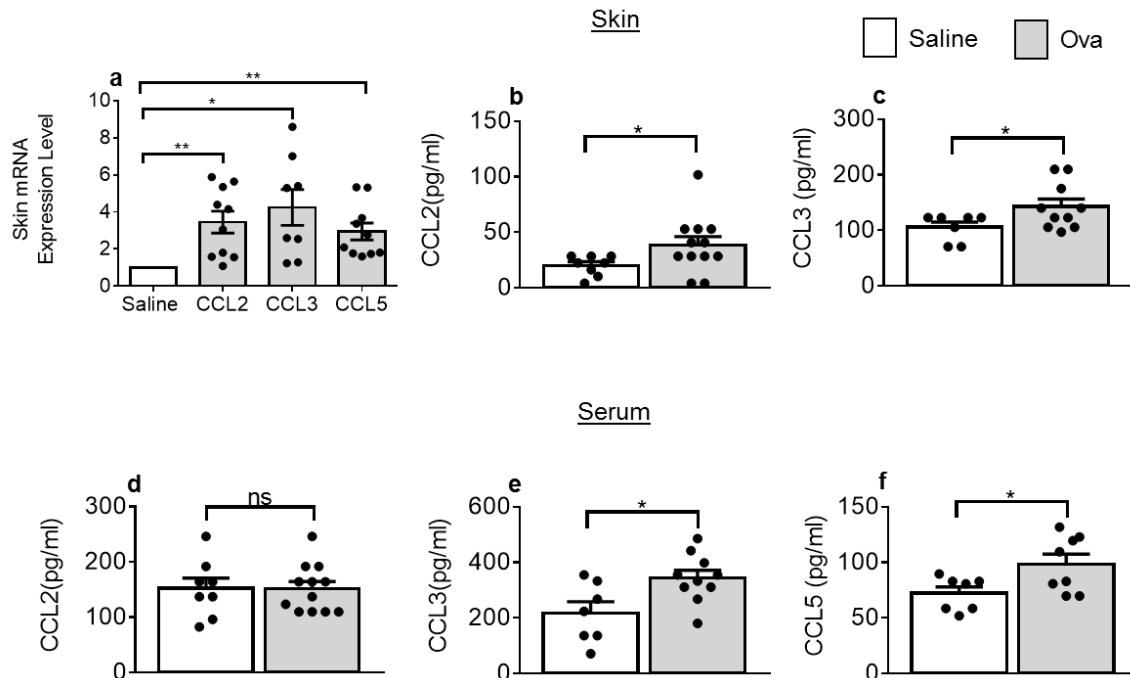


Figure 3.2 Chemokines are up-regulated after a single exposure to OVA. (a) CCL2, CCL3 and CCL5 mRNA levels in OVA-treated skin samples (grey bars), normalized to those in saline treated skins (empty bars) and quantified against GAPDH mRNA levels, $n = 6$ saline animals, 4-5 OVA animals with duplicate determinations. (b) CCL2 (* $p = 0.0383$) and (c) CCL3 protein levels in skin extracts (* $p = 0.0356$) (b, c) or serum (d, e: * $p = 0.0255$) and (f) serum CCL5 protein levels (* $p = 0.0307$) all collected from mice treated with saline or OVA. Protein determinations, $n = 4$ (saline) and 6 (OVA) with duplicate determinations. Statistical differences were determined with unpaired 2-tailed Student's t test with Welch's correction (a-f). * $p \leq 0.05$, ** $p \leq 0.01$, except otherwise indicated; ns, not significant.

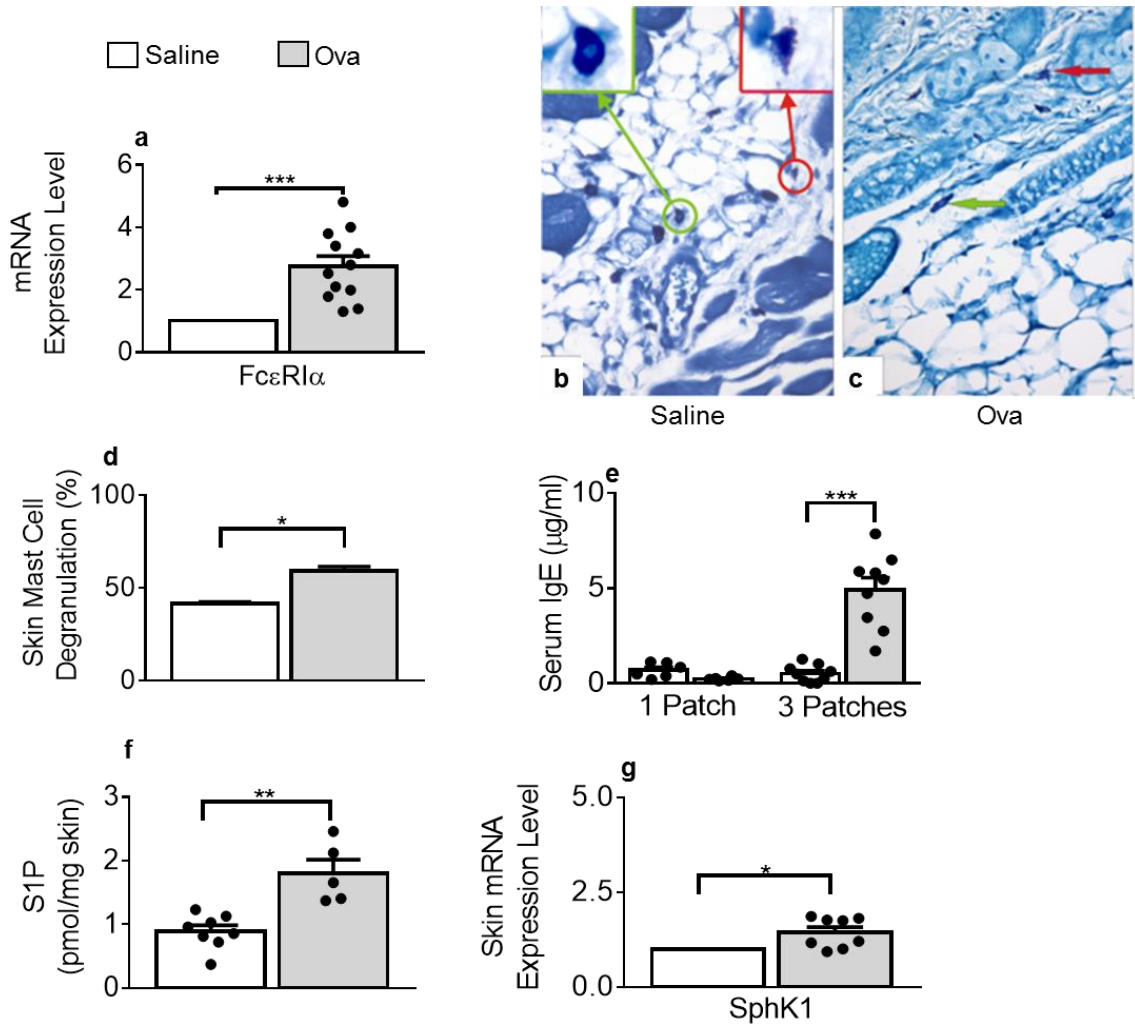


Figure 3.3 Mast cells degranulation and S1P levels increase in OVA-treated skin tissues. (a) Alpha chain for the high-affinity receptor for IgE mRNA levels in OVA-treated samples (grey bars), normalized to saline (empty bars) treated samples and GAPDH, $n = 4$ saline animals, 6 OVA animals with duplicate determinations (** $p = 0.0002$). (b, c) Methylene blue-stained skin sections after saline (b) or OVA (c) treatment. Arrows and inserts show examples of intact (green) or degranulated (red) mast cells (MC). Panels b-c are representative images. Bar = 50 μm . (d) Percent MC degranulation determinations in saline- and OVA-treated samples (* $p = 0.0352$, fifty 40x- total images/310-485 total MC; 4 skin sections/2 mice/treatment group). (e) Determinations of total serum IgE after one saline or OVA treatment (1 Patch), $n = 6$ animals/treatment group, averages of duplicate determinations and after three saline or OVA treatments (3 Patches), $n = 9$ animals/treatment group, averages of duplicate determinations (** $p = 0.0001$). (f) Sphingosine-1-phosphate (S1P) content of mouse skins after saline or OVA

treatment, n = 8 saline and 5 OVA samples. ** p = 0.0088 (g) Sphingosine kinase (SphK)1 mRNA levels in OVA-treated samples (n = 4), normalized to saline (n = 3) with duplicate measurements (* p = 0.0152). Statistical differences were determined with unpaired 2-tailed Student's t test with Welch's correction.

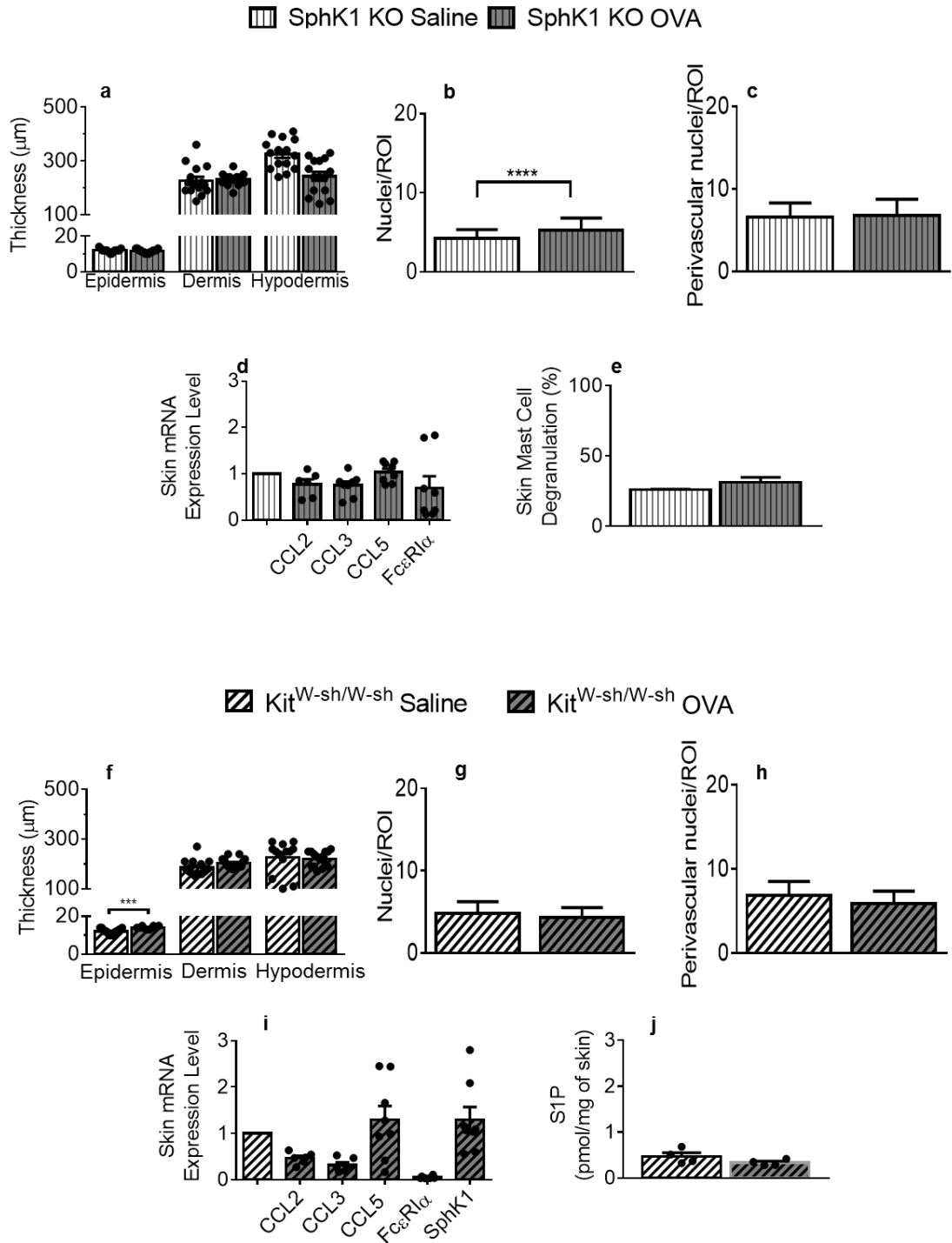


Figure 3.4 Skin remodeling and chemokine expression are mitigated in mice deficient for SphK1 or mast cells: S1P-mediated skin mast cell degranulation and mast cell-dependent local S1P production. Thickness of the epidermis, dermis and hypodermis layers in SphK1 KO mice (vertical line patterns) measured

in H&E-stained skin tissues. For epidermis thickness, n = 15 (saline, white bars), 15 (OVA, grey bars), for dermis, n = 15 and 13 and for hypodermis, n = 15 and 15 individual measurements collected from 3 animals/treatment group/skin layer. (b) Nuclei numbers per ROI within the hypodermis of saline-treated, compared to OVA-treated SphK1 KO mice. (c) Nuclei numbers per perivascular ROIs after saline or OVA treatment (d) CCL2, CCL3, CCL5 and FcεR1α mRNA expression in OVA-treated (n = 3-4) compared to saline-treated (n = 4) SphK1 KO skins, normalized to GAPDH, with duplicate determinations. (e) Percent mast cell degranulation measured in MB-stained saline- or OVA-treated SphK1-KO mouse skin samples. (f) Thickness of the epidermis, dermis and hypodermis layers of KitW-sh/W-sh mice (side-patterned bars), measured in H&E-stained tissues (n = 13-15 saline (white), 10-15 OVA (grey) individual measurements collected from 3 animals/treatment group/skin layer. (g) Nuclei numbers per ROI within the hypodermis of saline-treated compared to OVA-treated KitW-sh/W-sh mice. (h) Nuclei numbers around perivascular ROIs. (i) CCL2, CCL3, CCL5, FcεR1α and SphK1 mRNA expression from OVA-treated normalized to saline-treated KitW-sh/W-sh mouse skin samples, and to GAPDH, with duplicate determinations. (j) S1P content of KitW-sh/W-sh mouse skins after saline or OVA treatment (n = 4 mice/experimental group). All measurements were conducted as described in Figures 3.1-3.3. Statistical differences were determined with unpaired 2-tailed Student's t test with Welch's correction (a-j). **** p < 0.0001.

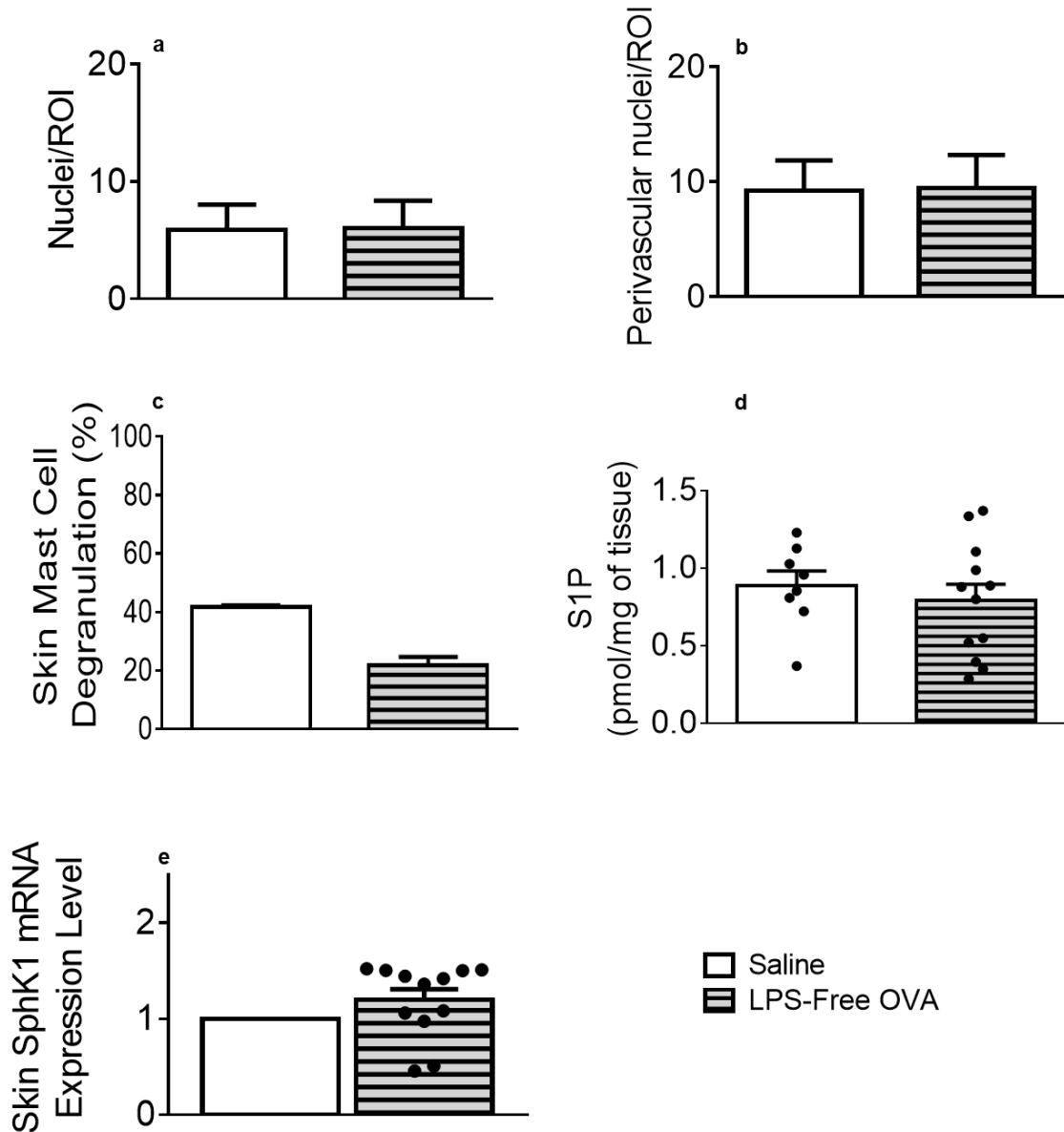


Figure 3.5 Cellular infiltration, mast cell degranulation and S1P increase are abated in mouse back skins exposed to LPS-free OVA. (a) Nuclei numbers per ROI within the hypodermis of saline (empty bars)-treated compared to LPS-free OVA (horizontal-patterned grey bars)-treated mice. (b) Nuclei numbers per perivascular ROIs after saline and LPS-free OVA treatments. (a, b) 20 ROI/animal, 3 mice/treatment. (c) Skin mast cell degranulation (%) measured in MB-stained saline- or LPS-free OVA-treated mouse skin samples. (d) S1P content of mouse skins after saline or OVA treatment. (c, d) $n = 8$ (saline), $n = 12$ (LPS-free OVA). (e) Skin SphK1 mRNA expression from LPS-OVA-treated ($n = 6$) normalized to

saline-treated (n = 6) mouse skin samples, and to GAPDH, with duplicate determinations. Statistical differences were determined with unpaired 2-tailed Student's t test with Welch's correction (a-e). All measurements were conducted as described in Figures 3.1-3.3.

Table 3.1 Mouse qPCR primer sequences

Target	Forward sequence	Reverse sequence
Mu_Gapdh	CAGAAGGGGCGGAGATGAT	AGGCCGGTGCTGCTGAGTATGTC
Mu_Ccl2	CACTCACCTGCTGCTACTCA	GCTTGGTGACAAAACTACAGC
Mu_Ccl3	GCCATATGGAGCTGACACCC	TAGTCAGGAAAATGACACCTGGC
Mu_Ccl5	TGCCCTCACCATCATCCTCACT	GGCGGTTCCCTTCGAGTGACA
Mu_SphK1	CGTGGACCTCGAGAGTGAGAA	AGGCTTGCTAGGCGAAAGAAG
Mu_FcεR1α	ATTGTGAGTGCCACCGTTCA	GCAGCCAATCTTGCGTTACA

CHAPTER 4: A MAST CELL-MEDIATED ELEVATION OF CERAMIDES TRIGGERS APOPTOSIS IN PRE-LESIONAL ATOPIC DERMATITIS.³

4.1 INTRODUCTION

Atopic dermatitis (AD), also known as eczema, is one of the most common chronic diseases, featuring severe itch and skin lesions. AD affects one-fifth of individuals residing in developed countries (Weidinger and Novak, 2016). It is well established that a disrupted skin barrier plays an integral role in AD etiology. The stratum corneum (SC) is the outermost layer of the epidermis that prevents water loss and protects underlying tissues from external factors including allergens and pathogens. It comprises a lipid matrix of cholesterol, free fatty acids and ceramides (CER) (Elias, 2014; Janssens *et al.*, 2012; Skolová *et al.*, 2014; van Smeden *et al.*, 2011).

CER are the most abundant SC lipids and play a critical role in maintaining homeostatic skin functions. Composed of a sphingoid base linked to a fatty acid chain, CER can be produced by three distinct pathways: the *de novo* synthesis pathway requires serine palmitoyl transferase and ceramide synthases (CerS) to generate CER, the *salvage* pathway involves degradation of complex sphingolipids to form CER, and subsequently sphingosine and sphingosine-1

³ Wedman P., Chumanevich A.P., Aladhani A., Castleberry K.M., Enos R.T., Gandy K.A., Velazquez K.T., Murphy E.A., Fuseler J.W., Nagarkatti M. and Oskeritzian C. A.. 2017. A Mast Cell-Mediated Elevation of Ceramides Triggers Apoptosis in Pre-Lesional Atopic Dermatitis. To be submitted to *J Lipid Res*.

phosphate (S1P), by ceramidases and lastly the *sphingomyelin* pathway which generates CER from sphingomyelin and sphingomyelinases (Aflaki *et al.*, 2012; Grösch *et al.*, 2012; Seumois *et al.*, 2007). CER regulate a variety of cellular responses including cell cycle arrest and apoptosis with specific behaviors being attributed to fatty acid chain length. CER are classified as short, long or very long chain, based on the number of carbons (C) they feature, C16-C24 being the most common chain lengths (Seumois *et al.*, 2007). Recent studies have highlighted the importance of CER chain length in skin barrier dysfunction, highlighting a decrease in very long chain C24 at the expense of long-chain C16 during the chronic phase of AD (Janssens *et al.*, 2012; Park *et al.*, 2012). However, the status of CER during the early phase of AD has not yet been explored.

In the current study, we investigated the pre-lesional CER composition of skin using a variation of a human-AD like mouse model after one 7-day exposure to Ovalbumin (OVA) or saline (vehicle control) to study disease initiation, the full model requiring 3 OVA exposures to induce chronic AD and skin lesions (Spergel *et al.*, 1998). We found that EC OVA treatment of mouse skin resulted in significantly increased total CER levels, compared to saline controls. In particular, levels of C16 and C24 CER species were increased in OVA-treated samples. Elevated CER result from increased synthesis and/or decreased catabolism. Therefore, local mRNA expression of CER synthase (*CerS*) and ceramidase (*Asah1/Asah2*) was evaluated. *CerS* 4,5 and 6 but also *Asah1* mRNA levels were statistically augmented following OVA exposure. Given the

overall pro-apoptotic nature of CER, *in situ* activation of Caspase 3, the executioner Caspase of apoptosis, was measured using a novel image analysis method we describe to quantify cleaved Caspase-3 (Casp3) in treated skin sections, and validated by protein analysis. Since apoptosis may occur as a result of endoplasmic reticulum (ER) stress, skin samples were further interrogated for key molecules of ER stress-induced apoptosis.

Mast cells (MC), skin-resident cells located near blood vessels, are well-known key players in the initiation of atopic diseases and an established source of a variety of pro-inflammatory mediators secreted upon activation by many stimuli (Galli and Tsai, 2012; Oskeritzian *et al.*, 2008; Oskeritzian *et al.*, 2015; Oskeritzian *et al.*, 2010). To substantiate the importance of MC in these processes, the AD model was repeated in MC-deficient *Kit^{Wsh/Wsh}* mice. The absence of MC prevented OVA-induced CER increase and local apoptosis. Moreover, primary mouse bone marrow-derived MC (BMMC) activated by exogenous S1P at different time-points *in vitro* exhibited elevation of CER C16 and C24 species with corresponding increased gene expression of CerS 4,5 and 6 and Asah1. We propose that the MC/CER axis is an essential pathogenic feature of pre-lesional AD. Targeting this axis may prevent disease development.

4.2 MATERIALS AND METHODS

Atopic dermatitis model

AD was induced female C57Bl/6J mice as previously described (Section 3.2). Mice were purchased from Charles River NCI (Frederick, MD) and The

Jackson Laboratory (Bar Harbor, ME). Animal experiments were approved and performed in accordance with IACUC guidelines.

Lipidomics

Lipids were extracted from snap-frozen skin tissues, as described in section 3.2, and S1P-activated BMMCs. CER were measured, and normalized to weight of skin sample or per 10^6 BMMCs.

Quantitative Real-Time qPCR

RNA was extracted from patched skin tissue, cDNA was synthesized and qPCR performed as described in section 3.2. The primer sequences (Thermo Fisher Scientific) used for real-time qPCR amplification are located in table 4.1. Data were analyzed with CFX Manager™ Software and are normalized expression to saline-treated samples for *in vivo* experiments or 0 hour S1P activation for *in vitro* experiments and directly proportional to the amount mRNA of the target gene relative to the amount of mRNA of the reference gene, GAPDH mRNA levels.

Immunofluorescent quantification of cleaved Caspase-3

Skin tissues collected from euthanized mice were fixed in 4% paraformaldehyde, paraffin-embedded, sectioned (4 μ m thickness) and mounted on microscope slides. Tissues underwent dewaxing, rehydration, antigen retrieval, blocking and permeabilization prior to overnight incubation with anti-cleaved Caspase-3 antibody (CST, Danvers, MA). Secondary AlexaFluor 488 donkey anti-rabbit IgG antibody (Jackson ImmunoResearch, West Grove, PA) was used to visualize cleaved Caspase-3. Images ((40x) magnification) were

collected as TIFF files and analyzed. Morphometric parameters were measured using the MetaMorph® 6.1 Image Analysis software (Molecular Devices, Sunnyvale, CA) as previously reported by our laboratory (Wedman *et al.*, 2015), and adapted to quantify cleaved Casp3.

Western blots

Proteins were extracted from snap-frozen skin tissues and the Bradford protein assay was used to measure concentration. Equal concentrations of protein were electrophoretically separated on a 4-20% Mini-PROTEAN®TGX™ gel (Bio-Rad, Hercules, CA) followed by electrophoretic transfer to a polyvinylidene difluoride (PVDF) membrane. Membranes were incubated overnight with primary antibodies (Cleaved Caspase-3, CHOP, BiP and GAPDH; CST, Danvers, MA). Proteins were detected using an HRP-linked secondary antibody and captured on film. Signal was quantified using ImageJ software (NIH).

Culture and activation of bone marrow-derived mast cells

Mouse BMMC were generated from progenitors isolated from femurs and cultured in RPMI 1640 medium (Invitrogen Life Technologies, Carlsbad, CA) containing 10% heat-inactivated FBS, 2 mM L-glutamine, 1% antibiotics, 1 mM sodium pyruvate, 1 mM HEPES (Biofluids, Rockville, MD), 2 ng/ml recombinant IL-3 and 20 ng/ml of stem cell factor (SCF, PeproTech, Rocky Hill, NJ). After 4 weeks of culture, BMMC were more than 98% pure and fully matured. S1P (100 nM) was used to stimulate BMMCs for lipidomics and qPCR analyses.

Engraftment of MC-deficient mouse skin with BMMC

Mature BMMC, generated from C57Bl/6 mice, were counted and resuspended in PBS (4×10^6 cells in 400 μ l). BMMC were injected intradermally into back skin of anesthetized mice (8 x 50 μ l injections in two rows down the length of the shaved back) (Kalesnikoff and Galli, 2011). Experiments were initiated 9 weeks after adoptive transfer of BMMC, allowing for proper reconstitution of skin MC.

Statistics

Data are expressed as means \pm SEM (unless otherwise stated) and were analyzed by using the unpaired 2-tailed Student *t* test, with Welch's correction for samples of unequal variance or nonparametric Mann Whitney test (Prism 6; GraphPad Software, La Jolla, CA).

4.3 RESULTS

In atopic dermatitis, a single OVA exposure triggers an increase in ceramides.

CER, the most abundant skin lipids, are known to be decreased in the SC during chronic AD, resulting in increased dryness and exposure to external environment (Park *et al.*, 2013). We have recently shown that localized changes occur very early in response to allergic stimuli (Oskeritzian *et al.*, 2015), thus we sought to investigate the status of CER at AD onset. Figure 4.1a shows that a single 7-day EC OVA exposure promoted CER production compared to saline-treated controls. Pertinent CER species were highlighted upon CER profiling, with CER C16 and C24 species being most augmented (Fig. 4.1b). To determine

if the accumulated CER were produced *de novo*, we explored the gene expression of ceramide synthases (*CerS*). Figure 4.1c shows increased detection of *CerS 4,5* and *6* but not *CerS 1* or *2* mRNA in OVA-treated mice compared to Saline, normalized to *Gapdh* (black line). We also observed increased gene expression for the acid ceramidase, *Asah1*, but not the neutral ceramidase *Asah2* (Fig. 4.1d). These results suggest that early accrual of CER C16 and C24 stems from both synthetic and catabolic pathways.

OVA exposure leads to increased detection of cleaved Caspase 3

De novo production of C16 and C24 species has previously been linked to apoptosis in neutrophils (Seumois *et al.*, 2007). Therefore, we next examined skin tissue sections for cleaved Casp3. Figure 4.2a shows a representative image of a fluorescently-labeled OVA-treated skin section. Using image analysis software, line scans were applied to detect positive signal while eliminating autofluorescence (Fig. 4.2b and c). We have recently shown that morphometric parameters can be applied to quantify cellular changes *in situ* (Wedman *et al.*, 2015). Similarly, we established specific parameters for the quantification of cleaved Casp3 fluorescence. In figure 4.2d, we show that the computer proceeds with thresholding of positive signal and measurement (in green) while simultaneously eliminating background staining (orange). By measuring the ratio of integrative optical density (IOD) over the total image area, we show a significant increase in cleaved Casp3 following OVA exposure compared to saline-treated animals (Fig. 4.2e). Presence of increased cleaved Casp3 was

further confirmed through Western blot analysis and quantification (Fig. 4.2f and g).

ER-stress contributes to local apoptosis following OVA exposure

Caspase 3, executioner enzyme of apoptosis, can be activated downstream of intrinsic signaling pathways during cellular stress. *De novo* synthesis of CER, by CerS, occurs within the ER (Futerman and Riezman, 2005) and increased production can trigger ER stress (Longato *et al.*, 2012). To determine if CER-induced apoptosis results from ER stress, we examined the skin tissues for stress-related markers. Local mRNA levels of binding immunoglobulin protein (*BiP*), activating transcription factor 4 (*Atf4*), x-box binding protein 1 (*Xbp-1*) and C/EBP-homologous protein (*Chop*) were all augmented following OVA exposure (Fig. 4.3a). Furthermore, significantly more CHOP (but not BiP) was detected by Western blot in OVA-treated skins compared to saline alone (Fig. 4.3b-d).

OVA-induced increase in ceramides C16 and C24, and resulting apoptosis, is dependent on mast cells

To substantiate how MC could contribute to ceramide regulation *in vivo*, we repeated similar experiments in MC-deficient *Kit^{W-sh/W-sh}* mice. Here we show that in the absence of MC, OVA exposure did not lead to ceramide accumulation (Fig. 4.4a and b) or changes in localized gene expression seen in WT mice (Fig. 4.1c and d) for *CerS 4, 5 and 6* or ceramidases (*Asah 1 and Asah 2*), in MC-deficient *Kit^{W-sh/W-sh}* mice (Fig. 4.4c and d). Furthermore, no change in cleaved Casp3 was measured upon OVA treatment (Fig. 4.4e and f) in *Kit^{W-sh/W-sh}* mice.

To further confirm the importance of MC in CER-driven apoptosis, skin of *Kit^{W/-}sh/W-sh* mice was reconstituted through adoptive transfer of BMMC. Reconstituted mice were similarly treated with OVA and saline, as a control. Figures 4.4g and h show that protein production of cleaved Casp3 and CHOP was restored in OVA-treated reconstituted mice.

Bone marrow-derived MC, activated in vitro by sphingosine-1-phosphate, display a CER profile comparable to OVA-treated WT mice skin samples

We recently highlighted the importance of S1P activation of MC in an acute pulmonary model of allergic response (Oskeritzian *et al.*, 2015). Since we demonstrated that MC are required for early CER changes in the skin following OVA exposure, we next investigated if exogenous S1P would also trigger CER production in MC. In figure 4.5, BMMC were *in vitro* stimulated with S1P at different time points. Total CER were measured (Fig. 4.5a) and CER profiling was conducted (Fig. 4.5b) at 0, 6 and 16 hours following S1P activation. Total CER levels were time-dependently increased with CER C16, C22 and C24 species being most prominent after 16 hours of stimulation. Further interrogation of BMMC showed increased gene expression of *Cers* 2, 4, 5 and 6 (Fig. 4.5c) and ceramidase *Asah* 1 (Fig. 4.5d) 3 hours following S1P stimulation, recapitulating the findings in mouse skin samples for the most part.

4.4 DISCUSSION

Ceramides are well known to play a role in chronic AD, but their function at AD onset is still unclear. Here, we report that ceramide accumulation can be observed in pre-lesional skin samples very early following a 7-day exposure to

OVA, compared to saline controls. OVA exposure resulted in significant elevation of total ceramides in particular, C16:0, C24:0 and C24:1 species. A recent study, conducted by YH Park *et al.*, reported increased C16:0 at the expense of C24 species in a preclinical model of chronic AD (Park *et al.*, 2012). However, it is important to note that 1) they extracted lipids from the SC layer only, and 2) mice had skin lesions, which are absent in our 7-day model. While ceramides are generally considered to be pro-apoptotic, it has been shown that C24 species can have protective effects (Grösch *et al.*, 2012). As both pro-apoptotic C16 (Mullen *et al.*, 2011) and protective C24 species accumulated following one week OVA exposure, it is tempting to speculate that pro-survival mechanisms were in effect to return to homeostatic conditions. Of note, accumulation of both C16 and C24 ceramides has been observed within malignant tumors of head and neck squamous cell carcinoma and breast cancer patients compared with normal and/or benign tumor tissues, suggesting that the balance between C16 and C24 species may control both apoptotic and survival pathways (Karahatay *et al.*, 2007; Schiffmann *et al.*, 2009).

In addition to increased ceramide levels, an increase in mRNA expression for ceramide-generating enzymes was also observed. Ceramide synthases (CerS) 1-6 link specific subsets of fatty acyl-CoAs to a sphingoid base generating ceramides with varying chain lengths, while ceramidases (acidic, neutral and alkaline) catalyze the cleavage of ceramides. Here we show increased expression of *CerS 4,5* and 6. It has previously been shown that *CerS 5* and 6 are specific for long chain ceramides, including C16. *CerS 4*, the least studied

CerS, is considered to be a broad-spectrum CerS. Expression of CerS 4 has previously been linked to increased C24 ceramide species (Mizutani *et al.*, 2009). Tirodkar *et al.* recently reported that elevation of CerS6 could mediate transcriptional activation of Asah1, which could explain the increased detection of acid ceramidase we observed following OVA exposure (Tirodkar *et al.*, 2015).

In this study, we report that topical OVA exposure induces an increase in C16 and C24 ceramide species compared to saline-exposed controls. Previous studies have linked *de novo* generation of C16 and C24 ceramides to spontaneous neutrophil apoptosis (Seumois *et al.*, 2007) and tumor-induced DC apoptosis (Kanto *et al.*, 2001). Similarly, we report that substantially increased C16 and C24 ceramides was linked to apoptosis, as measured by immunofluorescence staining of mouse skin sections upon OVA treatment. Detection of cleaved Casp3 was further validated and confirmed through quantification of cleaved Casp3 protein in OVA compared to saline-exposed skin samples using Western blot analysis. Thus, it appears the pro-apoptotic effects of C16 surpass protective C24 at the initiation of AD.

When injury occurs, the ER stress response initiates survival pathways. The chaperone protein, BiP, dissociates from IRE1, ATF6 and PERK activating the unfolded protein response (UPR). If the UPR fails, the ER-stress apoptosis pathway initiates, involving CHOP and the Caspase cascade (Chang *et al.*, 2013). Our results indicated *BiP* and transcription factors *Atf4*, *Xbp1* and *Chop*, were increased in skin samples following OVA application, with confirmed elevation of CHOP protein, key mediator of ER stress-induced apoptosis.

We have shown the importance of MC during early allergic lung inflammation (Oskeritzian *et al.*, 2015). Thus, we sought to investigate if MC were contributing to the augmentation of ceramides during early skin inflammation. In MC-deficient *Kit^{W-sh/W-sh}* mice, OVA application did not trigger ceramide elevation and cell survival was evident in the absence of cleaved Casp3. However, following MC reconstitution, cleaved Casp 3 levels returned to WT levels, also downstream of CHOP. Furthermore, we discovered that *in vitro* S1P activation of mouse BMMC stimulated ceramide production pathways leading to a comparable ceramide profile to the one observed in OVA-exposed WT mice skin samples.

In conclusion, targeting S1P/MC interactions may be a novel prophylactic approach to prevent ceramide-mediated apoptosis at the onset of AD.

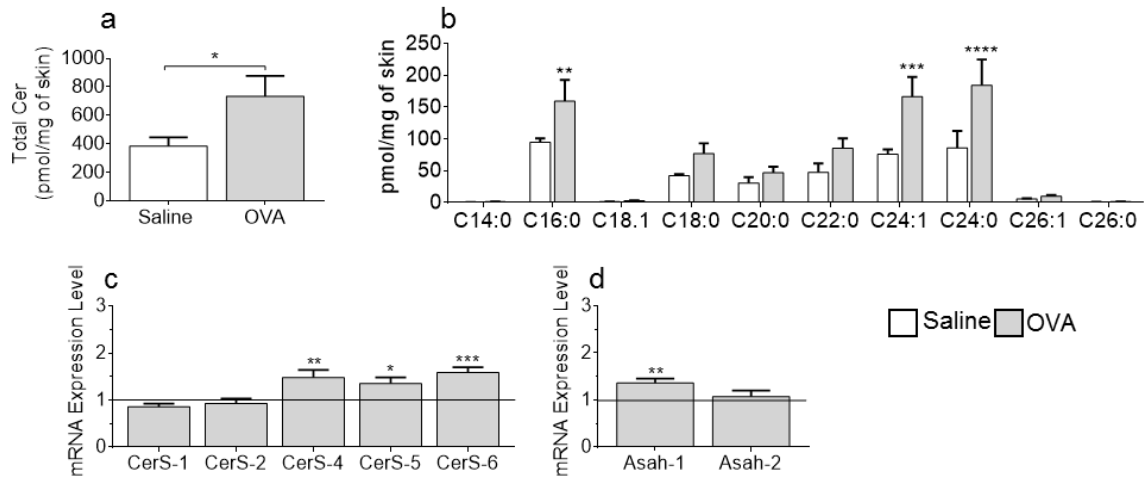


Figure 4.1 Skin exposure to OVA leads to increased ceramides in WT mice. A single, 7-day, OVA exposure resulted in elevation of total ceramides (a). Further analysis revealed specific increases in C16 and C24 ceramide species in OVA- compared to saline-treated mice (b). Elevated levels of mRNA for ceramide synthases (*CerS*) 4, 5 and 6 (c) and acid ceramidase (*Asah1*) (d) were observed in response to OVA.

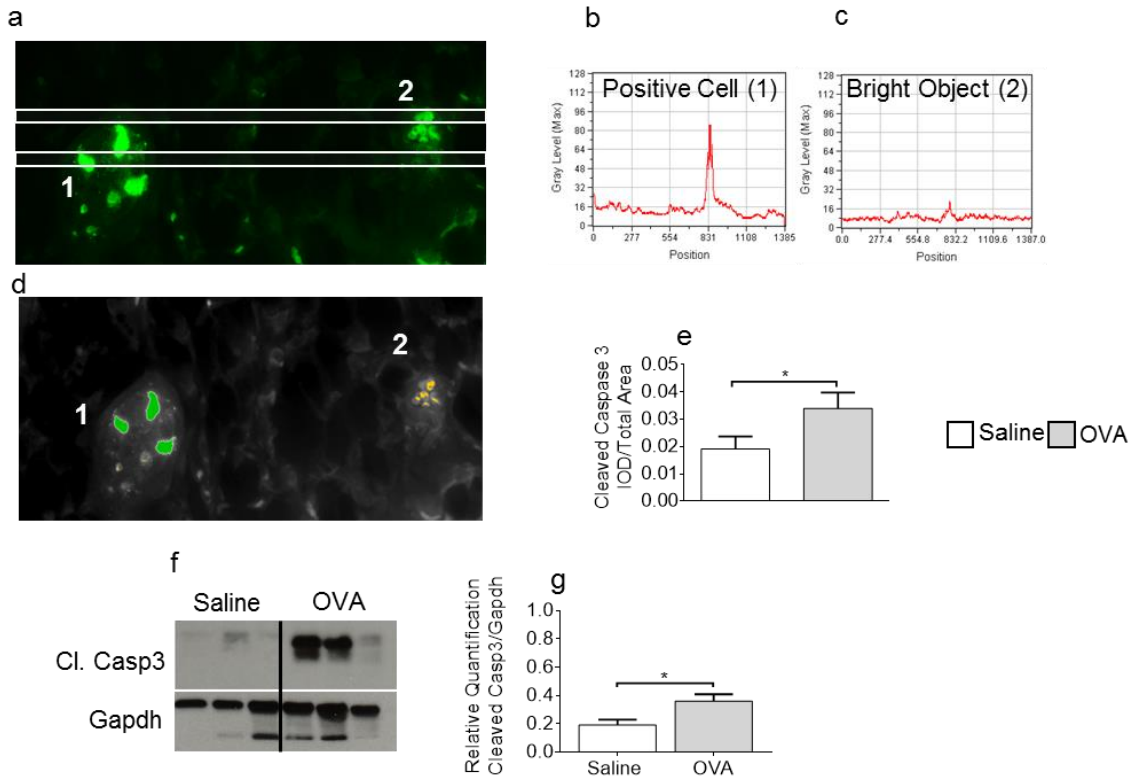


Figure 4.2 Increased cleaved Caspase 3 is observed following OVA exposure. Cleaved caspase-3 (Casp3) signal was analyzed in fluorescently labeled skin sections using a line scan histogram (a-c) and integrative optical density (IOD), which represents the mass or total amount of the fluorescent signal. Applying these parameters, images were thresholded to measure positive signal (d1, green). Significantly more cleaved Casp3 was quantified *in situ* in OVA-treated skins compared to saline (e). Protein analysis further confirmed production of cleaved Caspase 3 in OVA-treated skin samples (f-g).

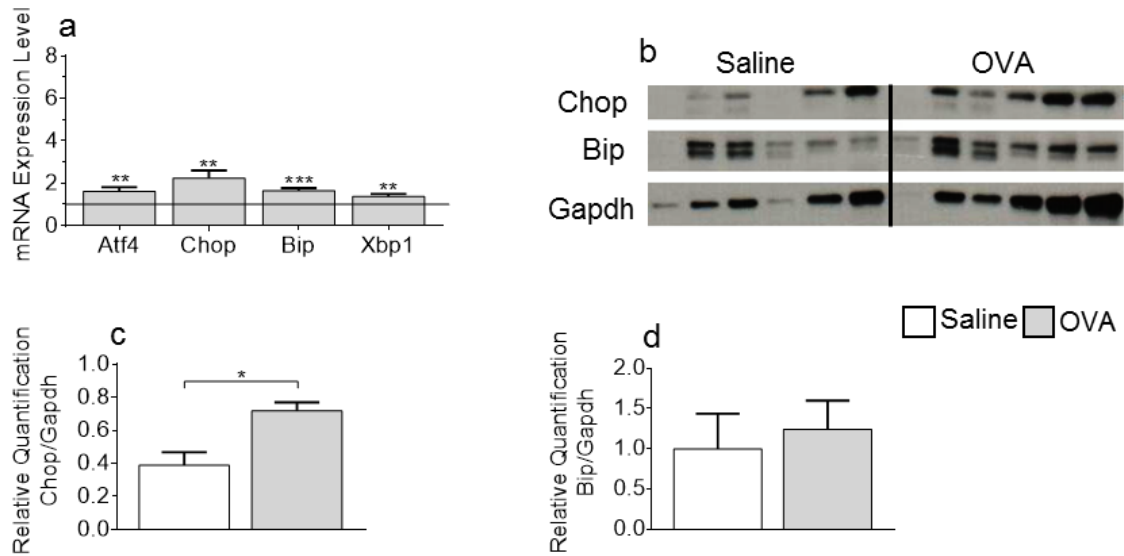


Figure 4.3 OVA treatment leads to endoplasmic reticulum stress-induced apoptosis. Gene expression of key ER-stress regulators was upregulated following OVA treatment (a). A significant increase in Chop protein (b, n = 6 mice/treatment group, c), but not Bip (b, d) was observed following OVA exposure.

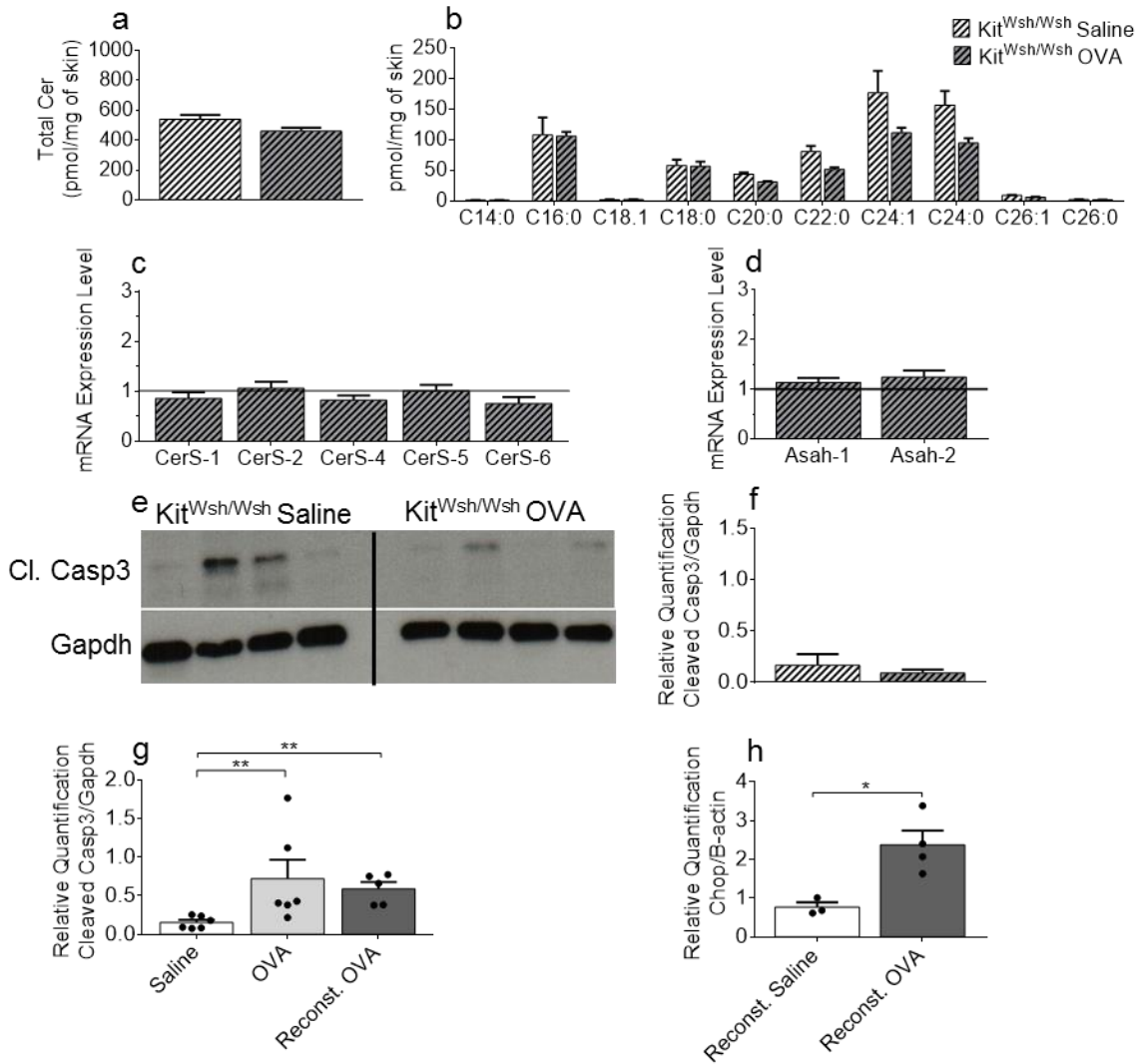


Figure 4.4 Ceramides, mRNA coding for genes involved in ceramide production remain unaltered and apoptosis undetectable upon OVA treatment of *Kit*^{W-sh/W-sh} MC-deficient mice. In the absence of MC, OVA exposure did not generate an increase in total ceramide levels (a), or in any specific ceramide species (b). The increased levels of mRNA for CerS 4, 5 and 6 and Asah 1, seen in WT mice treated with OVA (Fig. 4.1c, d), were unchanged in similarly treated MC-deficient *Kit*^{W-sh/W-sh} mouse skin samples (c, d). Western blot band quantification (f) showed no difference in Casp3 cleavage in OVA- or saline-treated MC-deficient *Kit*^{W-sh/W-sh} samples (e, n = 4 mice/each treatment group). Casp3 activation was restored in OVA-treated *Kit*^{W-sh/W-sh} following MC reconstitution (g), concomitant with increased production of CHOP protein (h).

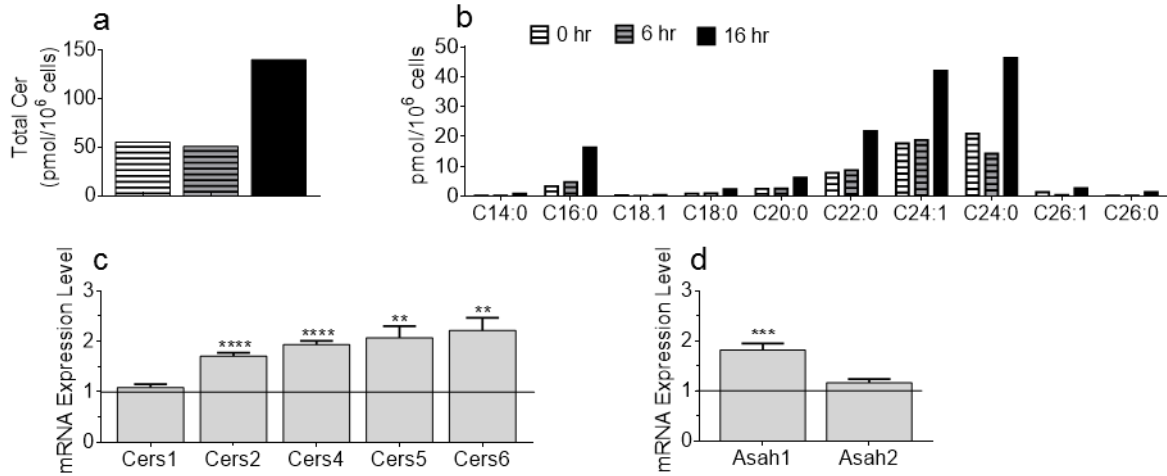


Figure 4.5 In vitro S1P stimulation triggers ceramide generation in BMMC. Increased production of total CER is observed after 16 hours of BMMC activation by S1P (a). Profiling highlights elevation of CER C16 and C24 species, also observed following OVA exposure *in vivo* (b and Fig. 4.1). Gene expression was significantly higher for CerS 2, 4, 5, 6 and Asah1 after 3 hours of S1P stimulation compared to untreated BMMC (c, d).

Table 4.1 Mouse qPCR primer sequences

Target	Forward sequence	Reverse sequence
Mu_Gapdh	CAGAAGGGGCGGAGATGAT	AGGCCGGTGCTGCTGAGTATGTC
Mu_Cers1	CCACCACACACATCTTTCGG	GGAGCAGGTAAGCGCAGTAG
Mu_Cers2	ATGCTCCAGACCTTGTATGACT	CTGAGGCTTTGGCATAGACAC
Mu_Cers4	TACCCACATCAGACCCTGAAT	TGAAGTCCTTGCGTTTGACATC
Mu_Cers5	CGGGGAAAGGTGTCTAAGGAT	GTTTCATGCAGTTGGCACCATT
Mu_Cers6	ATTCAACGCTGGTTTTGACAA	TTCAAGAACCGGACTCCGTAG
Mu_Aсах1	CACCAGCGTTGAGGATTTTAGT	TACCAGGCAGCTTTTGATCCA
Mu_Aсах2	GCAAAGCGAACCTTCTCCAC	ACTGGTAACAAACAAGAGGGTGA
Mu_Casp3	ATGGAGAACAACAAAACCTCAGT	TTGCTCCCATGTATGGTCTTTAC
Mu_Atф4	GGGTTCTGTCTTCCACTCCA	AAGCAGCAGAGTCAGGCTTTC
Mu_Chop	CCACCACACCTGAAAGCAGAA	AGGTGAAAGGCAGGGACTCA
Mu_Bip	TTCAGCCAATTATCAGCAAACCTCT	TTTTCTGATGTATCCTCTTCAACAGT
Mu_Xbp1	GAACCAGGAGTTAAGAACACG	AGGCAACAGTGTCAGAGTCC

CHAPTER 5: A MIRNA TRIAD EPIGENETICALLY REGULATES AD PATHOGENESIS⁴

5.1 INTRODUCTION

Atopic dermatitis (AD) is a chronic inflammatory skin disease relieved by symptom management but with no cure. Skin-resident MC express many receptors, including the high affinity receptor for IgE (FcεRI) (Galli *et al.*, 2008), which once cross-linked with Ag, initiates MC secretion of inflammatory histamine, cytokines and chemokines, many of which are pre-formed. IgE crosslinking also results in SphK1 activation, leading to the production of S1P, a multifunctional sphingolipid metabolite endowed with proinflammatory and chemotactic properties (Olivera *et al.*, 2006; Oskeritzian *et al.*, 2008). Once exported out of MC, S1P can ligate MC-expressed S1P receptors (S1PR) (Mitra *et al.*, 2006; Oskeritzian *et al.*, 2008; Oskeritzian *et al.*, 2007). S1PR2 signaling amplifies local allergic responses through further MC stimulation and immune cell recruitment (Oskeritzian *et al.*, 2015). We recently discovered that S1P ligation of S1PR2 on MC was a key driver of early inflammatory pathways in acutely inflamed lungs. Moreover, these studies identified a new MC-associated signaling pathway that encompasses activation of signal transducer and activator

⁴ Piper Wedman, Alena Chumanevich, Elizabeth Zumbrun, Prakash Nagarkatti, Mitzi Nagarkatti and Carole A. Oskeritzian. 2017. A miRNA triad epigenetically regulates AD pathogenesis. In progress.

of transcription 3 (Stat3) downstream of S1P/S1PR2, critical to MC-derived chemokine secretion (Oskeritzian *et al.*, 2015).

In recent decades, increased prevalence of AD was observed in developed countries. While research has identified genetic inheritability as one factor that contributes to AD manifestation, the rise in affected individuals cannot be attributed to genetic factors alone. With the discovery of miRNA, short non-coding RNA that can post-transcriptionally modify gene expression, new studies began to investigate the epigenetic regulation of AD. Such studies have focused on miRNA expressed in psoriasis and established AD (Sonkoly *et al.*, 2007), while others have investigated that status of miRNA in skin (Sonkoly *et al.*, 2010) and keratinocytes (Rebane *et al.*, 2014) of AD patients bearing chronic lesions compared to healthy controls. However, miRNA alterations at the pre-lesional phase of AD has yet to be explored.

We employed a well-established preclinical model that mimics human AD-like disease progression and consists in three 1-week EC exposures to OVA, each separated by two weeks of rest (Spergel *et al.*, 1998). We discovered that miRNA 34a, 485 and 486 were consistently down-regulated in skin samples exposed three times to OVA compared to saline-treated skins. *In silico* analysis of predicted target genes and pathways identified canonical cytokines and chemokines associated with AD anticipated to be de-repressed by decreased expression of these miRNA. Interestingly, SphK1 and Stat3 were also highlighted as target genes predicted to be up-regulated.

To investigate the relevance of this newly identified miRNA triad to AD pathogenesis, miRNA profiling was also performed on skin samples collected following a single OVA or saline exposure. Surprisingly, we observed that miRNA-34a, 485 and 486 were also significantly down-regulated at the early stage of AD, further highlighting their implications in disease development.

5.2 MATERIALS AND METHODS

Mice

Aged- and gender-matched C57Bl/6 mice were shaved on the back and skin was tape-stripped prior to OVA or saline exposure, as previously described (Chapter 3) (Spergel *et al.*, 1998). Skin samples were collected following the first and third exposures.

RNA extraction

Snap-frozen skin samples were homogenized and RNA was extracted using Qiagen miRNeasy kits, according to manufacturer's instructions.

MicroRNA expression profiling

RNA samples collected following three exposures were sent to Johns Hopkins University Deep Sequencing and Microarray core (Baltimore, MD) for miRNA microarray analysis, using the Affimetrix Genechip MiRNA 3.0 array platform and oligonucleotide probe sets for 1,111 mouse mature MiRNAs from Sanger miRbase. Four skin samples were analyzed from two OVA-treated and two saline-treated mice (n= two independent experiments). MiRNA microarray profiling of RNA collected at AD onset (i.e. following a single exposure to OVA or saline) was conducted using the Affimetrix GeneChip miRNA 4.0 platform with

oligo probe sets for ~3,200 mouse miR (n=three independent experiments – OVA compared to saline) at the Microarray Core Facility, SC College of Pharmacy at USC Columbia.

Computational pathway analysis

Ingenuity Pathway Analysis (IPA) software (Ingenuity[®] Systems) was used to identify target genes and pathways regulated by differentially expressed miRNA.

Real time qPCR

Total skin RNA were reverse transcribed to obtain cDNA using iScript synthesis kit (Bio-Rad). QPCR was completed using SensiFAST SYBR No-ROX kit (Bioline) on Bio-Rad CFX connect platform (see primer sequences in Table 5.1). To validate the miRNA microarray analysis, cDNA generated with the miScript II RT Kit was used as a template for qPCR with the miScript SYBR Green PCR Kit and miScript Primer Assays, according to manufacturer's instruction (Qiagen).

5.3 RESULTS

Skin miRNA profiles following repeated exposure to OVA

In a preclinical model of AD consisting in repeated EC exposure to OVA or saline (controls) (Spergel *et al.*, 1998), we identified, by miRNA microarray analysis, a triad of miRNA consistently down-regulated following OVA exposure: miR 34a, 485 and 486 (Figure 5.1a). Figure 5.1b shows qPCR validation of these miRNA, confirming the significant reduction of expression in OVA-treated samples compared to saline, after normalization to Small Nucleolar RNA, C/D

Box 96A (Snord96a) control. Furthermore, analysis of predicted target genes using bioinformatics computational tools identified canonical mediators associated with AD, including IgE receptors (FcεR1α and FcεR1γ chains), cytokines and chemokines (Figure 5.1c), upregulated by decrease of these miRNA. Further qPCR analysis confirmed increased expression of mRNA coding for CCL5, FcεR1α, and TNFα (Figure 5.1d). Of note, SphK1 and IL17a mRNA levels were not significantly altered.

MiRNA profiling of skin following *one* OVA exposure

Next, we sought to determine the contribution of these miRNA to the inception of AD as potential disease biomarkers and molecular targets. Figure 5.2a shows the average fold change of miRNA in skin samples collected from 3 independent *in vivo* experiments when comparing a single 1-week OVA exposure to saline controls. Mature miRNA may be generated from the 3' or 5' arms of pre-miRNA precursors. To further establish the relevance of this miRNA triad to AD onset, both 3p/5p miRNA species were investigated. A significant decrease in miRNA-34a-3p and -486-5p was established by microarray analysis (Figure 5.2a) that did not reach statistical significance for miRNA-485-5p and -486-3p. Validation of the microarray data by qPCR established down-regulation of miRNA-34a-5p, -485-5p, -486-3p and -5p species (Figure 5.2b). Analysis of predicted target genes revealed significant elevation of FcεR1α, SphK1 and chemokines CCL5, CCL19, CCL21 and CCL22 (Figure 5.2c).

5.4 DISCUSSION AND FUTURE DIRECTIONS

Little is known about the epigenetic regulation of AD. Among epigenetic modifiers, miRNA are small noncoding RNA that influence gene expression by inhibiting translation or inducing RNA degradation (Sonkoly *et al.*, 2010). Using a preclinical AD model (Spergel *et al.*, 1998), we discovered that three miRNAs, 34a, 485 and 486 were consistently down-regulated in diseased compared to healthy skin samples. Moreover, *in silico* analysis of predicted target genes and pathways for these miRNA identified canonical cytokines IL-5, IL-17a (Auriemma *et al.*, 2013) and chemokines CCL19, CCL21 (Kawakami *et al.*, 2009; Millrud *et al.*, 2014) associated with AD de-repressed by decrease of these miRNA. Interestingly, SphK1 and Stat3 were also triad-targeted. Because our lab focuses on unraveling early molecular events driving disease pathogenesis, the status of our newly discovered miRNA triad was evaluated following a single OVA exposure compared to saline control. Surprisingly, we found miRNA 34a, 485 and 486 were also significantly down-regulated at AD inception.

Sonkoly *et al.* reported the overexpression of miRNA-155 in chronic AD skin lesion compared to healthy human skin (Sonkoly *et al.*, 2010). Interestingly, they also described down-regulation of miRNA-486 in chronic human skin lesions. Rebane *et al.* evaluated miRNA expression in keratinocytes of chronic AD patients that featured upregulation of miRNA-146a expression. Of interest, miRNA-34a was also down-regulated in their study (Rebane *et al.*, 2014).

To further assess the functional contribution of these miRNA *in vivo*, down-regulation of these miRNA will be induced in saline-treated controls of our

AD preclinical model, using antisense oligonucleotides, antimiRs acting as miRNA inhibitors. Locked nucleic acid (LNA) modified oligonucleotides (LNA-antimiR, Exiqon, Woburn, MA, compared to LNA-mismatch antimir control) will be utilized because they allow long-lasting *in vivo* miRNA inhibition (Stenvang *et al.*, 2012). We anticipate that forcing down-regulation of these miRNA in control mice should recapitulate the remodeling, cellular and molecular findings of those obtained after OVA treatment. To monitor the anti-sense activity and effective miRNA inhibition, a functional read-out of miRNA silencing is recommended and will consist in measuring de-repression of direct targets by qPCR and protein assays (Western blots and ELISA) as an evidence for success. In a complementary approach, primary mouse and human MC will be transfected with miScript synthetic miRNA mimics (mimics and HiperFect transfection reagents from Qiagen) of each member of the miRNA triad separately or in combination. MC activation with S1P and subsequent chemokine production will be assessed *in vitro* and compared to non-transfected MC and MC transfected with mock mimics. We anticipate that miRNA overexpression will result in MC hyporesponsiveness.

To our knowledge, the current study is the first to investigate the epigenetic regulation of early inflammatory events featured in pre-symptomatic AD. These results highlight an important group of miRNA, downregulated at disease onset and during chronic-stage skin inflammation. We show that these miRNA target relevant AD-associated cytokines and chemokines and also MC/S1P signaling-related FcεRI, SphK1 and Stat3 gene expression. These

results suggest that the contribution of skin MC-derived chemokines and S1P we observed at AD initiation (Chapters 3 and 4) may be epigenetically regulated by miRNA 34a, 485 and 486.

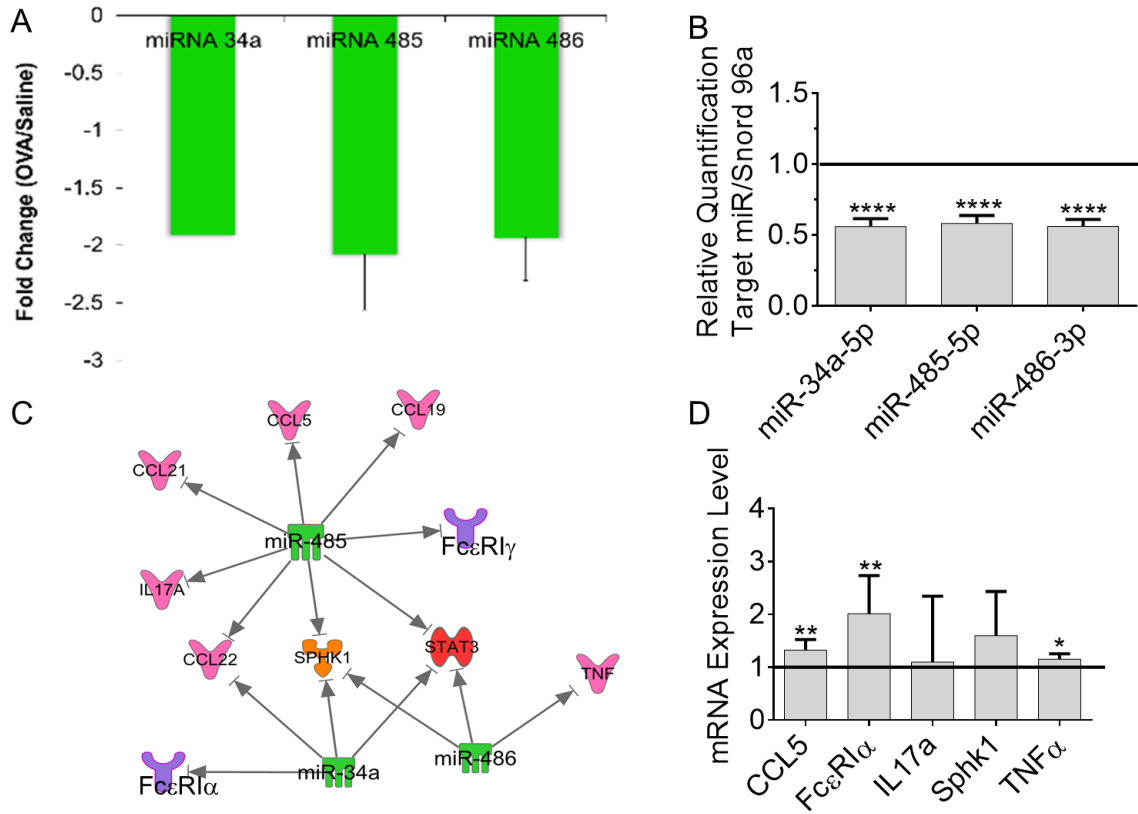


Figure 5.1 Down-regulation of skin miRNA up-regulates AD-associated gene expression. A miRNA triad, composed of miRNA 34a, 485 and 486 is consistently decreased following 3 OVA exposures compared to saline-treated skin (n = 2 independent trials). Down-regulation of miRNA was validated and Ingenuity Pathway Analysis (IPA) software (Ingenuity® Systems) was used to identify predicted target genes, including cytokines and chemokines (pink), FcεRI receptor sub-units (purple), Sphingosine kinase 1 (SphK1, orange) and transcription factor Stat3 (red) (b,c). To test the biological relevance of *in silico* predictions, qPCR was used to determine the mRNA levels of some of the predicted target genes in OVA- compared to saline-treated skin samples, normalized to GAPDH (d).

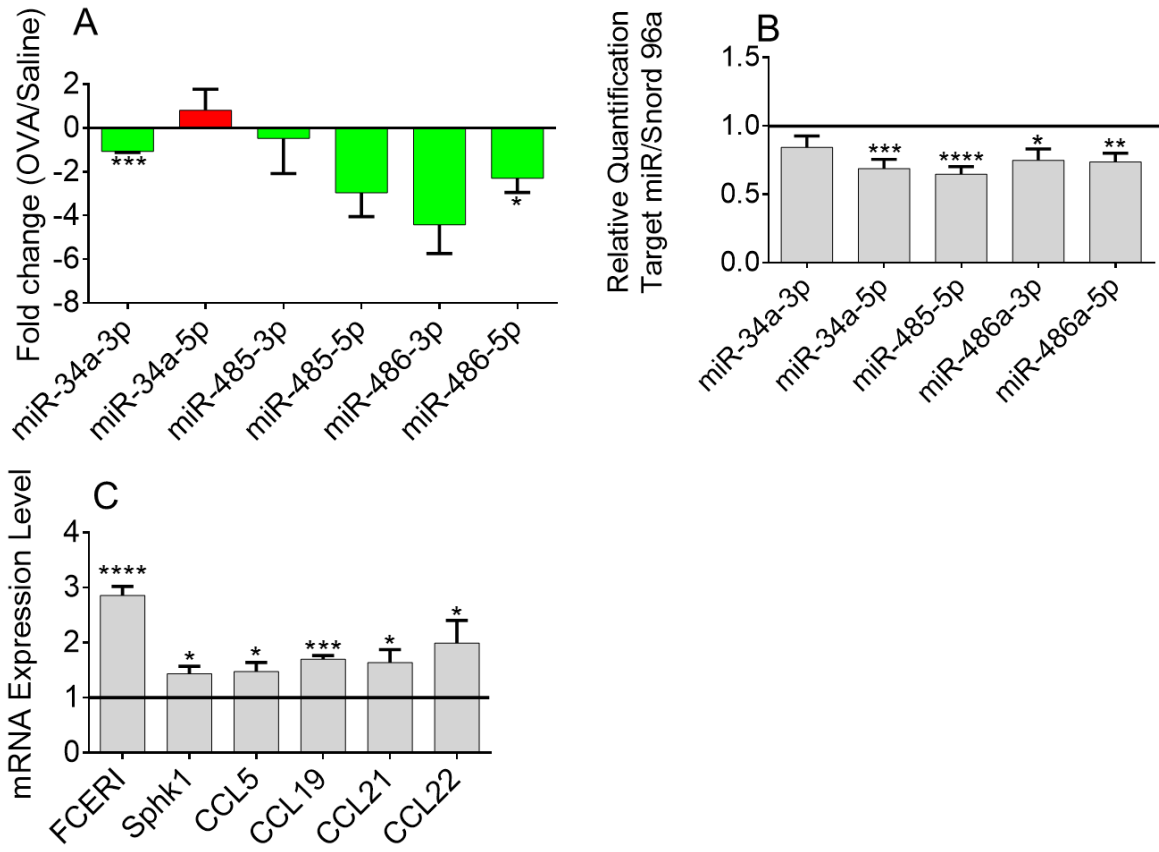


Figure 5.2 A newly identified AD-associated microRNA signature is also relevant to AD pathogenesis with validated target gene de-repression. To determine their contribution to AD onset, status of triad members was analyzed following a single OVA exposure, compared to saline, (n = 3 independent trials) and validated by qPCR, confirming significant decrease in miR34a-5p, miR485-5p, miR486a-3p and -5p (b). Gene expression for some disease-relevant predicted triad-targets was increased (c).

Table 5.1 Mouse qPCR primer sequences

Target	Forward sequence	Reverse sequence
Mu_IL17a	GCTCCAGAAGGCCCTCAGACT	CCAGCTTTCCTCCGCATTGA
Mu_TNF α	CCAGTGTGGGAAGCTGTCTT	AAGCAAAAGAGGAGGCAACA
Mu_Ccl19	GCCTGCTGTTGTGTTCCACC	CCTTTGTTCTTGGCAGAAGACT
Mu_Ccl21	TGAGCTATGTGCAAACCCTGAGGA	TGAGGGCTGTGTCTGTTCAAGTTCT
Mu_Ccl22	AGGTCCTATGGTGCCAATGT	CGGCAGGATTTTGAGGTCCA

CHAPTER 6: SUMMARY AND CONCLUSIONS

6.1 MOLECULAR MECHANISMS UNDERLYING EARLY SKIN REMODELING AT THE ONSET OF ATOPIC DERMATITIS

In 1998, Spergel *et al.* published a pre-clinical model of human-like AD. The model consists of shaving the back of the mouse and securing a patch containing ovalbumin (OVA, Ag) to the mouse for 3 consecutive 1-week periods, each separated by two weeks of rest (Spergel *et al.*, 1998). Our lab is most interested in investigating disease initiation, so we collected samples after the first 1-week exposure. Surprisingly, we observed skin thickening and increased cellular infiltration into the hypodermis during this early phase of inflammation. Quantitative image analysis revealed a significant increase in hypodermal nuclei following OVA exposure, most concentrated around blood vessels. Next, local and systemic levels of CD3⁺ T-cell recruiting chemokines were evaluated. We found that OVA-treated skin featured localized augmentation of CCL2, CCL3 and CCL5, chemokines we previously identified as key players of remodeling in Ag-challenged airways (Oskeritzian *et al.*, 2015).

6.2 SPHINGOSINE-1-PHOSPHATE AND MAST CELLS CONTRIBUTE TO SKIN INFLAMMATION IN EARLY-PHASE ATOPIC DERMATITIS

We conducted the first study that has identified that cellular infiltration initiated in the highly vascularized hypodermal skin layer. As previously mentioned, local resident MC reside within close proximity to Bv, allowing them

to play an active role in cell recruitment following release of chemokines. We established and published a method to evaluate MC activation status *in situ* by taking advantage of the metachromatic properties of methylene blue, which stains all nuclei blue while distinguishing MC from other cells through binding of granule-specific peptidoglycans resulting in purple coloration. MC status was evaluated in skin tissue collected from naïve C57Bl/6 mice and we identified a spectrum of morphometric parameters that could distinguish resting from degranulated MC *in situ* following a computer-assisted procedure. Applying these parameters to OVA-challenged skin samples highlighted a significant increase in localized MC degranulation compared to saline controls. MC are canonically activated through IgE/Ag stimulated pathways. However, we confirmed that a 7-day OVA exposure did not elicit augmented levels of total IgE, as Ab production takes 10-14 days. Moreover, mRNA expression of S1P producing enzyme SphK1, was significantly increased in skin of OVA-treated mice compared to saline controls and lipidomics analysis revealed a corresponding increase of S1P. SphK1 knockout and MC-deficient Kit^{Wsh/Wsh} mice failed to exhibit skin remodeling, hypodermal infiltration and associated chemokine production, following OVA exposure. Moreover, MC-deficient mice did not feature augmentation of S1P, identifying MC as a local source.

Interestingly, the very group from Harvard who established the AD mouse model, used by us and many other groups world-wide, recently reported that tape-stripping, a procedure included in the animal protocol that mimics the scratching response of human patients, resulted in the release of endogenous

TLR4 ligands (Yoon *et al.*, 2016). Commercially available OVA is notorious for its high content of TLR4-binding lipopolysaccharide (LPS). Our study is the first to compare the effects of OVA to LPS-free OVA in a mouse model of skin inflammation. Contrary to what we expected, based on a study describing the protective effects of LPS in airway allergic responses (Watanabe *et al.*, 2003) and another finding high LPS exposure protected Amish children from high occurrence of allergic disorders affecting genetically-related Hutterite children (Hutterites using industrialized more aseptic farming methods compared to Amish people who use traditional farming methods) (Stein *et al.*, 2016), local MC activation and S1P production were comparable to saline controls in LPS-free OVA-treated samples. Of note, other studies have reported pro-inflammatory responses following LPS/TLR4 signaling (Dong *et al.*, 2009; Eisenbarth *et al.*, 2002), perhaps due to differences in experimental procedures, timing of exposure and dose effect. Overall, our results suggest that LPS penetration of the skin through the compromised barrier may prime initial inflammatory responses, independently of Ag, as recently suggested (Yoon *et al.*, 2016),

6.3 OVA TRIGGERS MC-RELATED PRODUCTION OF PRO-APOPTOTIC CERAMIDES AT ATOPIC DERMATITIS ONSET

Ceramides (CER) are the dominant lipid species within skin and have a key role in skin barrier maintenance. Skin of AD patients displays decreased levels of very long chain CER. Analysis of CER species, following 7-day OVA exposure, highlighted augmentation of total skin CER compared to saline controls. CER profiling indicated that the observed increase was specific to CER C16 and C24 species. In general, CER are considered pro-apoptotic and further

investigation revealed increased detection of cleaved Casp3 in OVA-challenged skin. Further skin analysis revealed localized increase of CHOP, which initiates the Caspase cascade downstream of ER stress. Surprisingly changes in CER composition were not observed in OVA-treated MC-deficient *Kit^{Wsh/Wsh}* mice, but were restored following MC reconstitution, indicating a potential role for MC in CER accumulation. To further investigate this, we activated BMMC *in vitro* with S1P, a likely stimulus of MC as we have shown doubling of skin-associated S1P at the inception of AD in this model. Interestingly we detected a significant increase in C16 and C24 CER species following a 16-hour activation period. Furthermore, mRNA expression of ceramide producing enzymes CerS and ceramidase was increased within 3 hours of S1P stimulation.

Overall, this work features concerted interplay between MC/S1P/CER axis and early development of AD. These studies highlight MC and S1P as potential prophylactic targets that could interfere with disease onset and progression.

6.4 DOWN-REGULATION OF MIRNA 34A, 485 AND 486 REGULATES AD PATHOGENESIS

We report, for the first time, evidence for epigenetic regulation of pre-symptomatic remodeling in AD using an established mouse human AD-like model. We found that the skin exposure to Ag OVA triggered the downregulation of a unique miRNA triad whose predicted gene targets included AD-related cytokines/chemokines downstream of the MC/S1P signaling pathway. While the potential ability of these miRNA to regulate cellular infiltration has yet to be established, their down-regulation was accompanied with a significant increase in FC ϵ R1 α , SphK1 and CCL5 mRNA expression, predicted target genes coding for

cellular, enzymatic and molecular elements we already proved important to disease manifestation (Chapter 3).

Sonkoly *et al.* and Rebane *et al.* recently conducted miRNA profiling of human skin lesions and keratinocytes during chronic AD, compared to healthy controls (Rebane *et al.*, 2014; Sonkoly *et al.*, 2010). Importantly, their studies also identified down-regulation of miRNA 34a and 486, however without offering any mechanistic and/or functional insights. We demonstrate that these miRNA are similarly affected in mice and, more importantly, are affected at AD onset as well, highlighting their potential as prophylactic targets.

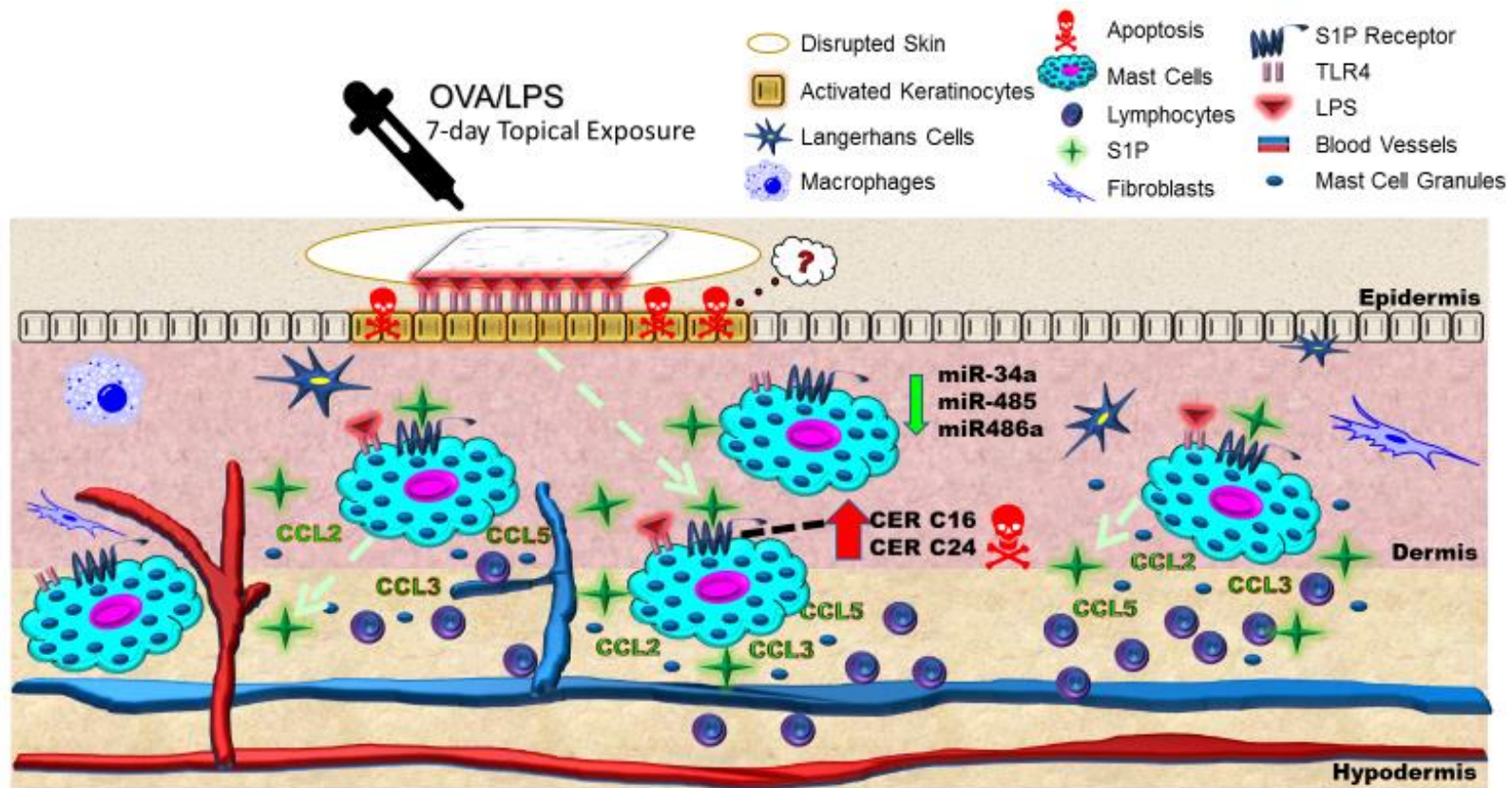


Figure 6.1 Inflammatory changes occur early after topical application of LPS-containing OVA in an established mouse human AD-like model. Skin shaving and tape-stripping first expose keratinocytes to LPS-containing OVA. LPS ligation of TLR4 on keratinocytes (and on MC) may result in S1P secretion that, in turn, can activate MC. MC activation leads to substantial local elevation of S1P and T cell-attracting chemokine CCL2, CCL3 and CCL5 release, resulting in cellular infiltration of the vascularized hypodermis. Furthermore, skin lipidomics revealed local increase in apoptosis-promoting ceramide (CER) species, due in part to MC. These pre-symptomatic effector mechanisms were epigenetically regulated by the down-regulation of miRNA 34a, 485 and 486a.

REFERENCES

- Aflaki, E., P. Doddapattar, B. Radović, S. Povoden, D. Kolb, N. Vujić, M. Wegscheider, H. Koefeler, T. Hornemann, W.F. Graier, R. Malli, F. Madeo, and D. Kratky. 2012. C16 ceramide is crucial for triacylglycerol-induced apoptosis in macrophages. *Cell Death Dis* 3:e280.
- Akin, C., P. Valent, and D.D. Metcalfe. 2010. Mast cell activation syndrome: Proposed diagnostic criteria. *J Allergy Clin Immunol* 126:1099-1104.e1094.
- Allende, M.L., T. Sasaki, H. Kawai, A. Olivera, Y. Mi, G. van Echten-Deckert, R. Hajdu, M. Rosenbach, C.A. Keohane, S. Mandala, S. Spiegel, and R.L. Proia. 2004. Mice deficient in sphingosine kinase 1 are rendered lymphopenic by FTY720. *J Biol Chem* 279:52487-52492.
- Anderson, J.C., A.L. Babb, and M.P. Hlastala. 2005. A fractal analysis of the radial distribution of bronchial capillaries around large airways. *J Appl Physiol* (1985) 98:850-855.
- Ando, T., K. Matsumoto, S. Namiranian, H. Yamashita, H. Glatthorn, M. Kimura, B.R. Dolan, J.J. Lee, S.J. Galli, Y. Kawakami, C. Jamora, and T. Kawakami. 2013. Mast cells are required for full expression of allergen/SEB-induced skin inflammation. *J Invest Dermatol* 133:2695-2705.

- Aon, M.A., M.R. Roussel, S. Cortassa, B. O'Rourke, D.B. Murray, M. Beckmann, and D. Lloyd. 2008. The scale-free dynamics of eukaryotic cells. *PLoS One* 3:e3624.
- Arock, M., E. Schneider, M. Boissan, V. Tricottet, and M. Dy. 2002. Differentiation of human basophils: an overview of recent advances and pending questions. *J Leukoc Biol* 71:557-564.
- Auriemma, M., G. Vianale, P. Amerio, and M. Reale. 2013. Cytokines and T cells in atopic dermatitis. *Eur Cytokine Netw* 24:37-44.
- Bieber, T. 2010. Atopic dermatitis. *Ann Dermatol* 22:125-137.
- Brown, J.H., V.K. Gupta, B.L. Li, B.T. Milne, C. Restrepo, and G.B. West. 2002. The fractal nature of nature: power laws, ecological complexity and biodiversity. *Philos Trans R Soc Lond B Biol Sci* 357:619-626.
- Butterfield, J.H., D. Weiler, G. Dewald, and G.J. Gleich. 1988. Establishment of an immature mast cell line from a patient with mast cell leukemia. *Leuk Res* 12:345-355.
- Chang, Y.C., J.D. Wang, K.K. Svoboda, R.P. Casillas, J.D. Laskin, M.K. Gordon, and D.R. Gerecke. 2013. Sulfur mustard induces an endoplasmic reticulum stress response in the mouse ear vesicant model. *Toxicol Appl Pharmacol* 268:178-187.
- Chumanevich, A., P. Wedman, and C.A. Oskeritzian. 2016. Sphingosine-1-Phosphate/Sphingosine-1-Phosphate Receptor 2 Axis Can Promote Mouse and Human Primary Mast Cell Angiogenic Potential through Upregulation

- of Vascular Endothelial Growth Factor-A and Matrix Metalloproteinase-2. *Mediators of Inflammation* 2016:8.
- da Silva, E.Z., M.C. Jamur, and C. Oliver. 2014. Mast cell function: a new vision of an old cell. *J Histochem Cytochem* 62:698-738.
- Damsgaard, T.E., A.B. Olesen, F.B. Sørensen, K. Thestrup-Pedersen, and P.O. Schiøtz. 1997. Mast cells and atopic dermatitis. Stereological quantification of mast cells in atopic dermatitis and normal human skin. *Arch Dermatol Res* 289:256-260.
- Darlenski, R., J. Kazandjieva, E. Hristakieva, and J.W. Fluhr. 2014. Atopic dermatitis as a systemic disease. *Clin Dermatol* 32:409-413.
- Di Ieva, A. 2012. Fractal analysis of microvascular networks in malignant brain tumors. *Clin Neuropathol* 31:342-351.
- Di Ieva, A., F. Grizzi, G. Ceva-Grimaldi, C. Russo, P. Gaetani, E. Aimar, D. Levi, P. Pisano, F. Tancioni, G. Nicola, M. Tschabitscher, N. Dioguardi, and R.R. Baena. 2007. Fractal dimension as a quantifier of the microvasculature of normal and adenomatous pituitary tissue. *J Anat* 211:673-680.
- Dillahunt, S.E., J.L. Sargent, R. Suzuki, R.L. Proia, A. Gilfillan, J. Rivera, and A. Olivera. 2013. Usage of sphingosine kinase isoforms in mast cells is species and/or cell type determined. *J Immunol* 190:2058-2067.
- Dioguardi, N., F. Grizzi, B. Fiamengo, and C. Russo. 2008. Metrically measuring liver biopsy: a chronic hepatitis B and C computer-aided morphologic description. *World J Gastroenterol* 14:7335-7344.

- Dioguardi, N., F. Grizzi, B. Franceschini, P. Bossi, and C. Russo. 2006. Liver fibrosis and tissue architectural change measurement using fractal-rectified metrics and Hurst's exponent. *World J Gastroenterol* 12:2187-2194.
- Dong, L., H. Li, S. Wang, and Y. Li. 2009. Different doses of lipopolysaccharides regulate the lung inflammation of asthmatic mice via TLR4 pathway in alveolar macrophages. *J Asthma* 46:229-233.
- Doubal, F.N., T.J. MacGillivray, N. Patton, B. Dhillon, M.S. Dennis, and J.M. Wardlaw. 2010. Fractal analysis of retinal vessels suggests that a distinct vasculopathy causes lacunar stroke. *Neurology* 74:1102-1107.
- Dudeck, A., J. Dudeck, J. Scholten, A. Petzold, S. Surianarayanan, A. Köhler, K. Peschke, D. Vöhringer, C. Waskow, T. Krieg, W. Müller, A. Waisman, K. Hartmann, M. Gunzer, and A. Roers. 2011. Mast cells are key promoters of contact allergy that mediate the adjuvant effects of haptens. *Immunity* 34:973-984.
- Eisenbarth, S.C., D.A. Piggott, J.W. Huleatt, I. Visintin, C.A. Herrick, and K. Bottomly. 2002. Lipopolysaccharide-enhanced, toll-like receptor 4-dependent T helper cell type 2 responses to inhaled antigen. *J Exp Med* 196:1645-1651.
- Elias, P.M. 2014. Lipid abnormalities and lipid-based repair strategies in atopic dermatitis. *Biochim Biophys Acta* 1841:323-330.
- Ewald, D.A., D. Malajian, J.G. Krueger, C.T. Workman, T. Wang, S. Tian, T. Litman, E. Guttman-Yassky, and M. Suárez-Fariñas. 2015. Meta-analysis derived atopic dermatitis (MADAD) transcriptome defines a robust AD

- signature highlighting the involvement of atherosclerosis and lipid metabolism pathways. *BMC Med Genomics* 8:60.
- Eyerich, K., and N. Novak. 2013. Immunology of atopic eczema: overcoming the Th1/Th2 paradigm. *Allergy* 68:974-982.
- Ferro, D.P., M.A. Falconi, R.L. Adam, M.M. Ortega, C.P. Lima, C.A. de Souza, I. Lorand-Metze, and K. Metze. 2011. Fractal characteristics of May-Grünwald-Giemsa stained chromatin are independent prognostic factors for survival in multiple myeloma. *PLoS One* 6:e20706.
- Feyerabend, T.B., A. Weiser, A. Tietz, M. Stassen, N. Harris, M. Kopf, P. Radermacher, P. Möller, C. Benoist, D. Mathis, H.J. Fehling, and H.R. Rodewald. 2011. Cre-mediated cell ablation contests mast cell contribution in models of antibody- and T cell-mediated autoimmunity. *Immunity* 35:832-844.
- Fuseler, J.W., A. Bedenbaugh, K. Yekkala, and T.A. Baudino. 2010. Fractal and image analysis of the microvasculature in normal intestinal submucosa and intestinal polyps in Apc(Min/+) mice. *Microsc Microanal* 16:73-79.
- Fuseler, J.W., D.M. Merrill, J.A. Rogers, M.B. Grisham, and R.E. Wolf. 2006. Analysis and quantitation of NF-kappaB nuclear translocation in tumor necrosis factor alpha (TNF-alpha) activated vascular endothelial cells. *Microsc Microanal* 12:269-276.
- Fuseler, J.W., C.F. Millette, J.M. Davis, and W. Carver. 2007. Fractal and image analysis of morphological changes in the actin cytoskeleton of neonatal

- cardiac fibroblasts in response to mechanical stretch. *Microsc Microanal* 13:133-143.
- Fuseler, J.W., and M.T. Valarmathi. 2012. Modulation of the migration and differentiation potential of adult bone marrow stromal stem cells by nitric oxide. *Biomaterials* 33:1032-1043.
- Futerman, A.H., and H. Riezman. 2005. The ins and outs of sphingolipid synthesis. *Trends Cell Biol* 15:312-318.
- Galli, S.J., N. Borregaard, and T.A. Wynn. 2011. Phenotypic and functional plasticity of cells of innate immunity: macrophages, mast cells and neutrophils. *Nat Immunol* 12:1035-1044.
- Galli, S.J., M. Grimbaldston, and M. Tsai. 2008. Immunomodulatory mast cells: negative, as well as positive, regulators of immunity. *Nat Rev Immunol* 8:478-486.
- Galli, S.J., and M. Tsai. 2012. IgE and mast cells in allergic disease. *Nat Med* 18:693-704.
- Galli, S.J., M. Tsai, T. Marichal, E. Tchougounova, L.L. Reber, and G. Pejler. 2015. Approaches for analyzing the roles of mast cells and their proteases in vivo. *Adv Immunol* 126:45-127.
- Gerber, P.A., B.A. Buhren, H. Schruppf, B. Homey, A. Zlotnik, and P. Hevezi. 2014. The top skin-associated genes: a comparative analysis of human and mouse skin transcriptomes. *Biol Chem* 395:577-591.
- Giannou, A.D., A. Marazioti, M. Spella, N.I. Kanellakis, H. Apostolopoulou, I. Psallidas, Z.M. Prijovich, M. Vreka, D.E. Zazara, I. Lilis, V.

- Papaleonidopoulos, C.A. Kairi, A.L. Patmanidi, I. Giopanou, N. Spiropoulou, V. Harokopos, V. Aidinis, D. Spyrtos, S. Telioussi, H. Papadaki, S. Taraviras, L.A. Snyder, O. Eickelberg, D. Kardamakis, Y. Iwakura, T.B. Feyerabend, H.R. Rodewald, I. Kalomenidis, T.S. Blackwell, T. Agaliofi, and G.T. Stathopoulos. 2015. Mast cells mediate malignant pleural effusion formation. *J Clin Invest* 125:2317-2334.
- Gittler, J.K., A. Shemer, M. Suárez-Fariñas, J. Fuentes-Duculan, K.J. Gulewicz, C.Q. Wang, H. Mitsui, I. Cardinale, C. de Guzman Strong, J.G. Krueger, and E. Guttman-Yassky. 2012. Progressive activation of T(H)2/T(H)22 cytokines and selective epidermal proteins characterizes acute and chronic atopic dermatitis. *J Allergy Clin Immunol* 130:1344-1354.
- Gonzalo, J.A., Y. Qiu, J.M. Lora, A. Al-Garawi, J.L. Villeval, J.A. Boyce, C. Martinez-A, G. Marquez, I. Goya, Q. Hamid, C.C. Fraser, D. Picarella, J. Cote-Sierra, M.R. Hodge, J.C. Gutierrez-Ramos, R. Kolbeck, and A.J. Coyle. 2007. Coordinated involvement of mast cells and T cells in allergic mucosal inflammation: critical role of the CC chemokine ligand 1:CCR8 axis. *J Immunol* 179:1740-1750.
- Graham, M.T., and K.C. Nadeau. 2014. Lessons learned from mice and man: mimicking human allergy through mouse models. *Clin Immunol* 155:1-16.
- Griffith, J.W., C.L. Sokol, and A.D. Luster. 2014. Chemokines and chemokine receptors: positioning cells for host defense and immunity. *Annu Rev Immunol* 32:659-702.

- Grimbaldeston, M.A., C.C. Chen, A.M. Piliponsky, M. Tsai, S.Y. Tam, and S.J. Galli. 2005. Mast cell-deficient *W-shash c-kit* mutant *Kit W-sh/W-sh* mice as a model for investigating mast cell biology in vivo. *Am J Pathol* 167:835-848.
- Grizzi, F., and N. Dioguardi. 1999. A fractal scoring system for quantifying active collagen synthesis during chronic liverdisease. *Int J Chaos Theo Appl* 21:262 – 266.
- Grizzi, F., C. Russo, P. Colombo, B. Franceschini, E.E. Frezza, E. Cobos, and M. Chiriva-Internati. 2005. Quantitative evaluation and modeling of two-dimensional neovascular network complexity: the surface fractal dimension. *BMC Cancer* 5:14.
- Grösch, S., S. Schiffmann, and G. Geisslinger. 2012. Chain length-specific properties of ceramides. *Prog Lipid Res* 51:50-62.
- Haas, N., K. Hamann, J. Grabbe, and B.M. Czarnetzki. 1993. Demonstration of the high-affinity IgE receptor (Fc epsilon RI) on Langerhans cells of oral mucosa. *Exp Dermatol* 2:157-160.
- Hait, N.C., J. Allegood, M. Maceyka, G.M. Strub, K.B. Harikumar, S.K. Singh, C. Luo, R. Marmorstein, T. Kordula, S. Milstien, and S. Spiegel. 2009. Regulation of histone acetylation in the nucleus by sphingosine-1-phosphate. *Science* 325:1254-1257.
- Hamilton, M.J., J.L. Hornick, C. Akin, M.C. Castells, and N.J. Greenberger. 2011. Mast cell activation syndrome: a newly recognized disorder with systemic clinical manifestations. *J Allergy Clin Immunol* 128:147-152.e142.

- Hart, P.H., M.A. Grimbaldston, E.K. Hosszu, G.J. Swift, F.P. Noonan, and J.J. Finlay-Jones. 1999. Age-related changes in dermal mast cell prevalence in BALB/c mice: functional importance and correlation with dermal mast cell expression of Kit. *Immunology* 98:352-356.
- Hart, P.H., M.A. Grimbaldston, G.J. Swift, A. Jaksic, F.P. Noonan, and J.J. Finlay-Jones. 1998. Dermal mast cells determine susceptibility to ultraviolet B-induced systemic suppression of contact hypersensitivity responses in mice. *J Exp Med* 187:2045-2053.
- He, R., M.K. Oyoshi, H. Jin, and R.S. Geha. 2007. Epicutaneous antigen exposure induces a Th17 response that drives airway inflammation after inhalation challenge. *Proc Natl Acad Sci U S A* 104:15817-15822.
- Janssens, M., J. van Smeden, G.S. Gooris, W. Bras, G. Portale, P.J. Caspers, R.J. Vreeken, T. Hankemeier, S. Kezic, R. Wolterbeek, A.P. Lavrijsen, and J.A. Bouwstra. 2012. Increase in short-chain ceramides correlates with an altered lipid organization and decreased barrier function in atopic eczema patients. *J Lipid Res* 53:2755-2766.
- Japtok, L., W. Bäumer, and B. Kleuser. 2014. Sphingosine-1-phosphate as signaling molecule in the skin: Relevance in atopic dermatitis. *Allergo J Int* 23:54-59.
- Japtok, L., K. Schaper, W. Bäumer, H.H. Radeke, S.K. Jeong, and B. Kleuser. 2012. Sphingosine 1-phosphate modulates antigen capture by murine Langerhans cells via the S1P2 receptor subtype. *PLoS One* 7:e49427.

- Jelinek, H.F., D. Ristanović, and N.T. Milošević. 2011. The morphology and classification of α ganglion cells in the rat retinae: a fractal analysis study. *J Neurosci Methods* 201:281-287.
- Jolly, P.S., M. Bektas, A. Olivera, C. Gonzalez-Espinosa, R.L. Proia, J. Rivera, S. Milstien, and S. Spiegel. 2004. Transactivation of sphingosine-1-phosphate receptors by FcepsilonRI triggering is required for normal mast cell degranulation and chemotaxis. *J Exp Med* 199:959-970.
- Kalesnikoff, J., and S.J. Galli. 2008. New developments in mast cell biology. *Nat Immunol* 9:1215-1223.
- Kalesnikoff, J., and S.J. Galli. 2011. Antiinflammatory and immunosuppressive functions of mast cells. *Methods Mol Biol* 677:207-220.
- Kanto, T., P. Kalinski, O.C. Hunter, M.T. Lotze, and A.A. Amoscato. 2001. Ceramide mediates tumor-induced dendritic cell apoptosis. *J Immunol* 167:3773-3784.
- Karahatay, S., K. Thomas, S. Koybasi, C.E. Senkal, S. Elojeimy, X. Liu, J. Bielawski, T.A. Day, M.B. Gillespie, D. Sinha, J.S. Norris, Y.A. Hannun, and B. Ogretmen. 2007. Clinical relevance of ceramide metabolism in the pathogenesis of human head and neck squamous cell carcinoma (HNSCC): attenuation of C(18)-ceramide in HNSCC tumors correlates with lymphovascular invasion and nodal metastasis. *Cancer Lett* 256:101-111.
- Kawakami, T., T. Ando, M. Kimura, B.S. Wilson, and Y. Kawakami. 2009. Mast cells in atopic dermatitis. *Curr Opin Immunol* 21:666-678.

- Kendall, A.C., and A. Nicolaou. 2013. Bioactive lipid mediators in skin inflammation and immunity. *Prog Lipid Res* 52:141-164.
- Kim, J.Y., M.S. Jeong, M.K. Park, M.K. Lee, and S.J. Seo. 2014. Time-dependent progression from the acute to chronic phases in atopic dermatitis induced by epicutaneous allergen stimulation in NC/Nga mice. *Exp Dermatol* 23:53-57.
- Kirshenbaum, A.S., C. Akin, Y. Wu, M. Rottem, J.P. Goff, M.A. Beaven, V.K. Rao, and D.D. Metcalfe. 2003. Characterization of novel stem cell factor responsive human mast cell lines LAD 1 and 2 established from a patient with mast cell sarcoma/leukemia; activation following aggregation of FcepsilonRI or FcgammaRI. *Leuk Res* 27:677-682.
- Kitamura, Y. 1989. Heterogeneity of mast cells and phenotypic change between subpopulations. *Annu Rev Immunol* 7:59-76.
- Lagunoff, D. 1974. Analysis of dye binding sites in mast cell granules. *Biochemistry* 13:3982-3986.
- Laidlaw, T.M., J.W. Steinke, A.M. Tiñana, C. Feng, W. Xing, B.K. Lam, S. Paruchuri, J.A. Boyce, and L. Borish. 2011. Characterization of a novel human mast cell line that responds to stem cell factor and expresses functional FcεRI. *J Allergy Clin Immunol* 127:815-822.e811-815.
- Leung, D.Y., and E. Guttman-Yassky. 2014. Deciphering the complexities of atopic dermatitis: shifting paradigms in treatment approaches. *J Allergy Clin Immunol* 134:769-779.

- Lilla, J.N., C.C. Chen, K. Mukai, M.J. BenBarak, C.B. Franco, J. Kalesnikoff, M. Yu, M. Tsai, A.M. Piliponsky, and S.J. Galli. 2011. Reduced mast cell and basophil numbers and function in Cpa3-Cre; Mcl-1fl/fl mice. *Blood* 118:6930-6938.
- Liu, F.T., H. Goodarzi, and H.Y. Chen. 2011. IgE, mast cells, and eosinophils in atopic dermatitis. *Clin Rev Allergy Immunol* 41:298-310.
- Longato, L., K. Ripp, M. Setshedi, M. Dostalek, F. Akhlaghi, M. Branda, J.R. Wands, and S.M. de la Monte. 2012. Insulin resistance, ceramide accumulation, and endoplasmic reticulum stress in human chronic alcohol-related liver disease. *Oxid Med Cell Longev* 2012:479348.
- Malajian, D., and E. Guttman-Yassky. 2015. New pathogenic and therapeutic paradigms in atopic dermatitis. *Cytokine* 73:311-318.
- Mandelbrot, B.B. 1983. The fractal geometry of nature. W.H. Freeman and Company, New York. 468 p., 416 p. of plates pp.
- Manera, M., B.S. Dezfuli, C. Borreca, and L. Giari. 2014. The use of fractal dimension and lacunarity in the characterization of mast cell degranulation in rainbow trout (*Onchorhynchus mykiss*). *J Microsc* 256:82-89.
- Marshall, J.S. 2004. Mast-cell responses to pathogens. *Nat Rev Immunol* 4:787-799.
- McAlpine, S.M., T.B. Issekutz, and J.S. Marshall. 2012. Virus stimulation of human mast cells results in the recruitment of CD56⁺ T cells by a mechanism dependent on CCR5 ligands. *FASEB J* 26:1280-1289.

- McNally, J.G., and D. Mazza. 2010. Fractal geometry in the nucleus. *EMBO J* 29:2-3.
- Metzger, H., G. Alcaraz, R. Hohman, J.P. Kinet, V. Pribluda, and R. Quarto. 1986. The receptor with high affinity for immunoglobulin E. *Annu Rev Immunol* 4:419-470.
- Miller, D.W., S.B. Koch, B.A. Yentzer, A.R. Clark, J.R. O'Neill, J. Fountain, T.M. Weber, and A.B. Fleischer. 2011. An over-the-counter moisturizer is as clinically effective as, and more cost-effective than, prescription barrier creams in the treatment of children with mild-to-moderate atopic dermatitis: a randomized, controlled trial. *J Drugs Dermatol* 10:531-537.
- Millrud, C.R., T. Hylander, S. Kumlien Georen, Å. Kågedal, O. Winqvist, and L.O. Cardell. 2014. Inverse immunological responses induced by allergic rhinitis and head and neck squamous cell carcinoma. *PLoS One* 9:e86796.
- Mitra, P., C.A. Oskeritzian, S.G. Payne, M.A. Beaven, S. Milstien, and S. Spiegel. 2006. Role of ABCC1 in export of sphingosine-1-phosphate from mast cells. *Proc Natl Acad Sci U S A* 103:16394-16399.
- Mizutani, Y., S. Mitsutake, K. Tsuji, A. Kihara, and Y. Igarashi. 2009. Ceramide biosynthesis in keratinocyte and its role in skin function. *Biochimie* 91:784-790.
- Moledina, S., A. de Bruyn, S. Schievano, C.M. Owens, C. Young, S.G. Haworth, A.M. Taylor, I. Schulze-Neick, and V. Muthurangu. 2011. Fractal branching quantifies vascular changes and predicts survival in pulmonary hypertension: a proof of principle study. *Heart* 97:1245-1249.

- Moon, T.C., A.D. Befus, and M. Kulka. 2014. Mast cell mediators: their differential release and the secretory pathways involved. *Front Immunol* 5:569.
- Mu, Z., Y. Zhao, X. Liu, C. Chang, and J. Zhang. 2014. Molecular biology of atopic dermatitis. *Clin Rev Allergy Immunol* 47:193-218.
- Mullen, T.D., R.W. Jenkins, C.J. Clarke, J. Bielawski, Y.A. Hannun, and L.M. Obeid. 2011. Ceramide synthase-dependent ceramide generation and programmed cell death: involvement of salvage pathway in regulating postmitochondrial events. *J Biol Chem* 286:15929-15942.
- Nakamura, Y., J. Oscherwitz, K.B. Cease, S.M. Chan, R. Muñoz-Planillo, M. Hasegawa, A.E. Villaruz, G.Y. Cheung, M.J. McGavin, J.B. Travers, M. Otto, N. Inohara, and G. Núñez. 2013. Staphylococcus δ -toxin induces allergic skin disease by activating mast cells. *Nature* 503:397-401.
- Nezadal, M., Z. O., and B. M. 2001. The Box-Counting: Critical Study, 4th Conference on Prediction, Synergetic and Mre. HarFa software. In The Faculty of Management, Institute of Information Technologies, Faculty of Technology, Tomas Bata University in Zlin .
- Nussbaum, C., S. Bannenberg, P. Keul, M.H. Gräler, C.F. Gonçalves-de-Albuquerque, H. Korhonen, K. von Wnuck Lipinski, G. Heusch, H.C. de Castro Faria Neto, I. Rohwedder, J.R. Göthert, V.P. Prasad, G. Haufe, B. Lange-Sperandio, S. Offermanns, M. Sperandio, and B. Levkau. 2015. Sphingosine-1-phosphate receptor 3 promotes leukocyte rolling by mobilizing endothelial P-selectin. *Nat Commun* 6:6416.

- Ohsawa, Y., and N. Hirasawa. 2012. The antagonism of histamine H1 and H4 receptors ameliorates chronic allergic dermatitis via anti-pruritic and anti-inflammatory effects in NC/Nga mice. *Allergy* 67:1014-1022.
- Oizumi, A., H. Nakayama, N. Okino, C. Iwahara, K. Kina, R. Matsumoto, H. Ogawa, K. Takamori, M. Ito, Y. Suga, and K. Iwabuchi. 2014. Pseudomonas-derived ceramidase induces production of inflammatory mediators from human keratinocytes via sphingosine-1-phosphate. *PLoS One* 9:e89402.
- Oldford, S.A., and J.S. Marshall. 2015. Mast cells as targets for immunotherapy of solid tumors. *Mol Immunol* 63:113-124.
- Olivera, A., N. Urtz, K. Mizugishi, Y. Yamashita, A.M. Gilfillan, Y. Furumoto, H. Gu, R.L. Proia, T. Baumruker, and J. Rivera. 2006. IgE-dependent activation of sphingosine kinases 1 and 2 and secretion of sphingosine 1-phosphate requires Fyn kinase and contributes to mast cell responses. *J Biol Chem* 281:2515-2525.
- Oskeritzian, C.A. 2015. Mast cell plasticity and sphingosine-1-phosphate in immunity, inflammation and cancer. *Mol Immunol* 63:104-112.
- Oskeritzian, C.A., S.E. Alvarez, N.C. Hait, M.M. Price, S. Milstien, and S. Spiegel. 2008. Distinct roles of sphingosine kinases 1 and 2 in human mast-cell functions. *Blood* 111:4193-4200.
- Oskeritzian, C.A., N.C. Hait, P. Wedman, A. Chumanevich, E.M. Kolawole, M.M. Price, Y.T. Falanga, K.B. Harikumar, J.J. Ryan, S. Milstien, R. Sabbadini, and S. Spiegel. 2015. The sphingosine-1-phosphate/sphingosine-1-phosphate receptor 2 axis regulates early airway T-cell infiltration in murine

- mast cell-dependent acute allergic responses. *J Allergy Clin Immunol* 135:1008-1018.e1001.
- Oskeritzian, C.A., S. Milstien, and S. Spiegel. 2007. Sphingosine-1-phosphate in allergic responses, asthma and anaphylaxis. *Pharmacol Ther* 115:390-399.
- Oskeritzian, C.A., M.M. Price, N.C. Hait, D. Kapitonov, Y.T. Falanga, J.K. Morales, J.J. Ryan, S. Milstien, and S. Spiegel. 2010. Essential roles of sphingosine-1-phosphate receptor 2 in human mast cell activation, anaphylaxis, and pulmonary edema. *J Exp Med* 207:465-474.
- Oskeritzian, C.A., W. Zhao, H.K. Min, H.Z. Xia, A. Pozez, J. Kiev, and L.B. Schwartz. 2005. Surface CD88 functionally distinguishes the MCTC from the MCT type of human lung mast cell. *J Allergy Clin Immunol* 115:1162-1168.
- Otsuka, A., M. Kubo, T. Honda, G. Egawa, S. Nakajima, H. Tanizaki, B. Kim, S. Matsuoka, T. Watanabe, S. Nakae, Y. Miyachi, and K. Kabashima. 2011. Requirement of interaction between mast cells and skin dendritic cells to establish contact hypersensitivity. *PLoS One* 6:e25538.
- Park, K., S. Lee, and Y.M. Lee. 2013. Sphingolipids and antimicrobial peptides: function and roles in atopic dermatitis. *Biomol Ther (Seoul)* 21:251-257.
- Park, Y.H., W.H. Jang, J.A. Seo, M. Park, T.R. Lee, D.K. Kim, and K.M. Lim. 2012. Decrease of ceramides with very long-chain fatty acids and downregulation of elongases in a murine atopic dermatitis model. *J Invest Dermatol* 132:476-479.

- Patrizi, A., A. Pileri, F. Bellini, B. Raone, I. Neri, and G. Ricci. 2011. Atopic dermatitis and the atopic march: what is new? *J Allergy (Cairo)* 2011:279425.
- Plank, M., S. Maltby, J. Mattes, and P.S. Foster. 2013. Targeting translational control as a novel way to treat inflammatory disease: the emerging role of microRNAs. *Clin Exp Allergy* 43:981-999.
- Price, M.M., C.A. Oskeritzian, Y.T. Falanga, K.B. Harikumar, J.C. Allegood, S.E. Alvarez, D. Conrad, J.J. Ryan, S. Milstien, and S. Spiegel. 2013. A specific sphingosine kinase 1 inhibitor attenuates airway hyperresponsiveness and inflammation in a mast cell-dependent murine model of allergic asthma. *J Allergy Clin Immunol* 131:501-511.e501.
- Qian, A.R., D. Li, J. Han, X. Gao, S.M. Di, W. Zhang, L.F. Hu, and P. Shang. 2012. Fractal dimension as a measure of altered actin cytoskeleton in MC3T3-E1 cells under simulated microgravity using 3-D/2-D clinostats. *IEEE Trans Biomed Eng* 59:1374-1380.
- Rafail, S., I. Kourtzelis, P.G. Foukas, M.M. Markiewski, R.A. DeAngelis, M. Guariento, D. Ricklin, E.A. Grice, and J.D. Lambris. 2015. Complement deficiency promotes cutaneous wound healing in mice. *J Immunol* 194:1285-1291.
- Rebane, A., T. Runnel, A. Aab, J. Maslovskaja, B. Rückert, M. Zimmermann, M. Plaas, J. Kärner, A. Treis, M. Pihlap, U. Haljasorg, H. Hermann, N. Nagy, L. Kemeny, T. Erm, K. Kingo, M. Li, M.P. Boldin, and C.A. Akdis. 2014. MicroRNA-146a alleviates chronic skin inflammation in atopic dermatitis

- through suppression of innate immune responses in keratinocytes. *J Allergy Clin Immunol* 134:836-847.e811.
- Reber, L.L., T. Marichal, and S.J. Galli. 2012. New models for analyzing mast cell functions in vivo. *Trends Immunol* 33:613-625.
- Reber, L.L., T. Marichal, J. Sokolove, P. Starkl, N. Gaudenzio, Y. Iwakura, H. Karasuyama, L.B. Schwartz, W.H. Robinson, M. Tsai, and S.J. Galli. 2014. Contribution of mast cell-derived interleukin-1 β to uric acid crystal-induced acute arthritis in mice. *Arthritis Rheumatol* 66:2881-2891.
- Reines, I., M. Kietzmann, R. Mischke, T. Tschernig, A. Lüth, B. Kleuser, and W. Bäumer. 2009. Topical application of sphingosine-1-phosphate and FTY720 attenuate allergic contact dermatitis reaction through inhibition of dendritic cell migration. *J Invest Dermatol* 129:1954-1962.
- Ribatti, D. 2013. Mast cells and macrophages exert beneficial and detrimental effects on tumor progression and angiogenesis. *Immunol Lett* 152:83-88.
- Rivera, J., R.L. Proia, and A. Olivera. 2008. The alliance of sphingosine-1-phosphate and its receptors in immunity. *Nat Rev Immunol* 8:753-763.
- Rogers, J.A., and J.W. Fuseler. 2007. Regulation of NF-kappaB activation and nuclear translocation by exogenous nitric oxide (NO) donors in TNF-alpha activated vascular endothelial cells. *Nitric Oxide* 16:379-391.
- Sawaguchi, M., S. Tanaka, Y. Nakatani, Y. Harada, K. Mukai, Y. Matsunaga, K. Ishiwata, K. Oboki, T. Kambayashi, N. Watanabe, H. Karasuyama, S. Nakae, H. Inoue, and M. Kubo. 2012. Role of mast cells and basophils in

- IgE responses and in allergic airway hyperresponsiveness. *J Immunol* 188:1809-1818.
- Schiffmann, S., J. Sandner, K. Birod, I. Wobst, C. Angioni, E. Ruckhäberle, M. Kaufmann, H. Ackermann, J. Lötsch, H. Schmidt, G. Geisslinger, and S. Grösch. 2009. Ceramide synthases and ceramide levels are increased in breast cancer tissue. *Carcinogenesis* 30:745-752.
- Schwartz, L. 2005. Analysis of MC_T and MC_{TC} Mast Cells in Tissue. *Methods in Molecular Biology*
- Schwartz, L.B., D.D. Metcalfe, J.S. Miller, H. Earl, and T. Sullivan. 1987. Tryptase levels as an indicator of mast-cell activation in systemic anaphylaxis and mastocytosis. *N Engl J Med* 316:1622-1626.
- Sedivy, R., S. Thurner, A.C. Budinsky, W.J. Köstler, and C.C. Zielinski. 2002. Short-term rhythmic proliferation of human breast cancer cell lines: surface effects and fractal growth patterns. *J Pathol* 197:163-169.
- Sehra, S., A.P. Serezani, J.A. Ocaña, J.B. Travers, and M.H. Kaplan. 2016. Mast Cells Regulate Epidermal Barrier Function and the Development of Allergic Skin Inflammation. *J Invest Dermatol* 136:1429-1437.
- Seumois, G., M. Fillet, L. Gillet, C. Faccinnetto, C. Desmet, C. François, B. Dewals, C. Oury, A. Vanderplasschen, P. Lekeux, and F. Bureau. 2007. De novo C16- and C24-ceramide generation contributes to spontaneous neutrophil apoptosis. *J Leukoc Biol* 81:1477-1486.
- Simon, D., and T. Bieber. 2014. Systemic therapy for atopic dermatitis. *Allergy* 69:46-55.

- Skolová, B., K. Hudská, P. Pullmannová, A. Kováčik, K. Palát, J. Roh, J. Fleddermann, I. Estrela-Lopis, and K. Vávrová. 2014. Different phase behavior and packing of ceramides with long (C16) and very long (C24) acyls in model membranes: infrared spectroscopy using deuterated lipids. *J Phys Chem B* 118:10460-10470.
- Smith, T.G., G.D. Lange, and W.B. Marks. 1996. Fractal methods and results in cellular morphology--dimensions, lacunarity and multifractals. *J Neurosci Methods* 69:123-136.
- Sonkoly, E., P. Janson, M.L. Majuri, T. Savinko, N. Fyhrquist, L. Eidsmo, N. Xu, F. Meisgen, T. Wei, M. Bradley, J. Stenvang, S. Kauppinen, H. Alenius, A. Lauerma, B. Homey, O. Winqvist, M. Stähle, and A. Pivarcsi. 2010. MiR-155 is overexpressed in patients with atopic dermatitis and modulates T-cell proliferative responses by targeting cytotoxic T lymphocyte-associated antigen 4. *J Allergy Clin Immunol* 126:581-589.e581-520.
- Sonkoly, E., T. Wei, P.C. Janson, A. Sääf, L. Lundeberg, M. Tengvall-Linder, G. Norstedt, H. Alenius, B. Homey, A. Scheynius, M. Stähle, and A. Pivarcsi. 2007. MicroRNAs: novel regulators involved in the pathogenesis of psoriasis? *PLoS One* 2:e610.
- Spergel, J.M., E. Mizoguchi, J.P. Brewer, T.R. Martin, A.K. Bhan, and R.S. Geha. 1998. Epicutaneous sensitization with protein antigen induces localized allergic dermatitis and hyperresponsiveness to methacholine after single exposure to aerosolized antigen in mice. *J Clin Invest* 101:1614-1622.

- Spiegel, S., and S. Milstien. 2011. The outs and the ins of sphingosine-1-phosphate in immunity. *Nat Rev Immunol* 11:403-415.
- Stein, M.M., C.L. Hrusch, J. Gozdz, C. Igartua, V. Pivniouk, S.E. Murray, J.G. Ledford, M. Marques dos Santos, R.L. Anderson, N. Metwali, J.W. Neilson, R.M. Maier, J.A. Gilbert, M. Holbreich, P.S. Thorne, F.D. Martinez, E. von Mutius, D. Vercelli, C. Ober, and A.I. Sperling. 2016. Innate Immunity and Asthma Risk in Amish and Hutterite Farm Children. *N Engl J Med* 375:411-421.
- Stenvang, J., A. Petri, M. Lindow, S. Obad, and S. Kauppinen. 2012. Inhibition of microRNA function by antimiR oligonucleotides. *Silence* 3:1.
- Streba, L., M.C. ForȚofoiu, C. Popa, D. Ciobanu, C.L. Gruia, S. Mogoantă, and C.T. Streba. 2015. A pilot study on the role of fractal analysis in the microscopic evaluation of colorectal cancers. *Rom J Morphol Embryol* 56:191-196.
- Sulcova, J., M. Meyer, E. Guiducci, T.B. Feyerabend, H.R. Rodewald, and S. Werner. 2015. Mast cells are dispensable in a genetic mouse model of chronic dermatitis. *Am J Pathol* 185:1575-1587.
- Sun, W.Y., D.P. Dimasi, M.R. Pitman, Y. Zhuang, R. Heddle, S.M. Pitson, M.A. Grimbaldeston, and C.S. Bonder. 2016. Topical Application of Fingolimod Perturbs Cutaneous Inflammation. *J Immunol* 196:3854-3864.
- Suárez-Fariñas, M., B. Ungar, J. Correa da Rosa, D.A. Ewald, M. Rozenblit, J. Gonzalez, H. Xu, X. Zheng, X. Peng, Y.D. Estrada, S.R. Dillon, J.G. Krueger, and E. Guttman-Yassky. 2015. RNA sequencing atopic dermatitis

- transcriptome profiling provides insights into novel disease mechanisms with potential therapeutic implications. *J Allergy Clin Immunol* 135:1218-1227.
- Szegedi, K., R. Lutter, P.C. Res, J.D. Bos, R.M. Luiten, S. Kezic, and M.A. Middelkamp-Hup. 2015. Cytokine profiles in interstitial fluid from chronic atopic dermatitis skin. *J Eur Acad Dermatol Venereol*
- Thamrin, C., G. Stern, and U. Frey. 2010. Fractals for physicians. *Paediatr Respir Rev* 11:123-131.
- Theoharides, T.C., K.D. Alysandratos, A. Angelidou, D.A. Delivanis, N. Sismanopoulos, B. Zhang, S. Asadi, M. Vasiadi, Z. Weng, A. Miniati, and D. Kalogeromitros. 2012. Mast cells and inflammation. *Biochim Biophys Acta* 1822:21-33.
- Tirodkar, T.S., P. Lu, A. Bai, M.J. Scheffel, S. Gencer, E. Garrett-Mayer, A. Bielawska, B. Ogretmen, and C. Voelkel-Johnson. 2015. Expression of Ceramide Synthase 6 Transcriptionally Activates Acid Ceramidase in a c-Jun N-terminal Kinase (JNK)-dependent Manner. *J Biol Chem* 290:13157-13167.
- Valent, P., H.P. Horny, M. Triggiani, and M. Arock. 2011. Clinical and laboratory parameters of mast cell activation as basis for the formulation of diagnostic criteria. *Int Arch Allergy Immunol* 156:119-127.
- van Smeden, J., L. Hoppel, R. van der Heijden, T. Hankemeier, R.J. Vreeken, and J.A. Bouwstra. 2011. LC/MS analysis of stratum corneum lipids: ceramide profiling and discovery. *J Lipid Res* 52:1211-1221.

- Voehringer, D. 2013. Protective and pathological roles of mast cells and basophils. *Nat Rev Immunol* 13:362-375.
- Walter, R.J., and M.W. Berns. 1981. Computer-enhanced video microscopy: digitally processed microscope images can be produced in real time. *Proc Natl Acad Sci U S A* 78:6927-6931.
- Wang, G., T. Savinko, H. Wolff, M.C. Dieu-Nosjean, L. Kemeny, B. Homey, A.I. Lauerma, and H. Alenius. 2007. Repeated epicutaneous exposures to ovalbumin progressively induce atopic dermatitis-like skin lesions in mice. *Clin Exp Allergy* 37:151-161.
- Watanabe, J., Y. Miyazaki, G.A. Zimmerman, K.H. Albertine, and T.M. McIntyre. 2003. Endotoxin contamination of ovalbumin suppresses murine immunologic responses and development of airway hyper-reactivity. *J Biol Chem* 278:42361-42368.
- Wawrzyniak, P., C.A. Akdis, F.D. Finkelman, and M.E. Rothenberg. 2016. Advances and highlights in mechanisms of allergic disease in 2015. *J Allergy Clin Immunol* 137:1681-1696.
- Wedman, P., A. Aladhami, M. Beste, M.K. Edwards, A. Chumanevich, J.W. Fuseler, and C.A. Oskeritzian. 2015. A New Image Analysis Method Based on Morphometric and Fractal Parameters for Rapid Evaluation of In Situ Mammalian Mast Cell Status. *Microsc Microanal* 21:1573-1581.
- Weidinger, S., and N. Novak. 2016. Atopic dermatitis. *Lancet* 387:1109-1122.
- Werfel, T., J.P. Allam, T. Biedermann, K. Eyerich, S. Gilles, E. Guttman-Yassky, W. Hoetzenecker, E. Knol, H.U. Simon, A. Wollenberg, T. Bieber, R.

- Lauener, P. Schmid-Grendelmeier, C. Traidl-Hoffmann, and C.A. Akdis. 2016. Cellular and molecular immunologic mechanisms in patients with atopic dermatitis. *J Allergy Clin Immunol* 138:336-349.
- Wernersson, S., and G. Pejler. 2014. Mast cell secretory granules: armed for battle. *Nat Rev Immunol* 14:478-494.
- Wick, N., S. Thurner, K. Paiha, R. Sedivy, I. Vietor, and L.A. Huber. 2003. Quantitative measurement of cell migration using time-lapse videomicroscopy and non-linear system analysis. *Histochem Cell Biol* 119:15-20.
- Wolters, P.J., J. Mallen-St Clair, C.C. Lewis, S.A. Villalta, P. Baluk, D.J. Erle, and G.H. Caughey. 2005. Tissue-selective mast cell reconstitution and differential lung gene expression in mast cell-deficient Kit(W-sh)/Kit(W-sh) sash mice. *Clin Exp Allergy* 35:82-88.
- Wu, Z., A.J. Macneil, R. Junkins, B. Li, J.N. Berman, and T.J. Lin. 2013. Mast cell FcεRI-induced early growth response 2 regulates CC chemokine ligand 1-dependent CD4+ T cell migration. *J Immunol* 190:4500-4507.
- Ying, S., L.T. Barata, Q. Meng, J.A. Grant, J. Barkans, S.R. Durham, and A.B. Kay. 1998. High-affinity immunoglobulin E receptor (Fc epsilon RI)-bearing eosinophils, mast cells, macrophages and Langerhans' cells in allergen-induced late-phase cutaneous reactions in atopic subjects. *Immunology* 93:281-288.
- Yoon, J., J.M. Leyva-Castillo, G. Wang, C. Galand, M.K. Oyoshi, L. Kumar, S. Hoff, R. He, A. Chervonsky, J.J. Oppenheim, V.K. Kuchroo, M.R. van den Brink,

- R.e.W. Malefyt, P.A. Tessier, R. Fuhlbrigge, P. Rosenstiel, C. Terhorst, G. Murphy, and R.S. Geha. 2016. IL-23 induced in keratinocytes by endogenous TLR4 ligands polarizes dendritic cells to drive IL-22 responses to skin immunization. *J Exp Med* 213:2147-2166.
- Zhang, L., J.Z. Liu, D. Dean, V. Sahgal, and G.H. Yue. 2006. A three-dimensional fractal analysis method for quantifying white matter structure in human brain. *J Neurosci Methods* 150:242-253.
- Zhu, Y., W.H. Pan, X.R. Wang, Y. Liu, M. Chen, X.G. Xu, W.Q. Liao, and J.H. Hu. 2015. Tryptase and protease-activated receptor-2 stimulate scratching behavior in a murine model of ovalbumin-induced atopic-like dermatitis. *Int Immunopharmacol* 28:507-512.
- Zouein, F.A., M. Kurdi, G.W. Booz, and J.W. Fuseler. 2014. Applying fractal dimension and image analysis to quantify fibrotic collagen deposition and organization in the normal and hypertensive heart. *Microsc Microanal* 20:1134-1144.

APPENDIX A: PERMISSION TO REPRINT

CAMBRIDGE UNIVERSITY PRESS LICENSE TERMS AND CONDITIONS

Apr 03, 2017

This Agreement between Piper A Wedman ("You") and Cambridge University Press ("Cambridge University Press") consists of your license details and the terms and conditions provided by Cambridge University Press and Copyright Clearance Center.

License Number	4080450996742
License date	
Licensed Content Publisher	Cambridge University Press
Licensed Content Publication	Microscopy and Microanalysis
Licensed Content Title	Microscopy and Microanalysis Aims and Scope
Licensed Content Author	
Licensed Content Date	Apr 29, 2005
Licensed Content Volume	12
Licensed Content Issue	S1
Start page	4
End page	4
Type of Use	Dissertation/Thesis
Requestor type	Author
Portion	Full article
Author of this Cambridge University Press article	Yes
Author / editor of the new work	Yes
Order reference number	
Territory for reuse	World
Title of your thesis / dissertation	Mast Cells and Lipid Cross-Talk in Skin Inflammation
Expected completion date	May 2017

Estimated size(pages)
Publisher Tax ID
Terms and Conditions

133
GB823847609

TERMS & CONDITIONS

Cambridge University Press grants the Licensee permission on a non-exclusive non-transferable basis to reproduce, make available or otherwise use the Licensed content 'Content' in the named territory 'Territory' for the purpose listed 'the Use' on Page 1 of this Agreement subject to the following terms and conditions.

1. The License is limited to the permission granted and the Content detailed herein and does not extend to any other permission or content.
2. Cambridge gives no warranty or indemnity in respect of any third-party copyright material included in the Content, for which the Licensee should seek separate permission clearance.
3. The integrity of the Content must be ensured.
4. The License does extend to any edition published specifically for the use of handicapped or reading-impaired individuals.
5. The Licensee shall provide a prominent acknowledgement in the following format: author/s, title of article, name of journal, volume number, issue number, page references, reproduced with permission.